Aus dem Zentrum für Innere Medizin der Universität zu Köln
Klinik und Poliklinik für Innere Medizin I
Direktor: Universitätsprofessor Dr. med. M. Hallek

# Drug combination studies of EZH2 inhibition combined with ATM, PI3-Kinase and CDK inhibitors in *BRCA1*-deficient breast tumors

Inaugural-Dissertation zur Erlangung der Doktorwürde
der Medizinischen Fakultät
der Universität zu Köln

vorgelegt von
Leandra Bartke
aus Hamburg, Deutschland

promoviert am 07. August 2023

Erklärung

Ich erkläre hiermit, dass ich die vorliegende Dissertationsschrift ohne unzulässige Hilfe Dritter und ohne Benutzung anderer als der angegebenen Hilfsmittel angefertigt habe; die aus fremden Quellen direkt oder indirekt übernommenen Gedanken sind als solche kenntlich gemacht.

Bei der Auswahl und Auswertung des Materials sowie bei der Herstellung des Manuskriptes habe ich Unterstützungsleistungen von folgenden Personen erhalten:

Frau Dr. med. Leonie Ratz
Herr Dr. med. Julian Puppe
Herr. Univ.-Prof. Dr. med. Christian Reinhardt

Weitere Personen waren an der Erstellung der vorliegenden Arbeit nicht beteiligt. Insbesondere habe ich nicht die Hilfe einer Promotionsberaterin/eines Promotionsberaters in Anspruch genommen. Dritte haben von mir weder unmittelbar noch mittelbar geldwerte Leistungen für Arbeiten erhalten, die im Zusammenhang mit dem Inhalt der vorgelegten Dissertationsschrift stehen.

Die Dissertationsschrift wurde von mir bisher weder im Inland noch im Ausland in gleicher oder ähnlicher Form einer anderen Prüfungsbehörde vorgelegt.

Dieser Arbeit zu Grunde liegenden Ideen, Konzepte und Umsetzungen der Experimente sind größtenteils unter Anleitung von Universitätsprofessor Dr. med. C. Reinhardt, Dr. med. Leonie Ratz, C.S. Brambillasca und Dr. med. Julian Puppe durchgeführt worden. Diese Arbeit ist in Anlehnung und Zusammenarbeit mit der Publikation „Combined inhibition of EZH2 and ATM is synthetic lethal in BRCA1-deficient breast cancer" von Ratz et al., publiziert im Journal Breast Cancer Research im Jahr 2022, entstanden. Weitere in der Publikation gelistete Mitautoren waren mittelbar an der Entstehung dieser Arbeit beteiligt.

Hinsichtlich meiner Arbeit möchte ich im Folgenden kurz darstellen, welche wesentlichen Beiträge ich geleistet habe und in welcher Zusammenarbeit diese Arbeit entstanden ist. Die Ziele und Inhalte dieser Arbeit entsprechen der oben genannten Publikation Ratz et al., welche durch meine Mithilfe entstanden ist. Die in vivo Experimente wurden vollständig von C.S. Brambillasca und Marieke van de Ven unter der Anleitung von Jos Jonkers am Netherlands Cancer Institute in Amsterdam ohne meine Mithilfe durchgeführt. Wie im Manuskript der Publikation aufgeführt, habe ich entscheidend zur Durchführung der in vitro Experimente beigetragen. Dies umfasst die Experimente aus den Abbildungen (figures) 3-11, die in enger Zusammenarbeit mit Dr. med. L. Ratz entstanden sind.

In diesem Zusammenhang möchte ich vermerken, dass für diese Arbeit ausschließlich Daten bis August 2020 erhoben wurden. Die Daten aus der Publikation beinhalten Revisionsexperimente, die von Dr. med. L. Ratz und weiteren in der Publikation vermerkten Autoren durchgeführt worden sind.  Aus diesem Grund sind die Daten bezüglich der Kombinationstherapie von EZH2-Inhibierung und ATM-Inhibierung aus den Abbildungen (figures) 3,4,7,10 und 11 nicht identisch mit den Daten, die in der Publikation gezeigt werden. In dieser Arbeit werden Inhalte, die aus der Publikation Ratz et al. mit freundlicher

Genehmigung übernommen wurden, entsprechend direkt zitiert. Inhalte, die auf Grund früherer Daten nicht exakt denen aus der Publikation entsprechen, aber in Zusammenarbeit mit den Autoren der Publikation entstanden sind, werden in dieser Arbeit entsprechend mit „beinhaltet Daten aus Ratz et al." bzw. auf Englisch entsprechend „contains data from Ratz et al." zitiert.

Des Weiteren beinhaltet diese Arbeit zwei zusätzliche Kombinationstherapien (EZH2-Inhibierung mit PI3K- oder CDK-Inhibierung), die in der Publikation nicht weiter ausgeführt werden, jedoch in gleicher Weise erhoben wurden. Die *in vitro* Experimente wurden unter der Beratung von Prof. Dr. med. C. Reinhard durch Dr. med. J. Puppe, Dr. med. L. Ratz und mich ausgeführt. Diese Arbeiten sind in Anlehnung an die Publikation von Ratz et al. entstanden. In diesem Fall werden die Experimente auf Basis der Publikation von Ratz et al. mit „in Anlehnung an", bzw. auf Englisch mit „based on Ratz et al." vermerkt.

Das schriftliche Einverständnis von Dr. med. J. Puppe über die Vorabveröffentlichung von nicht publizierten Inhalten meiner Dissertationsschrift liegt dem Promotionsbüro vor.

Erklärung zur guten wissenschaftlichen Praxis:

Ich erkläre hiermit, dass ich die Ordnung zur Sicherung guter wissenschaftlicher Praxis und zum Umgang mit wissenschaftlichem Fehlverhalten (Amtliche Mitteilung der Universität zu Köln AM 132/2020) der Universität zu Köln gelesen habe und verpflichte mich hiermit, die dort genannten Vorgaben bei allen wissenschaftlichen Tätigkeiten zu beachten und umzusetzen.

Köln, den 20.02.2023

Leandra Bartke

## ABBREVIATIONS

| | |
|---|---|
| **AGO** | Arbeitsgemeinschaft Gynäkologische Onkologie |
| **AKT/PKB** | Protein kinase B |
| **ATM** | Ataxia telangiectasia-mutated kinase |
| **ATP** | Adenosine triphosphate |
| **ATR** | Ataxia telangiectasia and Rad 3-related protein kinase |
| **BER** | Base excision repair |
| **BRCA1** | Breast cancer 1 |
| **BRCA2** | Breast cancer 2 |
| **BSA** | Bovine serum albumin |
| **CAL120** | Human cell line, TNBC, BRCA1$^{wt/wt}$ |
| **Cdc2** | Cell division cycle protein 2 |
| **CDH1** | Cadherin 1 |
| **CDK** | Cycline dependent kinase |
| **CDKN2A/p16** | Cyclin dependent kinase inhibitor 2A/protein 16 |
| **CFA** | Colony formation assay |
| **ChIP seq** | Chromatin Immuno Precipitation DNA-Sequencing |
| **CHK1** | Checkpoint kinase 1 |
| **CIN** | Chromosomal instability |
| **CT** | Computer tomography |
| **CTG** | CellTiter-Glo® Luminescent Cell Viability Assay |
| **DAPI** | 4′,6-Diamidin-2-phenylindol |
| **DDR** | DNA damage response |
| **DMEM-F12** | Dulbecco's Modified Eagle Medium and Ham's Nutrient Mixture F-12 |
| **DMSO** | Dimethylsulfoxid |
| **DNA** | Deoxyribonuleic acid |
| **Dox** | Doxycycline |
| **DSB** | Double-strand break |
| **dsDNA** | Double stranded DNA |
| **EMT** | Epithelial-mesenchymal transition |
| **ER** | Estrogen receptor |
| **ERK** | Extracellular regulated MAP kinase |
| **EZH2** | Enhancer of zeste homolog 2 |
| **FBS** | Fetal bovine serum |
| **FISH** | Fluorescence in situ hybridization |
| **FOXO3** | Forkhead box O3 |

| | |
|---|---|
| **GI** | Genomic instability |
| **H3K27me$^3$** | Trimethylation of lysine tail 27 on histone 3 |
| **HER2** | Human epidermal growth factor receptor 2 |
| **HIV** | Human immunodeficiency virus |
| **HOTAIR** | HOX transcript antisense RNA |
| **HOX genes** | Homeobox genes |
| **HR** | Homologous recombination |
| **IC$_{50}$** | Half maximal inhibitory concentration |
| **ID4** | Inhibitor of DNA binding 4 |
| **IHC** | Immunohistochemistry |
| **INK4-family** | Inhibitors of CDK 4/6-family (protein-15, -16, -18 and -19) |
| **KB1P** | K14Cre;Brca1fl/fl;Tp53fl/fl murine cell line |
| **Ki-67** | Proliferation marker |
| **KP** | K14Cre;Tp53$^{fl/fl}$ murine cell line |
| **MDM2** | Mouse double minute 2 homolog |
| **Mre11** | Meiotic recombination 11 |
| **MRI** | Magnetic resonance imaging |
| **mRNA** | Messenger Ribonucleic acid |
| **MSI** | Microsatellite instability |
| **MTD** | Maximum tolerable dose |
| **mTOR** | Mammalian Target of Rapamycin |
| **MYC** | MYC proto-oncogene |
| **Nab-** | Nanoparticle albumin bound |
| **NF-kb** | Nuclear factor kappa-light-chain-enhancer of activated B-cells |
| **NHEJ** | Non-homologous end joining |
| **NHEJ** | Non-homologous end joining |
| **Opti-MEM™** | Reduced Serum Medium, Minimum Essential Medium by thermo fisher |
| **PALB2** | Partner And Localizer Of BRCA2 |
| **PARP1/2** | Poly (ADP-Ribose)-polymerase 1/2 |
| **PBS** | Phosphate buffered saline |
| **PcG** | Polycomb group |
| **pCR** | Pathological complete response |
| **PCR** | Polymerase chain reaction |
| **PD-L1** | Programmed death ligand 1 |
| **PDX** | Patient derived xenograft |
| **PFA** | Paraformaldehyde |
| **PFS** | Progression-free survival |
| **PI3K** | Phosphatidylinositol-4,5-bisphosphate3-kinase |

| | |
|---|---|
| **PIK3CA** | Phosphatidylinositol-4,5-bisphosphate3-kinase catalytic subunit alpha |
| **PIKK** | Phosphatidylinositol-3-OH-kinase-like |
| **PIP3** | Phosphatidylinositol-3,4,5-triphosphate |
| **PMSF** | Phenylmethylsulfonylfluoride |
| **PR** | Progesterone receptor |
| **PRC2** | Polycomb repressive complex 2 |
| **PTEN** | Phosphatase and Tensin homolog |
| **RAD51** | Rad51 recombinase |
| **RAF1** | Raf-1 proto-oncogene |
| **RAS** | Rat sarcoma viral oncogene |
| **Rb** | Retinoblastoma protein |
| **RIPA** | Radioimmunoprecipitation assay buffer |
| **RNA** | Ribonucleic acid |
| **RPA** | Replication protein A |
| **SAM** | S-adenosyl-L-methionine |
| **SD** | Standard deviation |
| **SDS-PAGE** | Sodium dodecyl sulfate polyacrylamide gel electrophoresis |
| **shRNA** | Short hairpin RNA |
| **SSBs** | Single-strand breaks |
| **ssDNA** | Single stranded DNA |
| **SUM149** | Human cell line, TNBC, BRCA1 $^{fl/fl}$ |
| **TGF** | Transforming growth factor |
| **TNBC** | Triple negative breast cancers |
| *TP53* | Tumor progressor gene 53 |
| **UICC** | Union for International Cancer Control |
| **VEGF** | Vascular endothelial growth factor |
| **WHO** | World Health Organization |
| **yH2AX** | Phosphorylation of the histone H2A variant (H2AX) to gamma-H2AX |
| **(XYZ)i** | (XYZ)inhibitor |
| **53BP1** | Tumor suppressor p53-binding protein 1 |

# 1   SUMMARY

Current targeted treatment options for *BRCA1*-deficient breast cancer are limited. *BRCA1*-mutant breast cancers frequently show a triple-negative phenotype and are associated with poor survival. At the cellular level, BRCA1 is important for DNA double-strand break repair through the homologous recombination pathway. Our group previously showed that EZH2 is significantly higher expressed in *BRCA1*-associated breast tumors. EZH2, a member of the Polycomb repressive complex 2, acts as an epigenetic suppressor through its trimethyltransferase activity of H3K27me$^3$, a modification associated with a variety of pathways involved in stem cell self-renewal, cell cycle, cell differentiation, and cellular transformation. To further exploit EZH2 overexpression upon *Brca1*-deficiency, we designed a large-scale cell line-based drug synergy screen using EZH2 inhibitor GSK126 in combination with different inhibitors involved in DNA damage signaling or cell cycle regulation. We made use of cell lines that were derived from *Brca1*-deficient (*K14Cre;Brca1$^{fl/fl}$;Tp53$^{fl/fl}$*) and *Brca1*-proficient (*K14Cre;Tp53$^{fl/fl}$*) murine mammary tumors. Our screen revealed synergistic sensitivity of *Brca1*-deficient cells to treatment with the ATM inhibitor AZD1390, PI3K inhibitor BKM120 or CDK inhibitor dinaciclib combined with GSK126. Further validations by a variety of functional *in vitro* experiments showed significant growth inhibition and increased levels of unrepaired DNA damage upon treatment with the combination of GSK126 and AZD1390 in *Brca1*-deficient breast cancer cells indicating drug synergy. These findings could be confirmed for combined treatment with GSK126/AZD1390 in our *Brca1*-deficient murine model which show a significant survival benefit. Combined treatment of GSK126 and BKM120, as well as GSK126 and dinaciclib for *Brca1*-deficient breast cancer cells also demonstrated *in vitro* activity but were found to be of additive character. In summary, we hereby describe a novel synergistic combination treatment of GSK126/AZD1390 for the treatment of *BRCA1*-deficient breast cancer.

## ZUSAMMENFASSUNG

Die derzeitigen Behandlungsmöglichkeiten für *BRCA1*-defizienten Brustkrebs sind begrenzt. Mammakarzinome mit einer *BRCA1*-Mutation zeigen häufig einen triple-negativen Phänotyp und gehen mit einer schlechten Überlebensrate einher. Auf zellulärer Ebene ist BRCA1 wichtig für die DNA-Doppelstrangbruchreparatur durch den homologen Rekombinationsweg. Unsere Gruppe hat zuvor gezeigt, dass EZH2 in *BRCA1*-assoziierten Brusttumoren signifikant höher exprimiert wird. EZH2, Teil des Polycomb-Repressionskomplexes 2, wirkt als epigenetischer Suppressor und bewirkt mit seiner Trimethylase-Aktivität die Modifikation H3K27me$^3$, welche mit einer Vielzahl von Signalwegen verbunden ist, die an der Selbsterneuerung von Stammzellen, dem Zellzyklus, der Zelldifferenzierung und der Zelltransformation beteiligt sind. Um die EZH2-Überexpression bei *Brca1*-defizientem Brustkrebs weiter auszunutzen, entwarfen wir einen groß angelegten Zelllinien-basierten Arzneimittel-Synergie-Screen unter Verwendung des EZH2-Inhibitors GSK126 in Kombination mit verschiedenen Inhibitoren, die an der Reparatur von DNA-Schäden oder an der Zellzyklus-Regulation beteiligt sind. Wir verwendeten Zelllinien, die aus *Brca1*-defizienten (*K14Cre;Brca1$^{fl/fl}$;Tp53$^{fl/fl}$*) und *Brca1*-profizienten (*K14Cre;Tp53$^{fl/fl}$*) Mammatumoren der Maus gewonnen wurden. Unsere Untersuchungen ergaben eine synergistische Sensitivität von *Brca1*-defizienten Zellen gegenüber der Behandlung mit dem ATM-Inhibitor AZD1390, dem PI3K-Inhibitor BKM120 oder dem CDK-Inhibitor Dinaciclib in Kombination mit GSK126. Weitere Validierung durch funktionelle *in vitro* Experimente zeigten eine signifikante Wachstumshemmung und ein erhöhtes Niveau von nicht reparierten DNA-Schäden bei der Behandlung mit der Kombination von GSK126 und AZD1390 in *Brca1*-defizienten Brustkrebszellen und bestätigten den synergistischen Effekt dieser Kombination. Darüber hinaus konnten *in vivo* Versuche in unserem *Brca1*-defizienten Mausmodell für die kombinierte Behandlung von GSK126/AZD1390 ein signifikantes progressionsfreies Überleben zeigen und die *in vitro* Erkenntnisse bestätigen. Die kombinierten Behandlungen von *Brca1*-defizienten Brustkrebszellen mit GSK126 und BKM120 oder mit Dinaciclib zeigten einen additiven Effekt. Zusammenfassend beschreiben wir hiermit eine neuartige synergistische Kombinationsbehandlung von GSK126/AZD1390 zur Behandlung von Brustkrebs mit *BRCA1*-Defizienz.

# 2 INTRODUCTION

## 2.1 Cancer: a genetic disease as a global challenge

Cancer is the second leading cause of deaths worldwide [1]. It is distributed throughout all societies and socioeconomic classes, however 70% of cancer-related deaths occur in low- and middle-income countries [1]. It therefore remains a global challenge to reduce the cancer-related disease burden by identifying causes and disease mechanisms and improving treatment options for cancer patients. Manifold efforts throughout the history of cancer research have led to our current understanding of cancer as a complex genetic disease. A breakthrough of molecular cancer research in 1975 was the discovery of proto-oncogenes, which are ubiquitously expressed genes that have the potential to induce tumorigenesis when altered [2]. The current status of science was first displayed by the identification of six hallmarks of cancer by Douglas Hanahan and Robert Weinberg in 2000 [3]. According to their updated review from 2011, malignancies occur when cells acquire the capability of bypassing six essential regulatory cell circuits in a multistep process. Douglas Hanahan and Robert Weinberg describe that the six hallmark capabilities of cancer are: "sustaining proliferative signaling, evading growth suppressors, activating invasion and metastasis, enabling replicative immortality, inducing angiogenesis and resisting cell death" [4].

## 2.2 Oncogenes and tumor suppressor genes: involvement in genomic instability

### 2.2.1 Genomic instability in cancer

During the multistep progression of cancer, individual cells accumulate genetic aberrations that eventually lead to genomic instability (GI) and provide a proliferation and survival advantage [5]. GI is the cause for inter- and intra-tumor heterogeneity [5]. As it leads to the selection of mutations that enable the cells to best proliferate and disseminate, GI enables adaption of the tumor to environmental stress and promotes tumor aggressiveness [4].

The mutational scope can vary from point mutations on the nucleotide level to structural aberrations on the chromosomal level, which can result in microsatellite instability (MSI) as well as chromosomal instability (CIN). Most frequently, GI is acquired upon defects in pathways of DNA replication and DNA damage response (DDR) [5]. GI in hereditary cancers most frequently arises from impaired DNA damage repair through mutations of DNA repair genes, whereas GI in sporadic cancers is most likely a consequence of oncogene-induced stress

during replication [6]. Modern sequencing technologies provide an insight on GI-signatures of specific cancers, which enables categorization of cancer subtypes and novel targeted therapy options, thus highlighting its clinical relevance [5].

### 2.2.2 Oncogenes and tumor suppressor genes

As previously established, GI may cause the acquisition of essential hallmark capabilities in cancer development as it leads to the selection of clones with malignant alterations of potent oncogenes and tumor suppressor genes [4,5]. Such alterations are either consequences of diverse mutations or epigenetic modifications. Mutations most commonly seen in oncogenes are amplifications, hyper-activations or inhibition of negative feedback mechanisms, whereas losses of tumor suppressor genes are mostly caused by inactivating mutations [4].

Proto-oncogenes physiologically promote pathways of cell proliferation and metabolism in a controlled manner. However, gain of function of those genes upon mutation and/or amplification results in malignant transformation [7]. Prominent examples of oncogenes are *RAS* and *MYC* and their oncogenic potential has been pinpointed to the acquisition of all hallmark capabilities [4]. The physiological function of *RAS* is often impaired in cancers through mutation of its intrinsic GTPase activity, resulting in deregulation of its negative feedback mechanism, while the *MYC*-gene is frequently amplified in tumors [4]. As cancers are often very heterogeneous, they can be addicted to one oncogene in certain cases: this so-called "Achilles heel" of the cancer can be therapeutically targeted very specifically [8]. One clinically relevant example is the overexpression of human epidermal growth factor receptor 2 (HER2) in breast cancer, which is normally associated with a poor prognosis. Inhibition of HER2 in cancers that are addicted to this oncogene, however, leads to good therapeutic response rates [8].

Tumor suppressor genes acquire malignant potential upon loss of their function [7]. One of the first discovered tumor suppressor genes was the Retinoblastoma protein (RB), which is physiologically responsible for inhibition of cell cycle progression from G1 to S phase [9]. By studying the mechanism behind loss of function of *RB*, Knudson first described the "two hits" theory [10]. Upon inheritance of a mutated tumor suppressor gene (first hit), loss of function of the wild type allele as a second hit is obligatory for tumorigenesis [10]. Similar mechanisms have been described for other genes, such as *BRCA1*, which is autosomal dominantly inherited [6,7,11]. It leads to cancer development upon somatic loss of function of the wild type allele, a phenomenon also referred to as loss of heterozygosity [7]. One of the most frequently mutated tumor suppressor genes in many tumor entities is *TP53* [4,12]. By controlling crucial steps in cell cycle progression, the so-called "guardian of the genome" is essential for maintaining genome integrity [12]. The discovery of oncogenes and tumor suppressor genes paved the way for current

clinically available cancer therapies as it enables researchers to pinpoint cancer development to certain upregulated or inhibited pathways [7].

### 2.2.3 Epigenetic modifications

Epigenetic changes, which are chemical modifications of the DNA, impact transcription of both oncogenes and tumor suppressor genes [4]. DNA methylations often occur at CpG islands, which are regions characterized by a high frequency of cytosine nucleotides next to guanine nucleotides [13]. When looking at CpG islands of different cancer entities, certain DNA methylation patterns can be distinguished. Breast cancers, for example, frequently exhibit promoter methylations of the tumor suppressor genes *CDKN2A* (encoding for cyclin dependent kinase inhibitor 2A, also called p16), *BRCA1* and *CDH1* (encoding for E-Cadherin), which result in decreased gene-transcriptions and thus impaired downstream signaling [13]. The transcriptome can further be epigenetically impacted on chromosomes by histone modifications, such as acetylations or methylations of histone lysine tails. Polycomb group (PcG) proteins are representatives of these epigenetic suppressors and are known for participating in the regulation of stem cell maintenance and differentiation [14]. In that matter, dysfunction of PcG activity has been linked to tumorigenesis and could promote the oncogenic properties of cancer stem cells [14]. In breast cancer, among with many other cancer entities, histone methylations via the PcG proteins are associated with oncogenic signaling [15,16].

### 2.2.4 Cell cycle regulation

The cell cycle is the process that drives growth and proliferation. It consists of four stages: G1, S and G2 phase followed by mitosis. Under the influence of certain signaling events, G1 phase can be abrogated by activation of G0 phase, which is a resting and non-proliferative stage. Its complex role of converting mitogenic growth factors and stress signals into controlled cell cycle progression is regulated in each stage by a phase-specific checkpoint [17]. The transition from one phase to another is regulated by fluctuating levels of phase-specific cyclins, which activate cyclin-dependent kinases (CDK) that mediate cell cycle progression [17].

In G1 phase, D-type cyclins are upregulated by a variety of extracellular mitogenic signals [18]. D-type cyclins are then bound by CDK4/6 and progression to S phase is promoted. Upon transition from G1 to S phase, the cell passes the restriction point (R-point), after which cell cycle progression occurs independently from extracellular signals [2]. The R-point is controlled by the Retinoblastoma protein (RB), which regulates the activity of transcription factor E2F. Upon intracellular stress, RB is dephosphorylated and actively binds E2F [2]. If RB is hyperphosphorylated, E2F is unbound and can upregulate, among others, the transcription of E-type cyclins that mediate progression to S phase by activation of CDK2 [9]. The association

of cyclin A to CDK2 drives the S phase [17]. As DNA replication occurs during S phase, strict regulation of the R-point is crucial to avoid acquisition of DNA damage and cell cycle arrest occurs upon inhibition of specific cyclin-CDK complexes [19]. Most importantly, members of the INK4 family (p15, p16, p18 and p19) directly inhibit CDK4/6, whereas members of the WAF family (p21, p27 and p57) mediate inhibition of E-CDK2, A-CDK2 and B-CDK1 complexes [19]. P15, as part of G1 phase, is activated through extracellular TGF-ß signaling [20], whereas p21 and p27 are activated upon intracellular DNA damage signaling to inhibit replication of damaged DNA [17].

Following S phase, upregulation of CDK1-cyclin B complex is pivotal for G2 phase. During G2 phase a positive feedback loop acts to activate the CDK1 pathway to promote an increase of activated CDK1-cyclin B levels up to the cell's progression to mitosis [2,17]. This auto-activation loop can be disrupted upon DNA damage by CHK1-mediated inhibition of CDK1 and activation of the TP53 pathway [21]. Consequently, CHK1 inhibition is mandatory for enabling progression through the G2-M checkpoint to M phase [2,21].

In order to sustain proliferation or evade growth suppression, tumors cells can inactivate *RB*, inhibit CDK-regulators or enhance CDK activity [17,21]. The tumor suppressor gene *RB* is defective in a variety of cancers [4]. Further, inactivation of CDK-regulators can be mediated by epigenetic silencing, such as promoter methylation of CDKN2A [13]. High levels of cyclin E1 have been associated with a highly aggressive breast cancer type and decreased overall survival [22].

An important mediator of cell cycle progression is the phosphoinositide 3-kinase (PI3K), a lipid kinase that translates signals from growth factors and cytokines through phosphorylation of phosphatidylinositol-3,4,5-triphosphate (PIP3) via its regulatory subunit p85 and catalytic subunit p110 [23]. It has been linked to key hallmarks of cancer, mainly cell growth, proliferation, metabolism and survival [4,23]. Upon *PI3K* overexpression, mutation or loss of its negative regulator *PTEN*, AKT is increasingly phosphorylated [17]. AKT acts through inhibition of p21 and p27 activity, thereby promoting cell cycle progression through G1/S transition [17,23]. Additionally, it inhibits GSK-3ß and consequently activates ß-catenin, which results in upregulation of cyclin D and further progression to S phase [17,23]. As Luo et al. state, AKT promotes cell growth through activation of the metabolic mTOR signaling, while cell survival is caused by inactivation of the pro-apoptotic protein Bad, activation of the survival factor NF-kb (nuclear factor kappa-light-chain-enhancer of activated B-cells) and abrogation of TP53 [23]. The importance of oncogenic PI3K/AKT signaling is emerging, as it seems to be frequently altered in cancers, among others breast cancers. High-grade breast tumors correlate with increased activity of

pAKT (phosphorylated AKT) and consequently decreased levels of intra-nuclear p27 [24]. Additionally, cyclin D is overexpressed in 50% of breast cancers [18].

As an important mediator between cell cycle progression and DDR, the tumor suppressor TP53 [12] is activated upon phosphorylation by two key mediators of DNA damage repair: ATM (Ataxia telangiectasia mutated kinase) and CHK1/2 (checkpoint kinase 1/2) [2,21]. Upon deregulation of cellular signaling pathways, TP53 coordinates cell cycle arrest, DNA repair and induction of apoptosis [12]. As a negative feedback mechanism, TP53 is a transcription factor for its own inhibitor MDM2 [17]. MDM2 is furthermore positively regulated by the PI3K/AKT pathway [23]. Loss of function of *TP53* promotes accumulation of genomic aberrations leading to GI, as it is the case in about 25% of all breast cancers [25].

### 2.2.5 DNA damage response

Genomic integrity is impaired by ineffective DNA damage detection and repair. To prevent the accumulation of DNA damage, specialized repair mechanisms become activated by diverse DNA damage-inducing factors. Double strand breaks (DSBs) are repaired by homologous recombination (HR) or non-homologous end joining (NHEJ), whereas single-strand breaks (SSBs) are repaired by base excision repair (BER), which occurs throughout the entire cell cycle and is mediated and driven by PARP1/2 (poly (ADP-Ribose)-polymerase 1/2) [26]. If, however, the BER pathway is deficient, unrepaired SSBs cause a stall of replication forks during the next S phase, resulting in DSBs [26].

The phosphatidylinositol-3-OH-kinase-like (PIKK) family of protein kinases is pivotal for DNA damage signaling [27]. ATM is activated upon DSBs, whereas ATR (Ataxia telangiectasia and Rad 3-related protein kinase) is also activated upon stalled replication forks [28]. In the following, the kinases mediate DNA damage repair through phosphorylation of the histone H2A variant (H2AX) to gamma-H2AX (yH2AX), which leads to the recruitment of proteins essential for DSB repair [27]. Furthermore, ATM regulates cell cycle checkpoints (G1/S-, intra-S- and G2/M-checkpoint) in response to DSBs mediated by CHK1/2 and TP53, which consequently results in S- or G2-arrest, and it recruits BRCA1 to sites of DNA damage [28].

DSB repair by HR takes place during S and G2 phase, when DNA is present in its sister chromatids, which serve as a template for transcription of the missing DNA sequence [17]. BRCA1, a DNA damage signaling mediator, and BRCA2, an initiator of DNA repair, form a complex by binding through PALB2 [29]. BRCA1, when activated by ATM, is a regulator of intra-S-phase checkpoint [28]. Isono et al. report that BRCA1 promotes HR by dephosphorylating 53BP1 during S-phase, thus inhibiting the rather error prone NHEJ, while in its phosphorylated

state 53BP1 mediates NHEJ by inhibition of DNA end resection [30]. Upon BRCA1-mediated dephosphorylation of 53BP1, the recruitment of the MRN (MRE11, RAD50, NBS1) complex to sites of DSBs is enabled [30]. The MRN complex is pivotal in starting the pathway of HR, as well as DNA damage signaling, through further ATM activation [29]. After recognizing DSBs, the MRN complex initiates 5'-3' nucleolytic digestion of DNA ends, generating 3'-overhangs of single stranded DNA (ssDNA). In the following, Mre11/CtIP complexes induce protective RPA caps of the 3' ssDNA [21]. RPA caps are then replaced by Rad51, which is recruited by BRCA2 to sites of ssDNA. Next, Rad51 mediates single strand invasion to a homologous dsDNA, which then functions as a template for elongation of the missing nucleotides by DNA-Polymerase [29,31].

## 2.3 Combination therapies

Combination therapies follow the idea of combining drugs that are involved in either inhibiting different signaling pathways or different targets within the same pathway. It first originated in the therapy of infectious diseases, such as Tuberculosis and HIV in the mid 20th century to prevent and overcome resistances development of monotherapies [32]. This idea was adapted to novel cancer treatment strategies, since resistance to conventional chemotherapy remains a limiting factor of therapy response [33]. The effectiveness of this approach can be seen in the treatment of children with ALL (acute lymphoblastic leukemia) where combination of different chemotherapy drugs increased overall survival rates significantly [34].

The rational for combination therapy in cancer is the intra-tumor heterogeneity caused by clonal selection of cells with potent oncogenic mutations [5]. Even though some cancers that harbor an "oncogene-addiction" can be treated efficiently by solely inhibiting this oncogenic driver mutation [8], most cancers develop resistance by clonal selection of alternative potent oncogenes or compensatory upregulation of cell survival signaling pathways [35]. Furthermore, deletion of tumor suppressor genes such as *TP53* and *BRCA1* cannot be directly targeted. Hence, the only way of targeting such cancers is by inhibiting deleterious signaling which results from such driver mutations. In addition to that, Hanahan et al. state that "each of the core hallmark capabilities is regulated by partially redundant signaling pathways" [4], which further highlights the need of combinatory targeted treatments.

Combination therapies either result in an additive or synergistic effect of the applied drugs. An additive effect is the expected effect that would result from adding up the individual effects of each drug, while an observed synergistic effect of combination treatments is thus greater than the expected additive effect [33].

## 2.4 Breast cancer

### 2.4.1 Epidemiology

Breast cancer is the most prevalent cancer among women worldwide with increasing incident rates and most cancer related deaths among women according to the WHO [36]. In Germany, median age at diagnosis of breast cancer is at around 64 years and breast cancer incidence rate was 165.2 per 100.000 women, accounting for 29,5% of new cancer cases in 2016 [37]. Between 2003 and 2009 an increasing incidence by 23% has been registered, supposedly due to the implementation of the nation-wide mammography-screening program during this time period [38]. The mortality rate has been decreasing since 1998 in the range of 1-2% annually due to prevention programs, improved diagnostics, and the development in novel targeted therapeutic strategies [38]. Disease stage at the time of diagnosis is a crucial prognostic factor for breast cancer survival. In Germany, the 5-year survival rate for stage-two localized breast cancer is 94%, whereas stage-four diagnosed patients have a 5-year survival rate of 29% [37].

### 2.4.2 Diagnostics

Screening programs primarily involve clinical breast examination by palpation of the breast and mammography. The German AGO-Breast-Committee recommends yearly palpations of the breast by a specialized physician, as well as continuous self-examination by the patients [39]. In Germany, the national breast cancer prevention program involves mammography screenings every two years for women aged between 50 and 69 [39]. Suspicious findings will be controlled by ultrasound and if indicated biopsies of these lesions, as well as lymph nodes, are taken with guidance of ultrasound, mammography or MRI [40]. If a malignancy is histologically confirmed, staging with CT follows to rule out metastasis and to categorize the tumor according to the UICC stage, which the therapy recommendations are based on [40].

Patients with a positive family history of either breast and/or ovarian cancer or with cases of early cancer diagnosis have an increased risk for harboring a hereditary mutation [41]. If a mutation of a breast cancer susceptibility gene has been found in family members, women have the opportunity to undergo genetic testing [39]. Healthy women with germline mutations of the breast cancer susceptibility genes *BRCA1/BRCA2* subsequently benefit from both preventive bilateral mastectomy and bilateral salpingo-oophorectomy. These interventions lead to a risk reduction of 95% and 97% for breast and ovarian cancer, respectively [40]. Furthermore, early screening programs are indicated. Such screening programs start at the age of 25 or 5 years before the earliest cancer diagnosis in the family with semi-annual

palpation and ultrasound as well as yearly MRI, followed by yearly mammography starting at the age of 40 [39].

## 2.4.3 Pathology

Breast cancer is a very heterogeneous disease with many different genetic lesions and distinct phenotypes [5]. Most breast cancers arise from pre-cancerous lesions of either the epithelial or myoepithelial cells of the mammary ducts or the secretory milk-producing luminal cells of the lobules at the end of the milk ducts [42,43]. It is yet poorly understood which cells exactly initiate cancer development, however, most likely different stages of maturity from mammary stem cells are thought to be responsible [43]. The WHO histologically distinguishes an invasive carcinoma of no special type (NST) from certain invasive carcinomas with a mixed or special type, such as the invasive lobular carcinoma [42]. The molecular classification according to the receptor expression is of more clinical relevance since they determine prognosis and treatment options. Further, different cells of origin, driver mutations, gene expression profiles and methylation status can distinguish each subtype [43-45]. The five intrinsic molecular subtypes are defined by gene expression of Estrogen receptor (ER), Progesterone receptor (PR), HER2/neu and nuclear proliferation marker Ki67 and can histologically be distinguished with immunohistochemistry (IHC) or fluorescence in situ hybridization (FISH) [45]. International standardized discrimination between low and high levels of proliferation is currently lacking and the use of Ki67 as a surrogate marker for decision on therapy is controversial [5,45].

As Coates et al. sum up, the luminal A molecular subtype is characterized by high levels of ER and PR, while the luminal B type harbors only ER but not PR positivity and can be split into two subcategories by the HER2/neu-status and Ki67 levels [45]. The HER2-enriched molecular subtype only exhibits HER2/neu positivity. Furthermore, high HER2/neu status is associated with more aggressive tumors, as well as the proliferation marker Ki67, which is often increased upon hormone receptor negativity or HER2 positivity and associated with a poor prognosis [45]. Tumors negative of ER, PR and HER2 are referred to as triple negative breast cancers (TNBC) and their undifferentiated character is associated with more aggressive cancers and younger age of diagnosis compared to hormone receptor positive cancers [46]. Fifteen percent of all invasive breast cancers are TNBCs or basal-like cancers with mostly high histological grades, poor clinical outcomes in the first five years after diagnosis and often an association with loss of *BRCA1* function [46]. Eighty percent of TNBCs meet the criteria of the basal-like subgroup, a category defined by a basal-like gene expression profile of ductal carcinomas [46]. Basal-like cancers can further be identified by IHC staining of the cytokeratines CK5/6, CK 14 and CK17, which are expressed in normal basal myoepithelial cells of the breast ducts and are thus considered as basal markers [47]. TNBCs and the basal-like cancer cells show a distinct profile

of cell surface markers commonly expressed in breast-cancer stem cells, which are initiators and caretakers of malignant cells with metastatic development [48]. Basal-like breast cancer cells also frequently show a gene expression profile similar to cells undergoing epithelial-mesenchymal transition (EMT) [49]. Foulkes et al. state that even though TNBC and basal-like cancers tend to be an indicator for decreased 5-year overall survival and increased metastasis formation during this time period, survival reaches a steady state after 10 years [46]. In accordance with this, the risk for distant metastasis in non-TNBC is higher after 10 years since diagnosis, while TNBCs rarely recur anymore. TNBCs and basal-like cancers could thus be curatively treated if efficient therapies were to be available at diagnosis in order to prevent metastasis formation [46].

### 2.4.4 Treatment

Pharmacological therapy is based on the molecular subtypes. Hormone receptor positive luminal A type is predictive for good responses to anti-hormonal therapies such as tamoxifen (competitive inhibitor of ER) or anastrazole (lowering estrogen levels through aromatase inhibition), while luminal B type is less likely to respond to such treatments [45]. For hormone receptor positive and HER2 negative disease the type of adjuvant anti-hormonal therapy depends on the menopausal status and is commonly administered for five years [40]. The indication for neoadjuvant chemotherapy is evaluated depending on the risk stratification which is based on nodal status, tumor size, histological grading and Ki67 [40]. When chemotherapy is indicated for breast cancer therapy it starts with systemic neoadjuvant or adjuvant anthracycline- and taxane-based chemotherapy, which mostly shows good response rates in young patients, TNBC, HER2 positive and aggressive breast cancers [40]. HER2 positive cancers can be targeted efficiently by a combination of neoadjuvant chemotherapy and anti-HER2 treatment (pertuzumab/trastuzumab), followed by adjuvant maintenance of sole anti-HER2 inhibition. Furthermore, in case of no pathological complete response (pCR) a conjugate of trastuzumab-emtansin can be administered for a year [39].

TNBCs tend to be sensitive to carboplatin, an inter-strand crosslinking agent, and carboplatin is suggested for the neoadjuvant, adjuvant or palliative treatment of TNBCs [39]. The GeparSixto trial points out an increase of pCR for TNBC when adding carboplatin to the standard neoadjuvant chemotherapy regime (ClinicalTrials.gov identifier NCT01426880) [50]. Further efforts follow an anthracycline-free regime to provide for de-escalating neo-adjuvant therapy options. The WSG-ADAPT-TN trial found combined nab-paclitaxel/carboplatin therapy to improve pCR when compared with nab-paclitaxel/gemcitabine therapy in TNBC [51]. If pCR is achieved upon neoadjuvant therapy, especially the prognosis and survival for TNBCs is improved, however there is no evidence for prolonged overall survival [52].

If no lymph node metastasis is clinically diagnosed, a sentinel lymphnodectomy is indicated for pathological staging of lymph node dissemination [40]. Mastectomy has not improved overall survival rates in TNBCs and is thus not necessarily indicated if breast-conserving surgery is likely to achieve a free surgical margin (R0); however, breast-conserving surgery is then commonly followed by local radiation to additionally eradicate all residual microscopic lesions [40].

In stadium four, therapy regimens are increasingly complemented with novel targeted therapy options. Therapies depend on the patient's overall morbidity and location of metastasis. Recently, further targeted therapies have been emerging for the treatment of progressive breast cancer. A phase III clinical trial showed superiority of additional CDK 4/6 inhibition in combination with anti-hormonal therapy to overcome resistance of anti-hormonal treatment for hormone receptor positive breast cancers and is now implemented for the treatment of metastatic luminal A cancers (ClinicalTrials.gov identifier NCT01942135) [53]. If cancer progression is diagnosed under such treatment, mTOR inhibition (e.g. everolimus) in combination with the aromatase inhibitor exemestan can be indicated [40]. Recently, alpelisib in combination with fulvestrant has been approved for the treatment of *PIK3CA* mutated progressive luminal A cancer according to the SOLAR1-study [54]. Combined VEGF-inhibition and chemotherapy come into perspective for first line treatment of HER2 negative metastatic breast cancer, as it improved progression free overall survival in a phase III clinical trial (ClinicalTrials.gov identifier NCT00262067) [55]. For the treatment of TNBCs and basal-like breast cancer several potent inhibitors are currently being implemented into standard treatment, namely of PARP-1, PD-L1 and VEGF. The combination of nab-paclitaxel and atezolizumab has shown prolonged progression-free survival for patients with metastatic PD-L1 positive TNBC (ClinicalTrials.gov number NCT02425891) [56]. Upon PD-L1 negativity, combination therapy of paclitaxel, capecitabine and bevacizumab (anti-VEGF) is indicated [39]. So far chemotherapy appears to still be substantial for the treatment for aggressive cancers like TNBC, highlighting the need for the development of further novel targeted therapeutic strategies.

### 2.4.5 Hereditary breast cancer syndromes

Caretaker genes acting to maintain genome integrity take up essential tumor suppressive roles. An inherited pathogenic mutation in one allele of a caretaker gene, followed by loss of function of the wild type allele can lead to hereditary cancer [57]. Most inherited breast cancer syndromes result from defect tumor suppressor genes involved in DDR, cell cycle regulation and checkpoint control. To date, more than 25 mutated genes are frequently found in

hereditary breast cancers and approximately 5-10% of all breast cancer patients carry inherited mutations within a breast cancer risk gene [57]. The most frequent mutations are found in *BRCA1* and *BRCA2*, making up about 25% of all inherited breast cancer syndromes [58]. Women who are *BRCA1* germline mutation carriers have a lifetime risk of about 60% for developing breast cancer and the median age at diagnosis is approximately 10 to 15 years earlier than it is for non-hereditary cancers [41]. Other common syndromes with a predisposition to hereditary breast cancer are Li-Fraumeni, Cowden, Lynch and Ataxia telangiectasia [59]. Common heterozygous germline mutations with an association for hereditary breast cancer are found in the genes *RAD51*, *PALB2*, *ATM*, *TP53* and *CHK2* [57].

## 2.5   *BRCA1*-deficiency

### 2.5.1   Phenotype of *BRCA1*-deficient tumors in humans and murine model

*BRCA1*-mutation associated breast cancer is characterized by an aggressive and poorly differentiated phenotype [46]. Seventy percent of *BRCA1*-mutated breast cancers are TNBC [60] and the majority displays a basal-like phenotype [61]. Immunohistochemical and microarray analysis of *BRCA1*-mutated tumors are found to be concordant with the gene and protein expression profile of sporadic non-hereditary basal-like tumors [46,47,61]. In fact, there is evidence for down-regulation of *BRCA1* gene in sporadic tumors with basal-markers by i.e. high levels of ID-4, which is known to negatively regulate *BRCA1* [46]. *BRCA1* promoter methylation could be another mechanism of reduced *BRCA1* gene transcription and thus insufficient BRCA1 protein function in sporadic tumors [62].

The subgroup of sporadic cancers characterized by morphological features and defects in HR mimicking *BRCA1*-deficiency is referred to as a "*BRCA*ness" phenotype [63]. Twenty-five percent of sporadic breast cancer cases could be assigned to the "*BRCA*ness" phenotype [63]. Furthermore, *BRCA1*-mutated tumors show distinct DNA-copy number variations that are referred to as a "*BRCA1*-like" classifier and encompass *BRCA1*-mutated tumors, tumors with *BRCA1* promoter hyper-methylation and sporadic tumors with this distinct copy number variation-profile due to yet unknown genetic or epigenetic alterations[64,65]. The BRCA1-like classifier is of high clinical relevance since it is predictive of good response rates towards high dose alkylating- and platinum-based chemotherapy which is why it has been proposed that the BRCA1-like classifier could be employed to identify tumors lacking mechanisms for DSB-repair [64,66].

*BRCA1*-mutated tumors, as basal-like tumors, predominantly exhibit loss of TP53 function [67], which is associated with poor prognosis and considered as a potential predictor for resistance to platinum- and taxane-based chemotherapy [68]. A *TP53* mutation is assumed to be obligatory for the development of breast cancer upon *BRCA1*-deficiency. If *TP53* is abrogated upon high levels of GI, caused by insufficient HR due to *BRCA1*-deficiency, uncontrolled cell cycle progression occurs and enables cell survival despite genomic instability [67].

Liu et al. were able to create a conditional knockout murine model with somatic deletion of *Brca1* and *Tp53* in Cytokeratin 14 (expressed in myoepithelial cells of the breast ducts and specific for basal-like breast cancers [47]) exhibiting cells (*K14Cre;Brca1$^{fl/fl}$;Tp53$^{fl/fl}$*) [69]. The mice consequently develop autochthonous mammary tumors comparable to human basal-like breast cancers harboring a *BRCA1* mutation [69]. As this murine model proves initiation of mammary tumor development in the background of *Brca1-* and *Tp53*-deficiency, and faithfully mimics the human setting, we make use of cell lines derived from such *Brca1*-deficient tumors (*K14Cre;Brca1$^{fl/fl}$;Tp53$^{fl/fl}$*) in comparison with *Brca1*-wildtype tumors (*Brca1$^{wt/wt}$;Tp53$^{fl/fl}$*) to investigate novel synergistic therapies for *Brca1*-deficient breast cancers in this study [70].

### 2.5.2 Therapeutic options for *BRCA1*-deficient breast cancer patients

As for today, the German medical guidelines for pharmaceutical and surgical treatment of *BRCA1* mutated tumors are based on the evaluated therapy regimens for sporadic cancers. Nevertheless, new therapeutic approaches for *BRCA1*-deficient tumors are arising, among them platinum-based chemotherapy and PARP-inhibitors [40].

#### 2.5.2.1 Platinum-based chemotherapy

Since platinum-based chemotherapy is considered to be effective for the treatment of *BRCA1*-deficient tumors [40], several clinical trials are currently evaluating the benefit of this chemotherapy regimen for the treatment of TNBCs. In tumors with impaired DDR signaling, the assumed benefit of the alkylating platinum salts is due to accumulation of unrepaired DNA lesions subsequently leading to cell cycle arrest and apoptosis [71]. Three prospective clinical trials could show higher pCR rates upon additional treatment with carboplatin for *BRCA1* mutation carriers in the neoadjuvant [50,72] and metastasized setting [73]. However, a retrospective analysis of the GeparSixto trial, comparing the combination of carboplatin to the standard chemotherapy regimen for *BRCA1* mutated tumors with the standard chemotherapy regimen alone, did not show an additional effect of carboplatin (ClinicalTrials.gov identifier NCT01426880) [74].

### 2.5.2.2 Concept of synthetic lethality: PARP inhibition

The concept of synthetic lethality was first established in the mid 20th century as a genetic phenomenon, where alterations of alleles solely in their combination led to lethality [75]. A few decades later, this concept was then further developed and established as a new approach for cancer therapy. It aims for exploiting one crucially impaired oncogenic pathway with a second hit to provoke cell death. Each hit on its own is nonlethal and only their combination leads to a synergistically induced lethality [2]. In breast cancer, this novel approach is being implemented for treating tumors with a defect in DDR [75].

In 2005, poly ADP ribose polymerase (PARP)-inhibition was implemented as a novel target for treating tumors with loss of *BRCA1* and *BRCA2* [76]. As PARP is essential for ssDNA break repair by BER, its inhibition is assumed to cause stalling and collapsing of replication forks [77]. In the face of *BRCA1*-deficiency and thus defects in HR signaling, DSBs remain unrepaired, which eventually leads to cell death [77]. The PARP-inhibitor olaparib has been established in clinical trials for breast, ovarian and prostate cancer and shows very good anti-tumor activities and fewer side effects than chemotherapy [78]. Olaparib has recently been approved for the treatment of *BRCA1*-deficient and platin-sensitive ovarian cancer [79]. The EMBRACA trial observed improved progression-free survival rates of patients with advanced *BRCA1* germline-mutated breast cancers when treated with talazoparib (PARP1-inhibitor) in comparison to chemotherapy of the physician's choice as there is no standard chemotherapy for such cancers [80]. The OlympiA trial is studying the effect of adjuvant lynparza (PARP1-inhibitor) in comparison to placebo after definitive local treatment and first line chemotherapy (ClinicalTrials.gov identifier NCT02032823) [81]. As this approach represents an example for a complementary action between different DDR signaling pathways, this concept provides a rationale to investigate additional synthetic lethal targets [26].

### 2.6 EZH2: an epigenetic gene suppressor

### 2.6.1 Physiological function of EZH2

Enhancer of zeste homolog 2 (EZH2) is a subunit of the Polycomb repressive complex 2 (PRC2), which is physiologically expressed in dividing cells and has a histone methylase activity by trimethylation of lysine tail 27 on histone 3 (H3K27me$^3$) [82]. This methylation leads to transcriptional suppression of various genes and thus participates in shaping cell-fate determination [83]. EZH2 plays a crucial role during early embryogenesis. The consequences of mutations in Polycomb group (PcG) proteins vary from embryonic lethality to severe phenotypes in flies and mice [15,84]. One of the most studied targets of PcG proteins is the family

of *HOX* genes, which encode several transcription factors that are essential for specific segment identity of the anterior-posterior body axis [85]. During embryogenesis, EZH2-mediated methylation patterns are considered to be essential for the maintenance of the body plan [85]. Stem and progenitor cells exhibit high levels of EZH2 [86], which stresses the role of EZH2 in maintaining pluripotency and stem cell self-renewal [85]. In murine embryonic stem cells, *Prc2*-knockout failed to show gene expression changes, assuming that EZH2-mediated epigenetic suppression is crucial for preserving cell identity but not determining it [16]. PRC2-mediated silencing is thought to maintain the epigenetic profile rather than initiating suppression of certain genes [15].

### 2.6.2 Role in breast cancer

The role of EZH2 in cancer development is increasingly recognized. EZH2 has been associated with a variety of cancer entities like leukemia, kidney, lung, ovary, prostate, and breast cancer [15]. Based on its complex role in epigenetic gene silencing, EZH2 has been associated with both oncogenic and tumor suppressive signaling. However, to date there is no clear mechanistical understanding of the distinct role of EZH2-mediated tumorigenesis [15]. In that matter, Cometa et al. suggest its role to be rather "context - dependent" [15]. Numerous studies have described a positive correlation between EZH2 overexpression and tumor aggressiveness, most notably in prostate and breast cancer [87-89].

EZH2 overexpression has been linked to an increased formation of metastasis as Cao et al. observed a correlation between low levels of EZH2 and metastasis-free survival [90]. Furthermore, in breast cancer tissue increased EZH2 activity has been linked to reduced levels of E-Cadherin, an essential protein for cell-to-cell adhesion and thus an inhibitor for cell migration and cancer invasion [90]. In line with that, H3K27me$^3$ levels are associated with EMT related gene expression in breast cancer cells *in vitro* and *in vivo* [91]. EZH2 is also strongly associated with high rates of tumor proliferation as it is involved in cell cycle regulation and DDR [15]. H3K27me$^3$ modification leads to transcriptional repression of important tumor suppressors like *CDKN2A*, resulting in uncontrolled DNA replication due to loss of G1-arrest and thus promoting tumorigenesis [92]. The role of EZH2 in DDR signaling is controversial. Concerning DDR, there are different studies either supporting EZH2 as a promotor of DDR [93] or as an inhibitor of such [48], again suggesting that EZH2 has a context-dependent function. Chang et al*.* observed that high levels of EZH2 in breast tumor initiating cells lead to suppression of *Rad51* and consequently impaired DDR, increased genomic instability, as well as aberrant RAF1-ERK-ß-catenin signaling *in vitro* and *in vivo* [48]. Increased ß-catenin induces self-renewal and expansion of breast tumor initiating cells, as well as radiation resistance [48]. In contrast to that, others report an enhanced DDR upon EZH2 activation [93,94]. Upon DNA

damage, direct binding of BRCA1 to EZH2 is abrogated and its inhibition on EZH2 activity is released, leading to the assumption that EZH2 might transcriptionally repress crucial genes at sites of DNA damage to promote DDR [93]. In accordance with that, others have described an accumulation of PRC2 proteins at sites of DSBs and a decrease in DSB repair upon *EZH2*-deficiency [94].
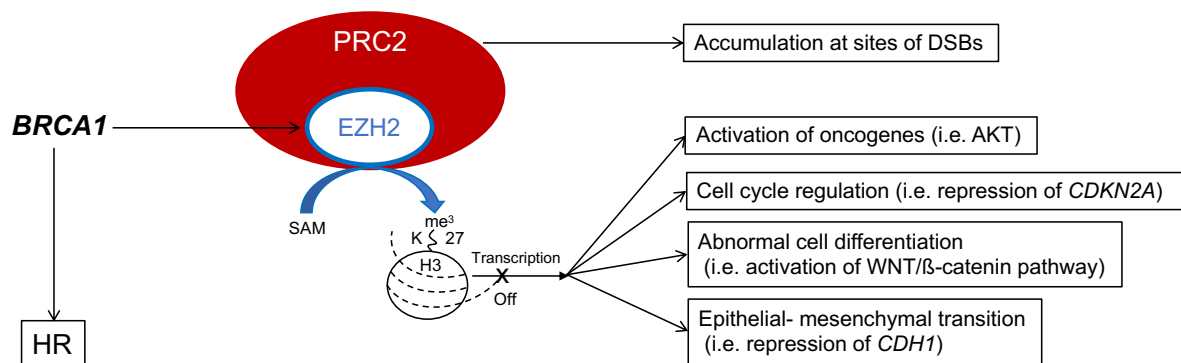


**Figure 1. Involvement of EZH2 in oncogenic signaling.**

EZH2 is part of the PRC2 protein complex and acts through trimethylating Histone 3 (H3) on lysine tail K27 (H3K27me$^3$), which consequently impacts a variety of pathways involved in tumorigenesis [95]. By repressing expression of certain genes, oncogenic signaling is promoted. Further, EZH2 specifically impacts cell cycle regulation, abnormal cell differentiation and metastasis formation [48,90,91,93,96]. Besides that, EZH2 activity is enhanced by BRCA1 upon DNA damage [93] and proteins of the PRC2 tend to accumulate at sites of DSBs [94]. EZH2 = Enhancer of zeste homolog 2; PRC2 = Polycomb repressive complex 2; HR = Homologues recombination; SAM = *S*-adenosyl-L-methionine

EZH2 promotes breast cancer progression by impacting a variety of oncogenic pathways such as EMT, cell differentiation, cell cycle regulation and DDR (fig. 1) [48,90,91,93]. In general, EZH2 overexpression in breast cancer can be considered as a prognostic marker for aggressive, undifferentiated cancers with poor prognosis and a high tendency for metastasis [65].

### 2.6.3   EZH2 as a promising target for treating *BRCA1*-deficient breast cancer

Concerning molecular subtypes of breast cancer, numerous studies describe a negative correlation of EZH2 levels and ER expression [97-99]. Our group previously revealed an association between high EZH2 levels and *BRCAness* [65]. Microarray analyses of *Brca1*-deficient murine mammary tumors show significantly higher EZH2 levels than *Brca1*-proficient tumors do (fig. 2) [65]. Increased EZH2 levels in *BRCA1*-mutant tumors are also evident from IHC data of human TNBCs (fig. 2) and this observation could be confirmed in various human breast cancer cohorts [65]. Interestingly, a subset of different human TNBCs exhibit significantly higher *EZH2* mRNA expression levels among tumors harboring either a *BRCA1* mutation, *BRCA1* promoter methylation or tumors with a *BRCA1*-like DNA copy number variation profile (according to the *BRCA1*-like classifier [64]) than tumors with no *BRCA1* association [65].
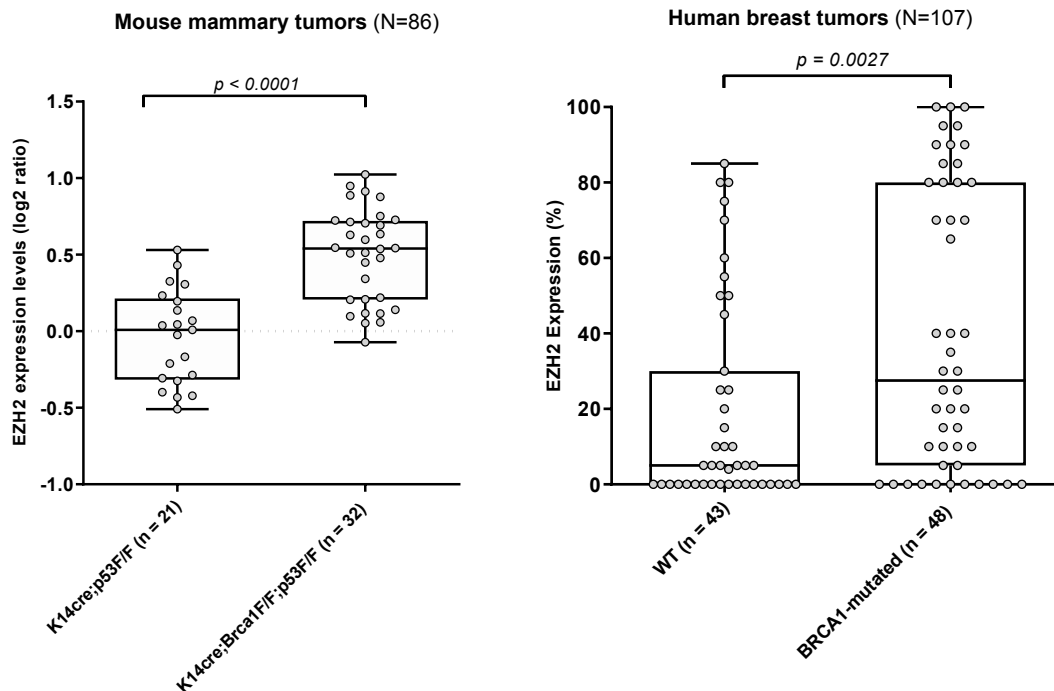
**Figure 2. EZH2 is overexpressed upon *BRCA1*-deficiency.**

EZH2 mRNA is significantly higher expressed in *Brca1*-deficient murine mammary tumors (micro array analysis). EZH2 protein levels are significantly higher expressed in *BRCA1*-deficient human mammary tumors (Immunohistochemistry). This figure was adapted with kind permission from Puppe et al. [65].

Having established a correlation between EZH2 and *BRCAness* [65], EZH2 gained our interest as a promising target in *BRCA1*-deficient tumors [70]. Puppe et al. previously described that an effective inhibition of EZH2 with the inhibitor 3-deazaneplanocin A (DNZep) resulted in increased cell death of *Brca1*-deficient in comparison to *Brca1*-proficient murine breast cancer cells [100]. A variety of selective small molecular compounds are available for competitive inhibition of the methyltransferase activity of EZH2 by targeting *S*-adenosyl-L-methionine (SAM). Several studies have investigated a potent anti-tumor effect of GSK126 in breast cancer cell lines *in vitro* [101,102] and similar effects have also been observed with a more recently developed inhibitor ZLD1039 [95]. GSK126 has recently shown good *in vivo* anti-tumor activity for different lymphoma entities [82,103-105]. Furthermore, our group could previously show good *in vivo* tolerability of GSK126 for the *Brca1*-deficient breast cancer murine model (*K14Cre;Brca1^{fl/fl};Tp53^{fl/fl}*) [65]. In that context, we found *Brca1*-deficient breast cancer cells to be more sensitive to EZH2 inhibition. However, GSK126 as single agent did not show significant anti-tumor activity *in vivo* [65]. The compound tazemetostat (EZH2i) is currently under investigation in many clinical phases I and II trials for various cancer entities as well as in a clinical phase III trial for advanced sarcoma (ClinicalTrials.gov identifier NCT04204941) [106]. EZH2 is a potential novel druggable target for *BRCA1*-deficient breast cancer (fig. 2) [65].

However, as it is involved in many pathways concerning genome integrity (cell cycle regulation, cell proliferation, DDR) [15], its anti-tumor activity might be enhanced in combination with other compounds targeting certain properties of *BRCA1*-deficient cancer according to the concept of synthetic lethality. Combination therapies with EZH2 inhibition could exploit *BRCA1*-deficiency in breast cancer and should therefore be investigated [70].

## 2.7   Aims of this study

We want to test if EZH2 inhibition is a sensitizer to other synthetic lethal partners in *BRCA1*-deficient breast cancer cells. This study aims to investigate the effect of dual inhibition of EZH2 in combination with the inhibition of signaling pathways involved in genome integrity. We want to identify synthetic lethal partners of EZH2 in *BRCA1*-deficient breast cancer. Compounds which are being evaluated in late preclinical states or that have previously been evaluated in clinical trials will be used for this analysis. A large-scale cell line-based screen will be performed to detect synergistic interactions between EZH2 inhibition and different pharmacological modulators of the DNA damage response (including PARP1, ATM, ATR, CHK1/2) as well as inhibitors of cell cycle regulation (including CDK, PI3K/AKT) in *Brca1*-deficient and *Brca1*-proficient triple negative breast cancer cells [70]. The most promising hits will be validated by different functional assays *in vitro*. In the following the anti-tumor effect of the potential drug combinations will be evaluated by *in vivo* experiments in a *Brca1*-deficient murine model.

Research aim**:**
To evaluate novel synergistic drug combinations with EZH2 inhibition in *BRCA1*-deficient breast tumors.

Study objectives:
i.   Identification of potential synergistic partners in combination with EZH2i for *Brca1*-deficient breast cancer
ii.   Growth inhibition analyses of combination treatments *in vitro*
iii.   Pharmacological validation of synergistic drug combinations
iv.   Genomic validation of EZH2 inhibition with synergistic drug combinations
v.   Effect of combination therapy on DNA damaging pathways
vi.   Validation of combination treatments *in vivo*

# 3   MATERIAL AND METHODS

## 3.1   MATERIAL

### 3.1.1   Supplies

| Name | Company | Catalogue Number |
|---|---|---|
| 96-well microplate, µCLEAR® | Greiner Bio | 655097 |
| Corning® 384-well microplate, white polystyrene | Corning | 3570 |
| Corning® 384-well Flat Clear Bottom Black | Corning | 3764 |
| Mini Trans-Blot® Cell | BioRad | 1703930 |
| Polyvinylidenfluorid-Membran (PVDF) | Merck Millipore | IPFL00010 |

### 3.1.2   Pharmacological Inhibitors

| Compound | Target | Company | Catalogue Number |
|---|---|---|---|
| Alpelisib | PI3K | Selleckchem | S2814 |
| AZD1390 | ATM | Selleckchem | S8680 |
| AZD7762 | CHK1/2 | Selleckchem | S1532 |
| BI2536 | PLK1 | Selleckchem | S1109 |
| BKM120 | PI3K | Selleckchem | S2247 |
| Crizotinib | ROS1 | Selleckchem | S1068 |
| Dinaciclib | Pan-CDK | Selleckchem | S2768 |
| Gefitinib | EGFR | Selleckchem | S1025 |
| GSK126 | EZH2 | Selleckchem | S7061 |
| JQ1 | BET | Selleckchem | S7110 |
| KU60019 | ATM | Selleckchem | S1570 |
| KU60648 | DNA-PK | Selleckchem | S8045 |
| LDC67 | CDK9 | Selleckchem | S7461 |
| MK1775 | Wee1 | Selleckchem | S1525 |

| NSC663284 | Cdc25 | Cayman Chemical | 383907-43-5 |
|-----------|-------|-----------------|-------------|
| Olaparib | PARP | Selleckchem | S1060 |
| Palbociclib | CDK4/6 | Selleckchem | S1579 |
| Panobinostat | HDAC | Selleckchem | S1030 |
| PF3644022 | MK2 | ApexBio | B5549 |
| PF477736 | CHK1 | Selleckchem | S2904 |
| purvalanol A | CDK1/2 | Selleckchem | S7793 |
| RO3306 | CDK1 | Selleckchem | S7747 |
| Selisitat | SIRT1 | Selleckchem | S1541 |
| selumetinib | MEK | Selleckchem | S1008 |
| senexin A | CDK8/19 | Selleckchem | S8520 |
| TH287 | MTH1/NUDT1 | Selleckchem | S7631 |
| THZ1 | CDK7 | Selleckchem | S7549 |
| VE822 | ATR | Selleckchem | S7102 |
| venetoclax | BCL2 | Selleckchem | S8048 |
| ZLD1039 | EZH2 | Aobious | AOB9716 |

### 3.1.3 Antibodies (WB and IF)

| Antibody | Catalogue Number | Kilo Dalton | Company | Host | Dilution |
|----------|------------------|-------------|---------|------|----------|
| 53BP1 | NB100-304 | 214 | Novusbio | Rabbit | 1:500 |
| AKT | 2920 | 60 | Cell signaling | Mouse | 1:2000 |
| Alexa Fluor 488 anti-mouse | A11001 | - | Life technologies | goat | 1:1000 |
| Alexa Fluor 647 anti rabbit | A21244 | - | Life technologies | goat | 1:1000 |
| ATM | 2873 | 350 | Cell signaling | rabbit | 1:1000 |
| CDK1 | 610037 | 34 | BD | mouse | 1:1250 |
| EZH2 | 612667 | 91 | BD | Mouse | 1:1000 |
| GAPDH | 2118 | 37 | Cell singaling | Rabbit | 1:1000 |
| H3 | 3638 | 17 | Cell signaling | Mouse | 1:2000 |
| H3K27Me$^3$ | 07-449 | 17 | MERCK | Rabbit | 1:500-1:1000 |
| H3K27me3 | CS 9733 | 17 | CST | rabbit | 1:1000 |

| HSP90 | 610418 | 90 | BD | mouse | 1:2000 |
|---|---|---|---|---|---|
| Kap | GTX102226 | 89 | Gene-Tex | rabbit | 1:1000 |
| p-AKT (Ser 473) | 4060S | 60 | Cell signaling | Rabbit | 1:2000 |
| p-ATM | AF1655 | 350 | RD-Systems | Rabbit | 1:250 |
| p-Kap (Ser824) | A300-767A | 100 | Biomol/Bethyl | Rabbit | 1:1000 |
| PI3K 110 alpha | Sc-293172 | 110 | Santa Cruz | rabbit | |
| yH2AX | 05-636 | 17 | Millipore | Mouse | 1:500 |

### 3.1.4 Other applied chemicals

| Substance | Company | Catalogue Number |
|---|---|---|
| 4′,6′-diamidino-2-phenylindole (DAPI) | Sigma | 10236276001 |
| Acrylamid-, Bisacrylamid-Stammlösung (Rotiphorese® Gel 30) | Carl Roth | 3029.2 |
| Amersham ECL Prime Western Blotting Detection Reagent | GE Healthcare | RPN2236 |
| Ammoniumpersulfat (APS) | Carl Roth | 9592.2 |
| BCA Protein Assay Kit (Pierce™) | ThermoFisher | 23225 |
| beta-Mercaptoethanol | Sigma-Aldrich | 6250 |
| Bromphenolblau | Carl Roth | T116.1 |
| CellTiter-Glo ® Luminescent cell viability assay | Promega | G7573 |
| cOmplete™ Mini Protease Inhibitor Cocktail | Sigma-Aldrich | 693124001 |
| Coomassie Plus™ (Bradford) Assay Kit | Thermo Scientific | 23236 |
| Dimethylsulfoxid (DMSO) | Carl Roth | A994.2 |
| Doxycycline | Sigma-Aldrich | D9891 |
| Dulbecco's Phosphate-Buffered Saline (PBS) | Life Technologies | 14190-169 |
| Goat serum | Sigma-Aldrich | G9023 |
| Kristallviolett | Sigma-Aldrich | HT90132 |
| N,N,N',N'-Tetramethylethylendiamin (TEMED) | Carl Roth | 2367.3 |
| PageRuler Plus Prestained Protein Ladder | LifeTechnologies | 26620 |

| | | |
|---|---|---|
| Paraformaldehyd (PFA) | Sigma-Aldrich | 158127 |
| PhosStop easy pack | Roche Diagnostics | 4906845001 |
| Bovine serum albumin  (BSA) | Sigma-Aldrich | A7906 |
| TritonX 100 | Carl Roth | 3051.3 |
| Tween20 | Sigma-Aldrich | P9416 |

### 3.1.5   Buffer and Solutions

| Name | Composition | Use |
|---|---|---|
| 6 x Laemmli buffer | 12% SDS, 0,06% Bromphenol blue, 47% Glycerol, 0,06 M Tris [pH 6,8], 2% ß-Mercaptoethanol, 0,6 M DTT | SDS-PAGE |
| Blockingsolution | 5% BSA, 2% normale Goat serum (Sigma-Aldrich), 0.01% Triton-X 100 | Immunofluorescence |
| Crystal violet solution | 0.5% Crystal violet, 25% Methanol | Colony formation assay |
| Lysis-Buffer (RIPA) | 50 mM Tris–HCl pH 7.5, 100 mM NaCl, 0.1% SDS, 0.5% Sodium deoxycholate | Protein lysis |
| Seperating Gel | 0.35 M Tris [pH 8.8], 0.1% SDS, 5-15% Acrylamid stock solution, 0.05% TEMED, 0.05% APS | SDS-PAGE |
| Stacking Gel | 0.125 M Tris [pH 6.8], 0.1% SDS, 4% Acrylamid stock solution, 0.1% TEMED, 0.07% APS | SDS-PAGE |
| TBST | 140 mM NaCl, 30 mM Tris [pH 7,5], 0,1% Tween 20 (TBST) | SDS-PAGE |

| | | |
|---|---|---|
| Transfer-buffer | 24 mM Tris, 70 mM Glycin, 20% Ethanol | SDS-PAGE |

### 3.1.6 Hardware

| Name | Company | Use |
|---|---|---|
| Axiovert mit Illuminator HXP 200C | Carl Zeiss | Microscope with camera |
| ChemiDoc XRS+, Image Lab | BioRad | Western Blot Gel analysis |
| Countess II FL Automated Cell Counter | Invitrogen | Cell counter |
| IncuCyte FLR | Essen Bioscience | Life cell imaging |
| Stemi™ 2000C Stereo microscope with AxioCam CC1 | Carl Zeiss | Microscope with camera |
| TECAN D300e digital dispenser | Tecan | Liquid dispenser |
| Tecan Infinite M1000 Pro | Tecan | Microplate reader |

### 3.1.7 Cell culture

| Name | Company | Catalogue Number |
|---|---|---|
| Cholera toxine | Sigma-Aldrich | C8052 |
| DPBS | Gibco | 14190-094 |
| Dulbecco's Modified Eagle Medium (DMEM/F12) | Gibco | 11320033 |
| EGF (epidermal growth factor) | Invitrogen | 53003-018 |
| Fetal Bovine Serum | Life Technologies | 10270106 |
| Insulin | Sigma Aldrich | 16634 |
| Penicillin Streptomycin | Life Technologies | 15070-063 |
| RPMI Medium 1640 | Gibco | 11554516 |
| Trypsin | Gibco | 25200056 |

## 3.2 METHODS

### 3.2.1 Cell lines and culturing

Murine cell lines:

Cell lines were derived from tumors arising in a conditional knockout murine model mimicking *Brca1*-mutant breast cancer [69]. By making use of Cre-loxP technology, conditional knockout of *Brca1* and *Tp53* were targeted to CK14 expressing epithelial cells, specific for mammary tissue. Cell lines with *Brca1^{fl/fl};Tp53^{fl/fl}* were named KB1P and accordingly cell lines with *Brca1^{wt/wt};Tp53^{fl/fl}* were named KP. Cell lines were derived as described by Silver et al. from individual spontaneous mammary tumors of the previously mentioned conditional knockout murine models [107]. Cell lines were cultured in DMEM-F12 medium, supplemented with 10% FBS, 50 U/ml penicillin, 50 mg/ml streptomycin, 5 mg/mL insulin, 5 ng/mL epidermal growth factor, and 5 ng/mL cholera toxin and incubated at 37 °C with 5% carbon dioxide under low oxygen conditions (3%) [65,70].

Human cell lines:

Following breast cancer cell lines derived from human tumor samples were used in this study: CAL120 (TNBC, *BRCA1^{wt/wt}*) and SUM149 (TNBC, *BRCA1^{fl/fl}*). Both cell lines were kindly provided by Jos Jonkers [70]. CAL120 cells were cultures in RPMI 1640 medium, substituted with 10% FBS, 50 U/ml penicillin and 50 mg/ml streptomycin. SUM149 cells were cultured in DMEM/F12 medium, substituted with 5% FBS, 50 U/ml penicillin, 50 mg/ml streptomycin, 1µg/ml hydrocortisone and 5µg/ml insulin. Using a PCR mycoplasma test kit (AppliChem, Cat#A3744), all cell lines were tested negative for mycoplasma contamination after thawing [70].

### 3.2.2 Growth analyses experiments

Colony formation assay:

25,000 cells per well were seeded in 6-well plates and 10,000 cells per well in 12-well plates. Cells were left to attach for one day and were then treated with compounds according to the experiment. Cells were treated with the according compounds for 7 days. For the fixation process cells were kept on ice. Medium was aspirated and wells were washed 2 times with 2 ml ice cold PBS. Next, 1 ml of ice-cold Methanol was put on the cells for 10 min. Then 1ml of Crystal violet solution was put in each well and left to incubate for 10 min. Finally, wells were washed 3 times with Milli-Q® and left to dry. For quantification of colonies, pictures with 0.54 magnifications were taken with the Stemi™ 2000C stereomicroscope (Carl Zeiss) and analyzed with the "*clono-counter*" [108]. Pictures for the figures were taken with 2.0 magnifications [70].

## Cell viability assay:

500 cells per well were seeded for the murine cell lines and 1000 cells per well for the human cell lines in 30μl medium with a multi-pipette in flat bottom white 384er-well plates to allow sub confluent growth over the time of the whole experiment. Cells were left to attach, and compounds were added the next day according to the protocol with the D300e Control software for each experiment by using the Tecan D300e Digital Dispenser. After 72 hours of incubation plates were taken out of the incubator for 20 minutes to reach room temperature. For the ATP Luminescent Cell Viability Assay 30 μl of 1:6 diluted CellTiter-Glo® Reagent (CTG) were added with a multi-pipette to a 386 well plate. Plates were allowed to equilibrate at room temperature for approximately 30 minutes. Afterwards plates were shaken, and luminescence was measured with the Tecan reader (Tecan Infinite M1000 Pro) [70].

## Calculation of half maximal inhibitory concentration ($ic_{50}$):

This experiment was carried out by Ratz et al. according to the description in the publication [70]. $IC_{50}$ values were calculated with CTG experiments. Drug concentrations were log-transformed, and the dose-response curve was plotted using GraphPad Prism (Version 8.0, Graphpad Software, Inc.). For further experiments, concentrations of the compounds were based around their $IC_{50}$ values. In a pre-screen, doses were titrated in the manner of two-fold dilutions to be then adjusted and optimized for the large-scale synergy screen. The displayed concentrations of compounds were chosen as they resulted in the highest levels of growth inhibition upon combination treatments in our murine breast cancer cell lines [70].

## Live-cell analysis:

To analyze cell growth over time the IncuCyte® was used. 500 cells per well were seeded of each cell lines in 50 μl medium per well in a black 384er-well plate with clear bottom. Cells were left to attach for one day in the incubator. Subsequently, compounds were by using the Tecan D300e Digital Dispenser and immediately put back into the Incucyte® incubator for hourly analysis of cell confluency up until 120h post treatment. Cell confluency was indicated as percentage (mean) of overgrown surface area of each well in triplicates. Proliferation was calculated from cell images with the IncuCyte software (Essen Bioscience) [70].

### 3.2.3   Cell-lysis and Western Blot experiments

Cell lysates were prepared in RIPA lysis buffer (RIPA buffer with 50 μl 20 % SDS/ml RIPA buffer and 1 mM PMSF). This was supplemented with phosphor-stop for validation of phosphor-sites in protein lysates with western blotting.  Bradford was performed with 5 μl of 1:10 diluted sample and 250 μl Coomassie and analyzed with 595 nm wavelength in the Tecan reader. Protein concentrations were calculated with protein standard curves. Samples were

diluted with Laemmli buffer 1:6, heated 5 min at 95 °C and then separated with SDS-PAGE in self-made polyacrylamide gels (percentage of gel according to the size of validated proteins 5 – 15 %). Gels were then blotted with a wet western blotting protocol in transfer buffer supplemented with 20 % Ethanol and transferred to a PVDF membrane for 16 hours at 4 °C. Next, the membrane was blocked in 10 ml of TBST with 5 % BSA for one hour at room temperature. Primary antibodies were also prepared in 5 % BSA in TBST and membranes were cut according to the size of proteins and incubated in the primary antibody for 16 hours at 4 °C. Membranes were then washed 3 times for 15 minutes in TBST and incubated in secondary – HRP antibody diluted 1:10.000 in 5 % BSA in TBST for one hour at room temperature. Membranes were washed again 3 times for 15 minutes in TBST and then developed with 1:1 ECL solution in the Bio-Rad reader with the ChemiDoc™ XRS+ Imager of the Image Lab™ software (Bio-Rad, Version 5.2.1). A list of used antibodies is attached. Quantitative analysis of the protein expression relative to GAPDH or HSP90 and to the according unphosphorylated sites, when phosphorylated proteins were analyzed, was calculated with Image Lab™ software [70].

### 3.2.4  Immunofluorescence

5000 cells per well in 100µl medium were plated in a clear bottom black 96-well plate. Cells were left to attach and treated with the drug printer and according to drug printer protocol the next day. After 48 h of incubation, cells were fixated with 100 µl of 8 % PFA to reach a concentration of 4 % PFA for 10 minutes. Wells were then washed 3 times with 100 µl of PBS. Next, wells were blocked with 100µl of blocking buffer for 1 hour at room temperature. The primary antibodies yH2AX and 53BP1 were diluted 1:500 in 1 % BSA in PBS and 50 µl were put in wells to incubate for 16 hours at 4 °C. After washing the wells 3 times with 100 µl of PBS, secondary antibodies Alexa Fluor 488 anti-mouse and Alexa Fluor 647 anti-rabbit (were diluted 1:1000 in PBS together with a 1:100 dilution of DAPI to incubated in 50 µl per well for one hour at room temperature in the dark.  Wells were washed again 3 times with 100 µl PBS and finally left with 200 µl PBS to be analyzed by Jörg Isensee as described by Ratz et al. and Erber et al. [33,70].

### 3.2.5  Doxycycline-inducible RNAi-mediated gene knockdown

Following cell lines were used: KB1P G3 sh-EZH2, KB1P G3 sh-random, KP 3.33 sh-EZH2 and KP 3.33 sh-random. Short hairpin cell lines were provided by Maarten van Lohuizen and Gaurav Pandey with a lentiviral single vector backbone of FH1tUTG with one cassette being a H1-TetO promoter-shRNA and a second cassette being a Ub-promoter-TetR-eGFP [109].

Doxycycline (Dox)-dependent shEZH2 knockdown was induced for 7 days. Dox was diluted to a concentration of 50 µg/ml. To reach a final concentration of 100 ng/ml, Dox was diluted 1:500 in 10 ml of medium. PBS was used as a control. The treatments were renewed every other day for 7 days. For a colony formation assay, cells were then seeded to a 12-well dish with 10.000 cells per well in 1 ml medium and left to attach for 24 hours. After renewing the medium with supplementary Dox compounds were added to the wells with the D300e Digital Dispenser (Tecan, Switzerland). Plates were incubated for 7 days after treatment and were then fixed and stained according to the protocol of the colony formation assay [70].

### 3.2.6 RNA sequencing

As reported by Ratz et al., first Illumina TruSeq mRNA libraries were developed and then sequenced with 50 to 65 base single reads on a HiSeq 2500 using v4 chemistry (Illumina Inc., San Diego) [70]. Then, in order to cut out all remaining adapter sequences, the arising reads were trimmed using Cutadapt (version 1.15). Furthermore, to ensure good mappability reads shorter than 20 bp following trimming were filtered. With the help of STAR (version 2.6.1a [110]) the trimmed reads were aligned to the GRCm38 reference genome. Using feautureCounts (version 1.5.0-p1 [111]), gene expression counts were generated with genome definitions from Ensembl GRCm38 version 76. DESeq median-of-ratios approach[112] was used to normalize expression values. This was done by adjusting differences in sequencing depth between samples. Statistical analyses were performed with ANOVA and pairwise t-test, corrected for multiple testing. The reported RNA sequencing data of this study can be found in the NCBI GEO database (GSE182448).

### 3.2.7 *In vivo* experiments

The in vivo experiments were carried out at the animal facility and mouse cancer clinic of the Netherlands Cancer Institute (NKI, Amsterdam, Netherlands) by our collaborating group (Jos Jonkers, Department of Molecular Pathology, NKI) and approved by the local ethic committee [70]. Cancer cells from a donor mouse (*K14Cre;Brca1^{fl/fl};Tp53^{fl/fl}*) were injected into mammary fatty pads of all mice provided for this experiment. Treatment was started once tumors reached the size of 100 mm$^3$. Tumor growth was measured every other day by caliper measurement and mice were sacrificed when tumor size was equal to or bigger than 1500 mm$^3$. Mice were treated with 150mg/kg bodyweight GSK126 daily (intraperitoneally) and twice 20mg/kg bodyweight AZD1390 daily (oral gavage).

### 3.2.8 Calculations of synergy

In order to decipher additive and synergistic effects, synergy scores can be calculated according to the *Bliss Independence Model*. Erber et al. describe the impact on the effect „a" of the interaction of two inhibitory compounds A and B, where the expected additive effect $a_{exp}$ was calculated according to *Bliss Independence* as followed: $a_{exp} = a^A + a^B - a^A * a^B$ [33]. If the delta ($\Delta$ a) of the observed effect $a_{obs}$ to $a_{exp}$ is greater than 10, the effect is described as synergistic in this study [70]. In accordance with that $\Delta$ a=0 displays an additive effect and $\Delta$ a<0 describes an antagonism of both drugs [33]. Synergies were depicted using the web-application tool "*SynergyFinder*" (version 2.0) [113].

# 4 RESULTS

## 4.1 Synergy screen identified three compounds that act synergistically in combinations with EZH2i especially in *Brca1*-deficient breast tumor cells: AZD1390 (ATMi), BKM120 (PI3Ki) and dinaciclib (panCDKi)

We could previously show that EZH2 overexpression is associated with a *BRCA*ness phenotype [65]. To further investigate this observation, we performed RNA-seq transcriptome analysis of tumors derived from our *Brca1*-deficient and *Brca1*-proficient murine model. Here, mammary tumors derived from *Brca1*-deficient mice exhibit higher levels of EZH2 compared to *Brca1*-proficient tumors (fig 3.A) [70]. Next, pharmacological inhibition of EZH2 with GSK126 shows that *Brca1*-deficient cell lines (KB1P) are significantly more sensitive to EZH2 inhibition than *Brca1*-proficient cell lines (KP) (fig. 3.C) [70]. Target inhibition analysis by western blotting confirmed that treatment with GSK126 reduced the histone methyltransferase activity of EZH2 by down-regulation of H3K27me$^3$ (fig. 3.B) [70].

We hypothesize that EZH2 inhibition (EZH2i) in combination with other compounds targeting genome integrity of *BRCA1*-deficient breast cancer cells could result in synthetic lethal interaction. Therefore, we performed a large-scale cell line-based drug synergy screen to identify synergistic drug combinations [70]. To study the dependency on homologous recombination deficiency, we made use of two cell lines (KB1P G3 and KB1P B11) derived from mammary tumors of a *K14Cre;Brca1$^{fl/fl}$;Tp53$^{fl/fl}$* mice and two cell lines (KP 3.33 and KP 6.3) derived from mammary tumors of *K14Cre;Brca1$^{wt/wt}$;Tp53$^{fl/fl}$* mice [69,107].

In this synergy screen, we used the EZH2 inhibitor GSK126 as a backbone and combined it with various compounds involved in cell cycle inhibition, DNA damage signaling and other inhibitors, which were already tested in early phase clinical trials [70]. As the prospect of this study is the identification of combination therapies for *BRCA1*-deficient breast tumors, we aimed to take a closer look at compounds with high synergy scores in *Brca1*-deficient cell lines and low scores in *Brca1*-proficient cell lines. To assess which combination treatments were valuable for further validation, the difference between the synergy scores of pooled *Brca1*-deficient and *Brca1*-proficient cell lines were calculated as delta (Δ) and depicted by rising delta values (fig. 3.D) [70]. We observed that inhibitors of the ATM /ATR axis (AZD1390, KU60019, PF-477736, VE822), CDK-Inhibitors (purvalanol A and dinaciclib) and the PARP inhibitor olaparib as well as an inhibitor of the PI3K/AKT pathway (BKM120) were under the top hits [70].

In previous studies, others and we could already reveal synergy of GSK126 and olaparib, indicating that this screen was reliable to detect synergistic effects [114,115]. We picked three compounds to further evaluate in combination with GSK126 in this study as followed: AZD1390 to represent ATM mediated DDR-pathway [70], BKM120 to represent proliferative signaling via PI3K/AKT pathway and dinaciclib as inhibitor of CDKs (fig. 3.E, F, G).

**EZH2i and ATMi drug combination:**

AZD1390 (ATMi) shows the highest synergy with a Bliss synergy score of 26.56% in KB1P cell lines and -1.86% in KP cell lines (Δ: 28,42) when combined with EZH2i (fig. 3.E) [70]. Other compounds of the DNA damage response pathway including the ATM/CHK2 and ATR/CHK1 axis also scored high: KU60019 (ATMi), VE822 (CHK1i) and PF477736 (ATRi) (fig. 3.D) [70]. To confirm on-target efficiency of the ATMi AZD1390 we analyzed a common downstream target of ATM (phosphorylated Kap1) by western blotting. Treatment of KB1P cells with AZD1390 (2 µM) led to a down-regulation of phosphorylated Kap1 protein levels (fig. 3.E) [70]. Moreover, AZD1390 monotherapy was more effective in *Brca1*-deficient breast cancer cell lines (KB1P G3 IC$_{50}$: 6,66µM vs. KP IC$_{50}$: 26,90 µM), indicating that *Brca1*-deficient tumors are sensitive to monotherapy with ATM inhibitors (fig. 3.E) [70].
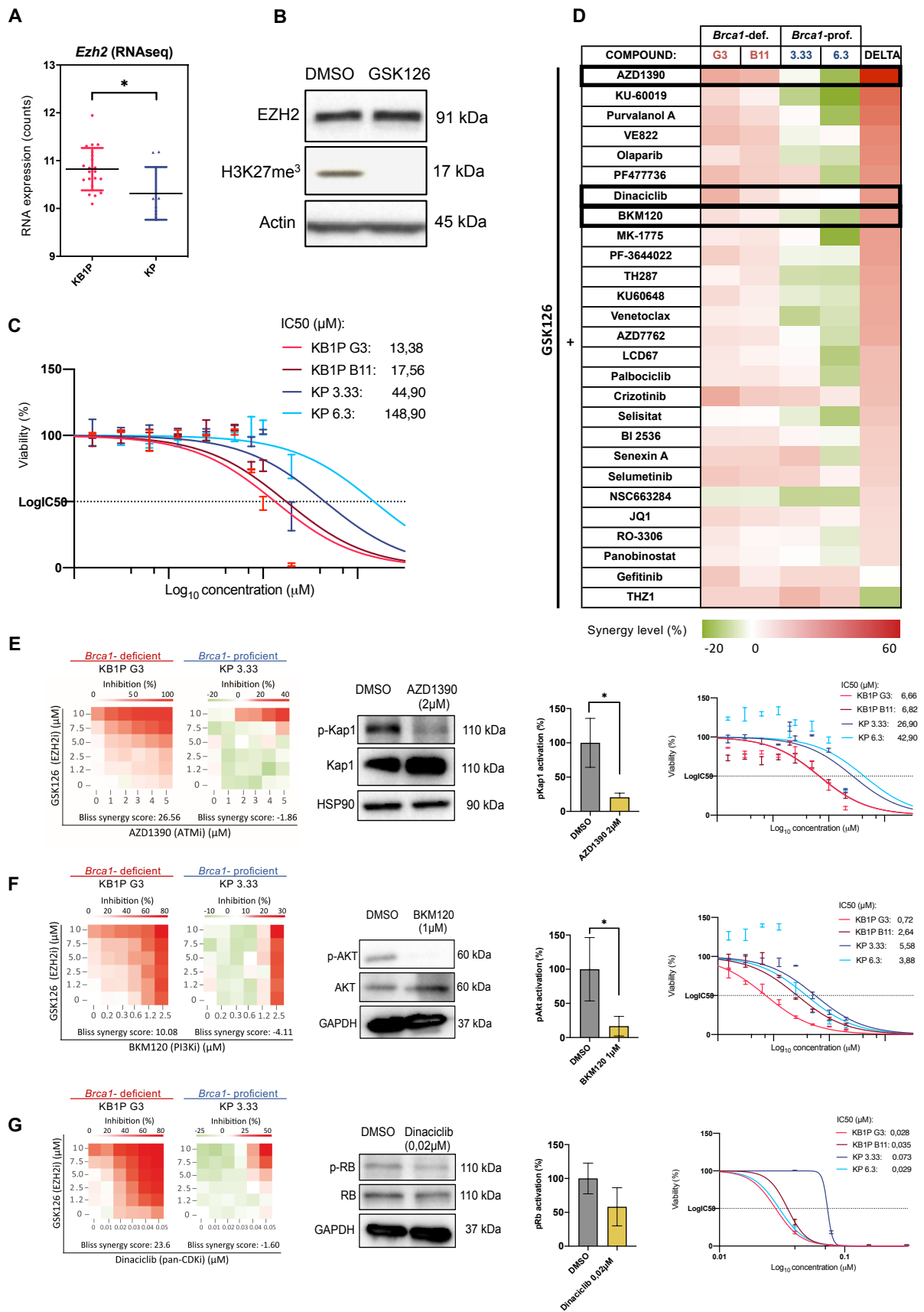
**EZH2i and PI3Ki drug combination:**

Combination therapy of GSK126 and BKM120 (PI3Ki) also scored well upon *Brca1*- deficiency (fig. 3.D) [70]. Drug target efficacy of BKM120 was demonstrated by a down-regulation of phosphorylated AKT on a protein level (fig. 3.F). IC$_{50}$ studies with BKM120 show a higher sensitivity of KB1P cell lines to the PI3Ki BKM120 compared to KP cell lines (fig. 3.F). These experiments are based on Ratz et al. [70].

**EZH2i and CDKi drug combination:**

In addition, two inhibitors of cyclin-depending kinases (CDKs), dinaciclib (panCDKi, especially CDK1/2/5/9), as well as purvalanol (CDK1i) were among the compounds with highest scores in *Brca1*-deficient cell lines (fig. 3.D) [70]. We could confirm by western blot analyses that dinaciclib showed target efficacy by down-regulation of pRB (fig. 3.G). However, no difference between *Brca1*-deficient and -proficient cells could be observed after dinaciclib treatment (fig. 3.G). These experiments are based on Ratz et al. [70].

**A**

Ezh2 (RNAseq)

**B**

| | DMSO | GSK126 | |
|---|---|---|---|
| EZH2 | | | 91 kDa |
| H3K27me³ | | | 17 kDa |
| Actin | | | 45 kDa |

**C**

IC50 (µM):
KB1P G3: 13,38
KB1P B11: 17,56
KP 3.33: 44,90
KP 6.3: 148,90

**D**

| COMPOUND: | Brca1-def. | | Brca1-prof. | | DELTA |
|---|---|---|---|---|---|
| | G3 | B11 | 3.33 | 6.3 | |
| AZD1390 | | | | | |
| KU-60019 | | | | | |
| Purvalanol A | | | | | |
| VE822 | | | | | |
| Olaparib | | | | | |
| PF477736 | | | | | |
| Dinaciclib | | | | | |
| BKM120 | | | | | |
| MK-1775 | | | | | |
| PF-3644022 | | | | | |
| TH287 | | | | | |
| KU60648 | | | | | |
| Venetoclax | | | | | |
| AZD7762 | | | | | |
| LCD67 | | | | | |
| Palbociclib | | | | | |
| Crizotinib | | | | | |
| Selisitat | | | | | |
| BI 2536 | | | | | |
| Senexin A | | | | | |
| Selumetinib | | | | | |
| NSC663284 | | | | | |
| JQ1 | | | | | |
| RO-3306 | | | | | |
| Panobinostat | | | | | |
| Gefitinib | | | | | |
| THZ1 | | | | | |

GSK126 +

Synergy level (%)
-20   0   60

**E**

Brca1-deficient KB1P G3 / Brca1-proficient KP 3.33

Bliss synergy score: 26.56 / Bliss synergy score: -1.86

| | DMSO | AZD1390 (2µM) | |
|---|---|---|---|
| p-Kap1 | | | 110 kDa |
| Kap1 | | | 110 kDa |
| HSP90 | | | 90 kDa |

pKap1 activation (%)

IC50 (µM):
KB1P G3: 6,66
KB1P B11: 6,82
KP 3.33: 26,90
KP 6.3: 42,90

**F**

A   Brca1-deficient KB1P G3 / Brca1-proficient KP 3.33

Bliss synergy score: 10.08 / Bliss synergy score: -4.11

Brca1-deficient KB1P G3 / Brca1-proficient KP 3.33

Bliss synergy score: 23.6 / Bliss synergy score: -1.60

B   KB1P G3   KB1P B11

| | DMSO | BKM120 (1µM) | |
|---|---|---|---|
| p-AKT | | | 60 kDa |
| AKT | | | 60 kDa |
| GAPDH | | | 37 kDa |

C   KB1P G3   KB1P B11

IC50 (µM):
KB1P G3: 0,72
KB1P B11: 2,64
KP 3.33: 5,58
KP 6.3: 3,88

**G**

Brca1-deficient KB1P G3 / Brca1-proficient KP 3.33

Bliss synergy score: 23.6 / Bliss synergy score: -1.60

KP 3.33   KP 6.3

| | DMSO | Dinaciclib (0.02µM) | |
|---|---|---|---|
| p-RB | | | 110 kDa |
| RB | | | 110 kDa |
| GAPDH | | | 37 kDa |

pRb activation (%)

IC50 (µM):
KB1P G3: 0,028
KB1P B11: 0,035
KP 3.33: 0,073
KP 6.3: 0,029

**D**   KB1P G3   KB1P B11

**E**   KB1P G3   KB1P B11

KP 3.33   KP 6.3

DMSO
GSK126
Dinaciclib
GSK126 + Dinaciclib

KP 3.33   KP 6.3

DMSO
GSK126
BKM120
GSK126 + BKM120

Fig and AZD1390 (ATMi),
BK

40

**(A)** RNA expression of Ezh2 in murine mammary tumor cells derived from the primary tumor of *Brca1*-deficient (KB1P) and *Brca1*-proficient (KP) mice was determined with RNA-seq. This experiment was conducted and analyzed by L. Ratz.**(B)** Intracellular protein levels of H3K27me$^3$ and EZH2 were determined by western blot upon GSK126 (5μM) treatment and DMSO (0,1%) as control treatment. One representative image out of 3 is displayed. This experiment was conducted by J.Puppe and L. Bartke. **(C)** IC$_{50}$ values of GSK126 were determined by analysis of the viability in CTG experiments. Two *Brca1*-deficient (KB1P G3 and KB1P B11) and two *Brca1*-proficient (KP3.33 and KP6.3) murine mammary tumor cell lines were treated. This experiment was conducted and analyzed by J. Puppe, L. Ratz and L. Bartke. **(D)** Cell line-based drug synergy screen was performed with GSK126 as a backbone in combination with various compounds in two *Brca1*-deficient (KB1P G3 and KB1P B11) and two *Brca1*-proficient (KP3.33 and KP6.3) cell lines with CTG experiments. The synergy is displayed by color: Green color indicates negative synergy score; red color indicates high synergy score. Delta values were calculated between pooled *Brca1*-proficient and pooled *Brca1*-deficient cell lines. This experiment was conducted and analyzed by J. Puppe, L. Ratz and L. Bartke. **(E)** Synergy matrices are derived from the *"Synergy finder"*. Protein levels of p-Kap1 and Kap1 were determined in KB1P G3 cells by western blot upon treatment with AZD1390. One representative image out of 3 is displayed. Western blot-based activation of p-Kap1 activity upon AZD1390 treatment is quantified. IC$_{50}$ values of AZD1390 were determined by analysis of the cell viability in CTG experiments. Two *Brca1*-deficient (KB1P G3 and KB1P B11) and two *Brca1*-proficient (KP3.33 and KP6.3) murine mammary tumor cell lines were treated. **(F)** Synergy matrices were analyzed with *"Synergy finder"*. Protein levels of p-AKT and AKT were determined in KB1P G3 cells by western blot upon treatment with BKM120. One representative image out of 3 is displayed. Western blot-based activation of p-AKT activity upon BKM120 treatment is quantified. IC$_{50}$ values of BKM120 were determined by analysis of cell viability in CTG experiments. **(G)** Synergy matrices were analyzed with *"Synergy finder"*. Protein levels of p-RB and RB were determined in KB1P G3 cells by western blot upon treatment with dinaciclib. One representative image out of 3 is displayed. Western blot-based activation of p-RB activity upon dinaciclib treatment is quantified. IC$_{50}$ values of dinaciclib were determined by analysis of cell viability in CTG experiments. These western blot experiments were conducted and analyzed by L. Bartke.  This figure is adapted and contains data from Ratz et al. [70] with kind permission.

If not otherwise specified, shown experiments exhibit values from at least three independent experiments.

Statistical analysis was done using the Student's t-test (ns= not significant; *, p<0,0332; **, p<0,0021; ***, p<0,0002; ****, p<0,0001) with GraphPad Prism (Version 8.0, Graphpad Software, Inc.).

## 4.2   Growth inhibition analyses confirm synergy of combined EZH2i and ATMi in *Brca1*-deficient but not *Brca1*-proficient breast tumor cells.

To validate synergistic growth inhibition of combination treatments, we analyzed each combination treatment for KB1P (*Brca1*-deficient) and as a control for KP (*Brca1*-proficient) cell lines with following assays: CellTiter-Glo® (CTG) assay, Life cell imaging (Incucyte®) and Colony Formation Assay (CFA). All of these experiments contain data from Ratz et al. for the EZH2i/ATMi combination and are based on Ratz et al. for the EZH2i/PI3Ki and EZH2i/CDKi combinations [70].
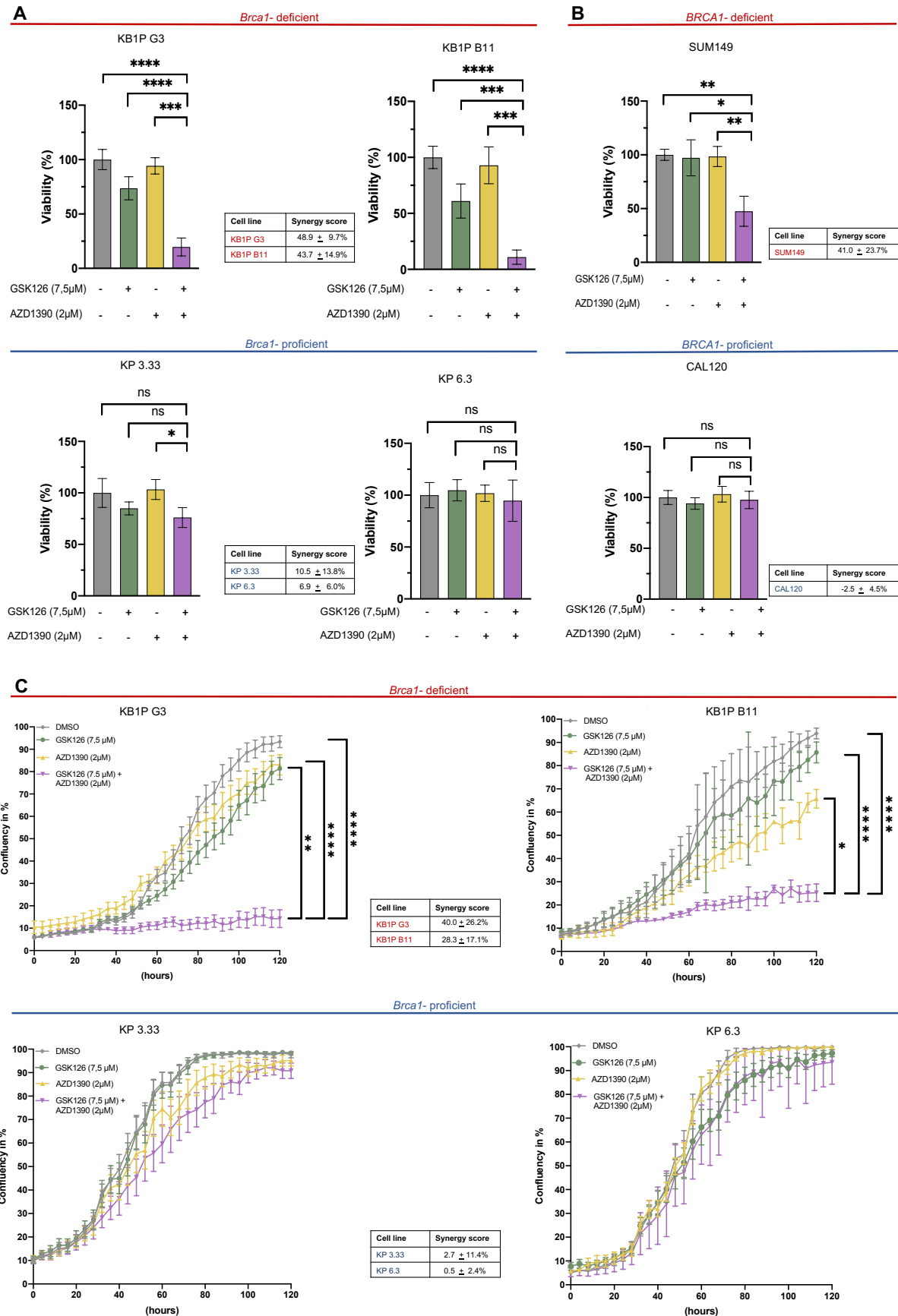
**Combination treatment of EZH2i and ATMi leads to synergistic growth inhibition in *Brca1*-deficient breast tumor cell lines.**

Cell viability in KB1P cell lines was significantly lower when treated with combination therapy of GSK126 (EZH2i) and AZD1390 (ATMi) than in vehicle control, as well as single agent treatments. Here, combination treatment led to about 80 % growth inhibition upon *Brca1*-

deficiency (fig. 4.A). In contrast to that, no effect of combination therapy could be observed for *Brca1*-profient cell lines (KP). Synergy scores for combination treatment were higher in KB1P cell lines (KB1P G3: 48.9 %; SD +/- 9.7 % and KB1P B11: 43.7 % SD +/- 14.9 %) compared to KP cell lines (KP 3.33: 10.5 %; SD +/- 13.8 % and KP 6.3: 6.9 %; SD +/- 6.0 %) (fig. 4.A). Therefore, combination treatment of GSK126 and AZD1390 could be considered as synergistic for *Brca1*-deficient cell lines [70]. Furthermore, we investigated the effect of this drug combination after long-term treatment. Life Cell Imaging with the Incucyte® system for 5 days (fig. 4.C) and cell colony formation (CFA) experiments for 7 days (fig. 4.D) were conducted [70]. Both methods also demonstrated a substantial growth inhibition upon combination therapy solely in *Brca1*-deficient cell lines, confirming the results of the previous cell viability experiments [70]. Here, data from the Incucyte® experiments showed synergy scores of up to 40% (SD +/- 26.2 %) (fig. 4.C) and 43.8 % (SD +/- 8.7 %) in CFA study (fig. 4.D) for KB1P cell lines, which therefore can be considered as synergistic.

Next, we wanted to validate the synergistic effect of GSK126 and AZD1390 in the human setting and used cell lines derived from human mammary tumors (fig. 4.B) [70]. CTG assays of SUM149 (TNBC, *BRCA1*-mutant) showed comparable results to CTG assays of *Brca1*-deficient murine cell lines with a significant growth inhibition upon combination therapy [70]. CAL120 (TNBC, *BRCA1*-wild type) cells did not exhibit significant growth inhibition when treated with GSK126 and AZD1390. Combination of EZH2i/ATMi can be considered as synergistic in *BRCA1*-mutant human breast cancer cell lines with synergy score of 41.0 % (SD +/- 23.7 %), whereas synergy scores of -2.5 % (SD +/- 4.5 %) indicate no synergy in the *BRCA1*-wildtype human breast cancer cells (fig. 4.B).

**Figure 4.** Growth inhibition analyses confirm synergy of combination with EZH2i and ATMi in *Brca1*-deficient cell lines.

**D**
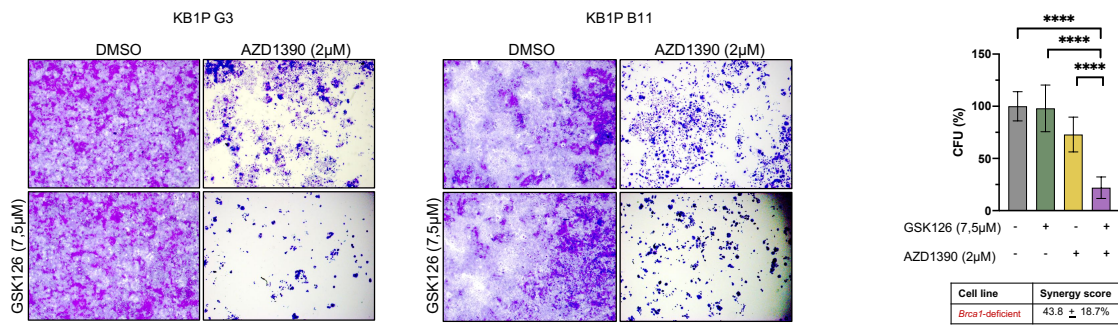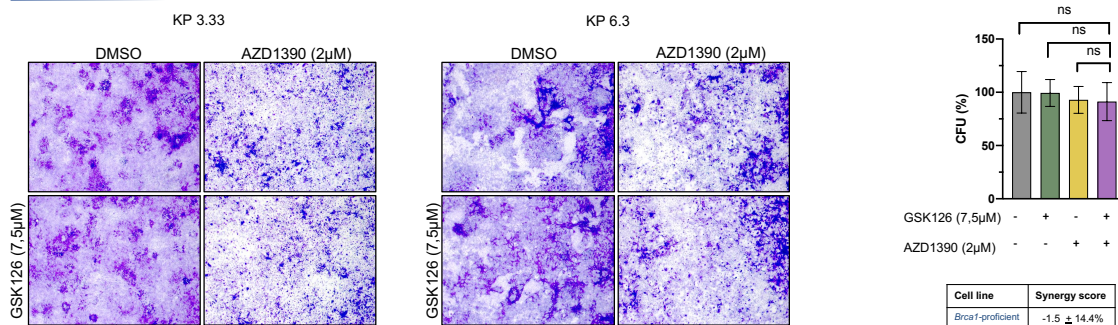


**Figure 4. Growth inhibition analyses confirm synergy of combination with EZH2i and ATMi in *Brca1*-deficient cell lines.**
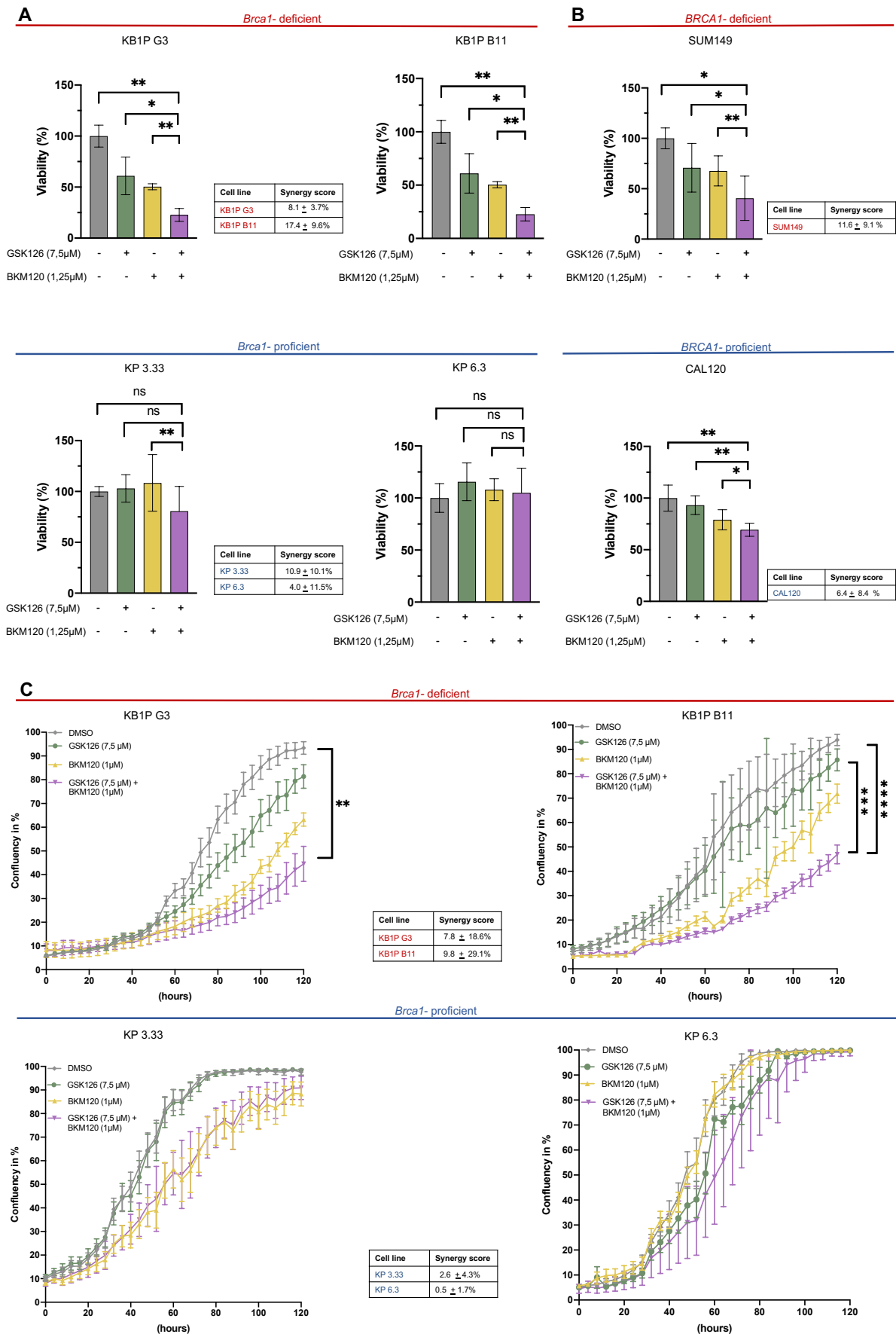
(**A**) Viability of cells (KB1P G3, KB1P B1, KP 3.33 and KP 6.3) treated with DMSO, GSK126, AZD1390 and combined GSK126 and AZD1390 was determined with a CTG assay after 72 h of treatment. Growth inhibition was normalized to the mean of DMSO control values. N=6. These experiments were conducted and analyzed by L. Ratz and L. Bartke. (**B**) Viability of human breast cancer cell lines (SUM149 and CAL120) treated with DMSO, GSK126, AZD1390 and combined GSK126 and AZD1390 was determined with a CTG assay after 72 h of treatment. Growth inhibition was normalized to the mean of DMSO control values. These experiments were conducted and analyzed by L. Ratz and L. Bartke. (**C**) Confluency of cells was measured with the Life Cell Imaging for 120 h. Confluency of cells (KB1P G3, KB1P B1, KP 3.33 and KP 6.3) treated with DMSO, GSK126, AZD1390 and combined GSK126 and AZD1390 was normalized to the mean confluency-values of DMSO treated cells. Significance was evaluated with Tukey's multiple comparison tests. Three replicate values from four independent experiments are displayed for both cell lines KB1P G3 and KP 3.33 N=4. Three replicate values from three independent experiments are displayed for both cell lines KB1P B11 and KP 6.3 N=3. These experiments were conducted and analyzed by L. Ratz and L. Bartke. (**D**) Pictures of 2x magnified colony formation assays after 7 days of incubation for DMSO, GSK126, AZD1390 and combined GSK126 and AZD1390 are shown for KB1P G3, KB1P B11, KP 3.33 and KP 6.3 cell lines. Quantification of colony forming units (CFU) in 0.56 magnified pictures was normalized to the mean values of DMSO control for pooled *Brca1*-deficient cell lines of three independent experiments for KB1P G3 and two independent experiments for KB1P B11 experiments, as well as for *Brca1*-proficient cell lines of two independent experiments for KP 3.33 cell lines and three independent experiments for KP 6.3 cell lines. These experiments were conducted and analyzed by L. Ratz and L. Bartke. This figure contains data from Ratz et al. [70]. If not otherwise specified, shown experiments exhibit values from at least three independent experiments. Synergy scores (in %) were calculated according to the *Bliss Independence Model.* Significances were calculated with Tukey's multiple comparison testing (ns= not significant; *, p<0,0332; **, p<0,0021; ***, p<0,0002; ****, p<0,0001) with GraphPad Prism (Version 8.0, Graphpad Software, Inc.).
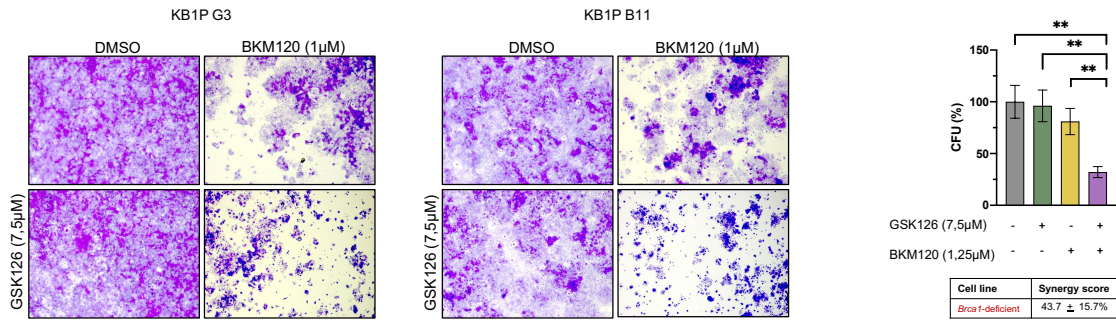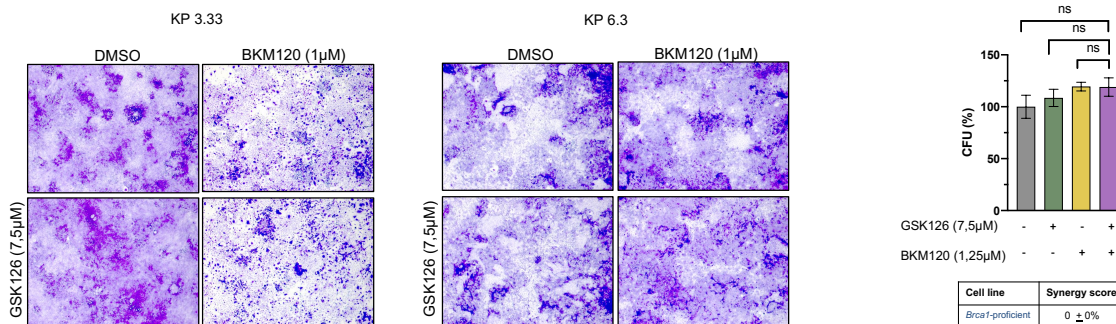
**Combination treatment of EZH2i and PI3Ki leads to additive growth inhibition in *Brca1*-deficient murine and human breast cancer cell lines.**

Combination treatment of GSK126 (EZH2i) and BKM120 (PI3Ki) led to a significant growth inhibition in comparison to vehicle control especially in *Brca1*-deficient cell lines. CTG experiments (fig. 5.A) as well as Incucyte® data (fig. 5.C) and CFA assays (fig. 5.D) demonstrated a significant growth inhibition compared to vehicle control in *Brca1*-deficient breast cancer cells. No effect of combination treatment could be observed in *Brca1*-proficient cell lines. Synergy score for KB1P cell lines was 43.7 % (SD +/- 15.7 %) in CFA (fig. 5.D), indicating synergy. However, synergy scores of CTG (KB1P G3: 8.1 %; SD +/- 3.7 % and KB1P B11: 17.4 %; SD +/- 9.6 %) (fig. 5.A) and Incucyte® experiments (KB1P G3: 7.8 %; SD +/- 18.6 % and KB1P B11: 9.8 %; SD +/- 29.1 %) (fig. 5.C) showed broader variation between synergy scores and cell lines. When applying the previously defined 10 % threshold for drug synergy, this drug combination would rather be considered as additive and not synergistic.

Fig. 5.B displays combination treatment of GSK126 and BKM120 for human breast cancer cell lines. For SUM149 cell line, a varying growth inhibition between 30% and 80% was observed upon GSK126 and BKM120 combination treatment. This is a significantly higher growth inhibition than seen in vehicle control and single agent treatments. Combination treatment of SUM149 cannot be considered as synergistic according to the synergy score of 11.6% due to the standard deviation of +/- 9.1%. An additive effect of GSK126 and BKM120 could also be observed in the *BRCA1*-proficient CAL120 cell line (synergy score of 6.4%; SD +/- 8.4%).

**Figure 5.** Growth inhibition analyses reveal an additive effect of combination with EZH2i and PI3Ki in *Brca1*-deficient cell lines.

**Figure 5. Growth inhibition analyses reveal an additive effect of combination with EZH2i and PI3Ki in *Brca1*-deficient cell lines.**

(**A**) Viability of cells (KB1P G3, KB1P B1, KP 3.33 and KP 6.3) treated with DMSO, GSK126, BKM120 and combined GSK12 and BKM120 was determined with a CTG assay after 72h of treatment. Growth inhibition was normalized to the mean of DMSO control values. These experiments were conducted and analyzed by L. Bartke. (**B**) Viability of human breast cancer cell lines (SUM149 and CAL120) treated with DMSO, GSK126, BKM120 and combined GSK126 and BKM120 was determined with a CTG assay after 72h of treatment. Growth inhibition was normalized to the mean of DMSO control values. These experiments were conducted and analyzed by L. Bartke. (**C**) Confluency of cells was measured with the life cell imaging by the Incucyte for 120h. Confluency of cells cells (KB1P G3, KB1P B1, KP 3.33 and KP 6.3) treated with DMSO, GSK126, BKM120 and combined GSK126 and BKM120 was normalized to the mean confluency-values of DMSO treated cells. Three replicate values from four independent experiments are displayed for both cell lines KB1P G3 and KP 3.33 N=4. Three replicate values from three independent experiments are displayed for both cell lines KB1P B11 and KP 6.3 N=3. These experiments were conducted and analyzed by L. Ratz and L. Bartke. (**D**) Pictures of 2x magnified colony formation assays after 7 days of incubation for DMSO, GSK126, BKM120 and combined GSK126 and BKM120 are shown for (KB1P G3, KB1P B1, KP 3.33 and KP 6.3) cell lines. Quantification of colony forming units (CFU) in 0.56 magnified pictures was normalized to the mean values of DMSO control for pooled *Brca1*-deficient cell lines of three independent experiments for KB1P G3 and two independent experiments for KB1P B11 experiments, as well as for *Brca1*-proficient cell lines of two independent experiments for KP 3.33 cell lines and three independent experiments for KP 6.3 cell lines. These experiments were conducted and analyzed by L. Bartke. This figure is based on the paper of Ratz et al. [70]. If not otherwise specified, the displayed graphs exhibit values from at least three independent experiments. Synergy scores (in %) were calculated according to the *Bliss Independence Model*. Significances were calculated with Tukey's multiple comparison testing (ns= not significant; *, $p<0{,}0332$; **, $p<0{,}0021$; ***, $p<0{,}0002$; ****, $p<0{,}0001$) with GraphPad Prism (Version 8.0, Graphpad Software, Inc.).
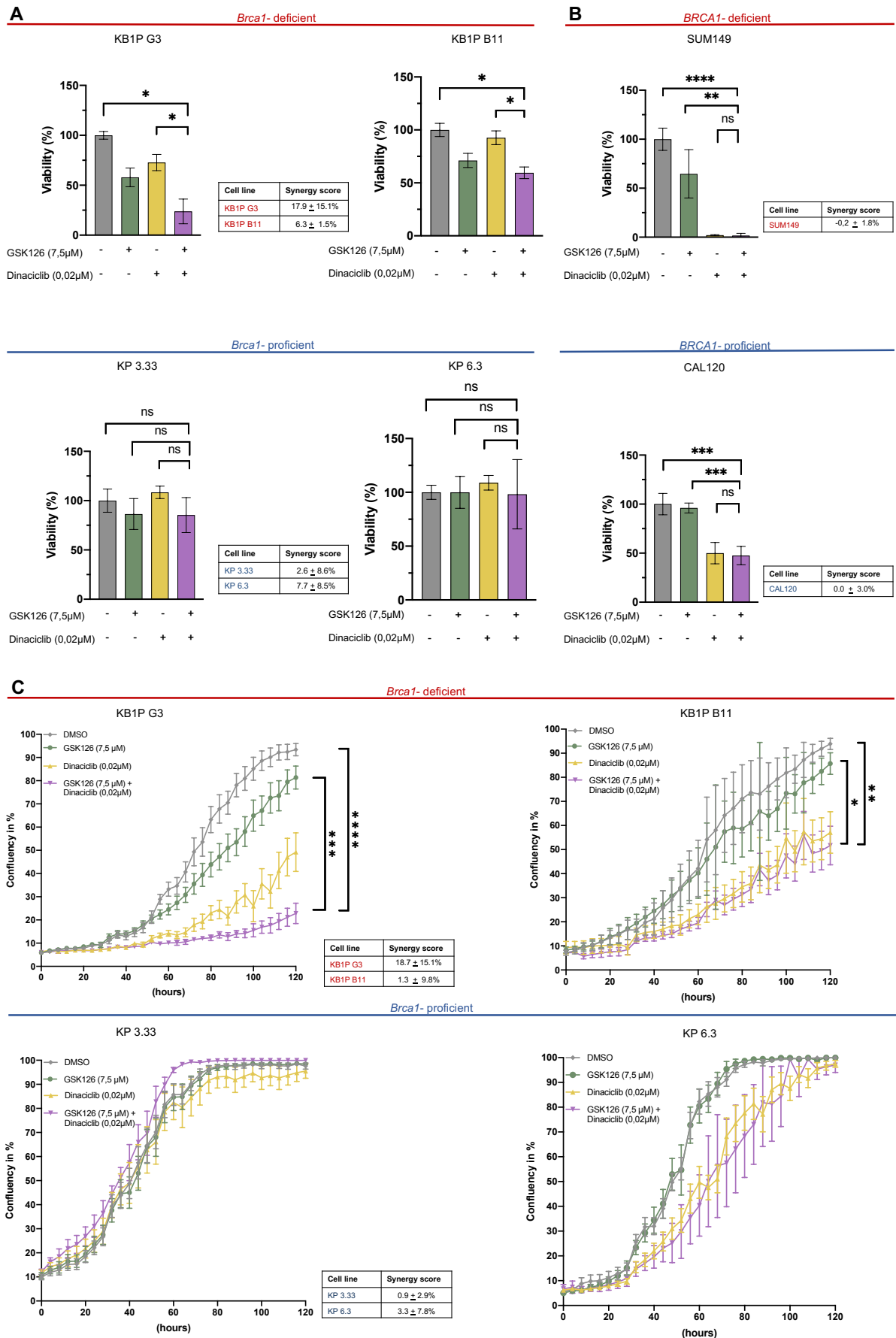
**Combination treatment of EZH2i and panCDKi leads to additive growth inhibition in *Brca1*-deficient murine breast cancer cell lines.**

In CTG assays, we found that combination treatment of GSK126 (EZH2i) and dinaciclib (panCDKi) leads to a significant growth inhibition in *Brca1*-deficient breast tumor cell lines compared to *Brca1*-proficient breast tumor cell lines (fig. 6.A). Incucyte® experiments (fig. 6.C) and CFA (fig. 6.D) validated this significant growth inhibition of combination treatment upon *Brca1*-deficiency. No effect on cell viability was observed for KP cell lines. However, synergy scores for *Brca1*-deficient cell lines for CTG assays (KB1P G3: 17.9 %; SD +/- 15.1 % and KB1P B11: 6.3 %; SD +/- 1.5 %) (fig. 6.A) as well as life cell imaging (KB1P G3: 18.7 %; SD +/-15.1 % and KB1P B11: 1.3 %; SD +/- 9.8 %) (fig. 6.C) and colony formation assays (16.0 %; SD +/- 12.1 %) (fig. 6.D) cannot be safely pinpointed to significant values of over 10 % as standard deviation indicates contradictory values within each experiment. Therefore, we can merely describe an additive growth inhibition when combining GSK126 and dinaciclib.
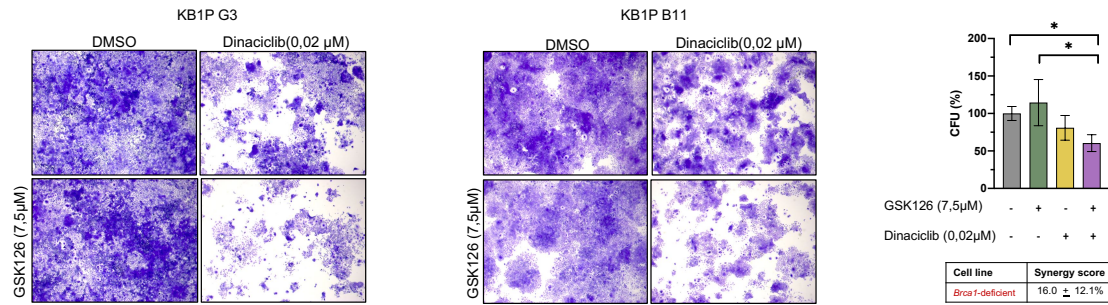
Treatment of human *BRCA1*-deficient breast cancer cell line SUM149 with dinaciclib led to a significant growth reduction of almost 100 % (fig. 6.B). Combination treatment with GSK126 resulted in the same level of growth inhibition as dinaciclib monotherapy in both *BRCA1*-proficient and -deficient human breast cancer cell lines. For this combination, synergy scores of -0.2 % (SD +/- 1.8 %) for SUM149 indicate a rather additive effect of combination treatment.

**Figure 6.** Growth inhibition analyses reveal an additive effect of combination with EZH2i and panCDKi in *Brca1*-deficient cell lines.
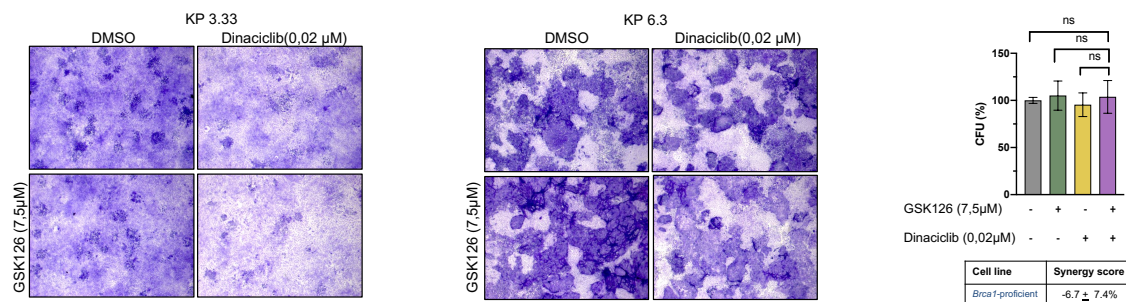
**Figure 6. Growth inhibition analyses reveal an additive effect of combination with EZH2i and panCDKi in *Brca1*-deficient cell lines.**

(**A**) Viability of cells (KB1P G3, KB1P B1, KP 3.33 and KP 6.3) treated with DMSO (7,5 µM), GSK126, and dinaciclib was determined with a CTG assay after 72h of treatment. Growth inhibition was normalized to the mean of DMSO control values. These experiments were conducted and analyzed by L. Bartke. (**B**) Viability of human breast cancer cell lines (SUM149 and CAL120) treated with DMSO (7,5 µM), GSK126, dinaciclib and combined GSK126 and dinaciclib was determined with a CTG assay after 72h of treatment. Growth inhibition was normalized to the mean of DMSO control values. These experiments were conducted and analyzed by L. Bartke. (**C**) Confluency of cells was measured with the life cell imaging by the Incucyte for 120h. Confluency of cells (KB1P G3 and KP 3.33) treated with DMSO (7,5 µM), GSK126, and dinaciclib and combined GSK126 and dinaciclib was normalized to the mean confluency-values of DMSO treated cells. Three replicate values from four independent experiments are displayed for both cell lines KB1P G3 and KP 3.33 N=4. Three replicate values from three independent experiments are displayed for both cell lines KB1P B11 and KP 6.3 N=3. These experiments were conducted and analyzed by L. Ratz and L. Bartke. (**D**) Pictures of 2x magnified colony formation assays after 7 days of incubation for DMSO (7,5 µM), GSK126, dinaciclib and combined GSK126 and dinaciclib are shown for KB1P G3 and KP 3.33 cell lines. Quantification of colony forming units (CFU) in 0.56 magnified pictures was normalized to the mean values of DMSO control for pooled *Brca1*-deficient cell lines of three independent experiments for KB1P G3 and two independent experiments for KB1P B11 experiments, as well as for *Brca1*-proficient cell lines of two independent experiments for KP 3.33 cell lines and three independent experiments for KP 6.3 cell lines. These experiments were conducted and analyzed by L. Bartke. This figure is based on the paper of Ratz et al. [70]. If not otherwise specified, shown experiments exhibit values from at least three independent experiments. Synergy scores (in %) were calculated according to the Bliss Independence Model. Significances were calculated with Tukey's multiple comparison testing (ns= not significant; *, p<0,0332; **, p<0,0021; ***, p<0,0002; ****, p<0,0001) with GraphPad Prism (Version 8.0, Graphpad Software, Inc.).

50

**4.3 Compound exchange of EZH2i as well as ATMi leads to synergistic growth inhibition in *Brca1*-deficient breast tumor cells.**
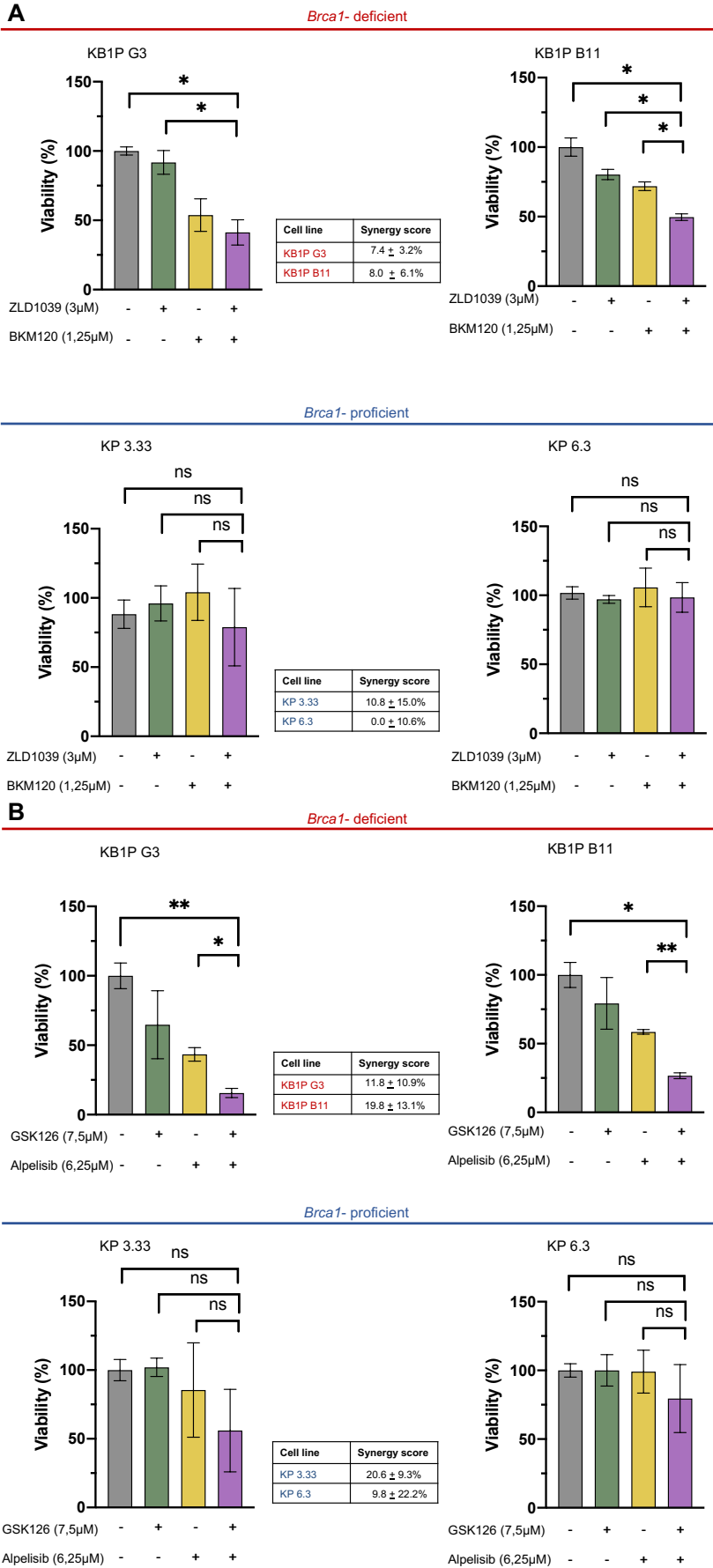
For a pharmacological validation, we used different EZH2 and ATM inhibitors. For the CTG experiments we used ZLD1039, another EZH2 inhibitor, which is in preclinical development for the treatment of breast cancer [95] [70]. Besides AZD1390, we used the ATM inhibitor KU60019 [116] [70]. The displayed CTG assays contain data from Ratz et al. [70]. Combination treatment of ZLD1039 and AZD1390 led to a growth inhibition of about 40 % for KB1P G3 and 50 % for KB1P B11 cell line (fig. 7.A). Combinatory treatment of GSK126 and KU60019 resulted in a growth inhibition of about 80 % for KB1P G3 and 50 % for KB1P B11 cell line (fig. 7.B). Synergy scores for KB1P cell lines of combined ZLD1039 and AZD1390 treatment as well as GSK126 and KU60019 treatment can be pinpointed to levels over the 10% threshold of synergy with synergy scores of 44.2 % (SD +/- 10.6 %) for KB1P G3 cells and 27.1 % (SD +/- 13.0 %) for KB1P B11 cells. Therefore, both combination treatments with different EZH2 and ATM inhibitors have shown synergy, indicating that the synergistic effect is related to the inhibition of both pathways and not an off-target effect of the compounds [70].
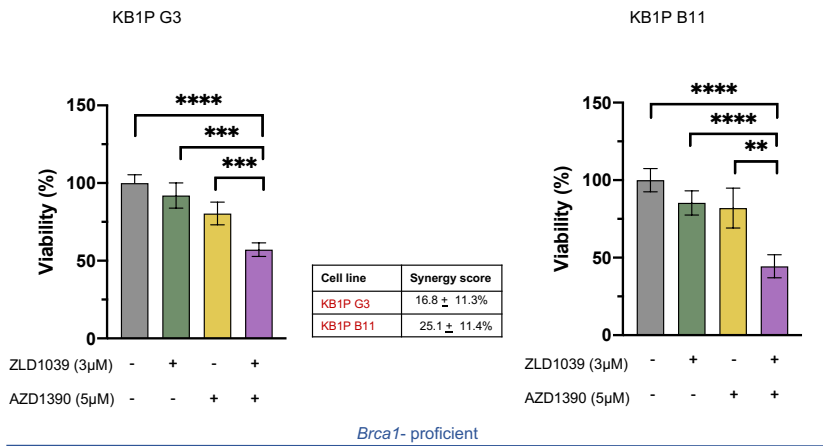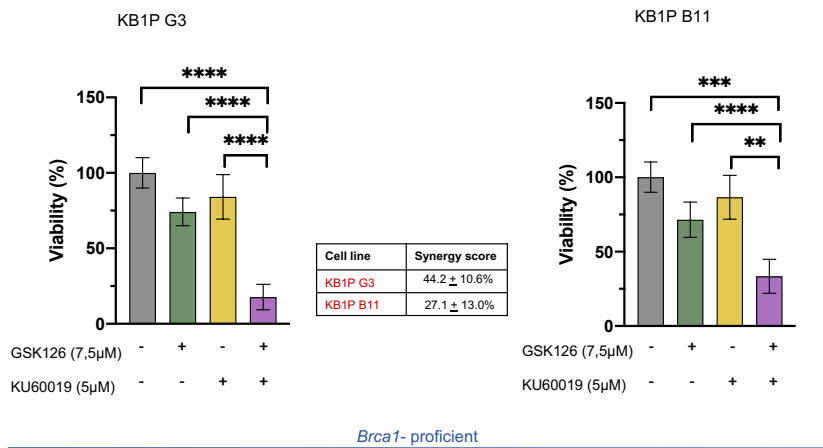
**Figure 7. Compound exchange of EZH2i as well as ATMi leads to synergy in *Brca1*-deficient cell lines.**

Pharmacological exchange of compounds was analyzed with CTG experiments for 72 h for (KB1P G3, KB1P B1, KP 3.33 and KP 6.3) cell lines. DMSO served as a vehicle control. Viability (in %) of cells is normalized to DMSO values. (**A**) Cells were treated with ZLD1039 in combination with AZD1390. (**B**) Cells were treated with GSK126 in combination with in combination with KU60019. These experiments were conducted and analyzed by L. Ratz and L. Bartke. This figure contains data from Ratz et al. [70]. If not otherwise specified, shown experiments exhibit values from at least three independent experiments. Synergy scores ( in %) were calculated according to the Bliss Independence Model. Significances were calculated with Tukey's multiple comparison testing (ns= not significant; *, p<0,0332; **, p<0,0021; ***, p<0,0002; ****, p<0,0001 )with GraphPad Prism (Version 8.0, Graphpad Software, Inc.).

## Compound exchange of EZH2i as well as PI3Ki leads to an additive growth inhibition in *Brca1*-deficient cell lines.

Combinatory treatment of ZLD1039 (EZH2i) and BKM120 revealed significantly higher growth inhibition than vehicle control in *Brca1*-deficient cell lines (fig. 8.A). Instead of BKM120 we used the PIK3CA inhibitor alpelisib, which inhibits the alpha unit of PI3K specifically and is already approved for breast cancer treatment according to the SOLAR-1 study [54]. Combination therapy of GSK126 with the novel PI3K inhibitor alpelisib resulted in significantly higher growth inhibition than vehicle control in KB1P cell lines (fig. 8.B). No effect on cell viability was observed for either combination therapy in *Brca1*-proficient cell lines. Single agent alpelisib led to significantly higher growth inhibition than vehicle control specifically in *Brca1*-deficient cell lines. Combination treatments in *Brca1*-deficient cell lines were additive according to the synergy scores of 7.4 % (SD +/- 3.2 %) for KB1P G3 and 8.0 % (SD +/- 6.1 %) for KB1P B11 when exchanging the EZH2i (fig. 8.A) and 11.8% (SD +/- 10.9 %) for KB1P G3 and 19.8 % (SD +/- 13.1 %) for KB1P B11 when exchanging the PI3Ki (fig. 8.B). These experiments are based on Ratz et al. [70].

**A**

*Brca1*- deficient

KB1P G3

| Cell line | Synergy score |
|-----------|---------------|
| KB1P G3 | 7.4 ± 3.2% |
| KB1P B11 | 8.0 ± 6.1% |

KB1P B11

*Brca1*- proficient

KP 3.33

| Cell line | Synergy score |
|-----------|---------------|
| KP 3.33 | 10.8 ± 15.0% |
| KP 6.3 | 0.0 ± 10.6% |

KP 6.3

**B**

*Brca1*- deficient

KB1P G3

| Cell line | Synergy score |
|-----------|---------------|
| KB1P G3 | 11.8 ± 10.9% |
| KB1P B11 | 19.8 ± 13.1% |

KB1P B11

*Brca1*- proficient

KP 3.33

| Cell line | Synergy score |
|-----------|---------------|
| KP 3.33 | 20.6 ± 9.3% |
| KP 6.3 | 9.8 ± 22.2% |

KP 6.3

**Figure 8. Compound exchange of EZH2i as well as PI3Ki leads to an additive growth inhibition in *Brca1*-deficient cell lines.**

Pharmacological exchange of compounds was analyzed with CTG experiments for 72 h for (KB1P G3, KB1P B1, KP 3.33 and KP 6.3) cell lines. DMSO served as a vehicle control. Viability (in %) of cells is normalized to DMSO values. (**A**) Cells were treated with ZLD1039 in combination with BKM120. (**B**) Cells were treated with GSK126 in combination with alpelisib. These experiments were conducted and analyzed by L. Bartke. This figure is based on the paper of Ratz et al. [70]. If not otherwise specified, shown experiments exhibit values from at least three independent experiments. Synergy scores ( in %) were calculated according to the Bliss Independence Model. Significances were calculated with Tukey's multiple comparison testing (ns= not significant; *, p<0,0332; **, p<0,0021; ***, p<0,0002; ****, p<0,0001) with GraphPad Prism (Version 8.0, Graphpad Software, Inc.).

## Compound exchange of EZH2i in combination with dinaciclib does not significantly inhibit growth of *Brca1*-deficient cell lines.

Combinatory ZLD1039 (EZH2i) and dinaciclib treatment did not lead to a significant growth inhibition of KB1P cell lines (fig. 9). No effect of ZLD1039 and dinaciclib combinatory treatment can be observed for KP cell lines. Dinaciclib was not exchanged in this experiment. Due to the inhibition of different CDKs no comparable compound could be identified. These experiments are based on Ratz et al. [70].
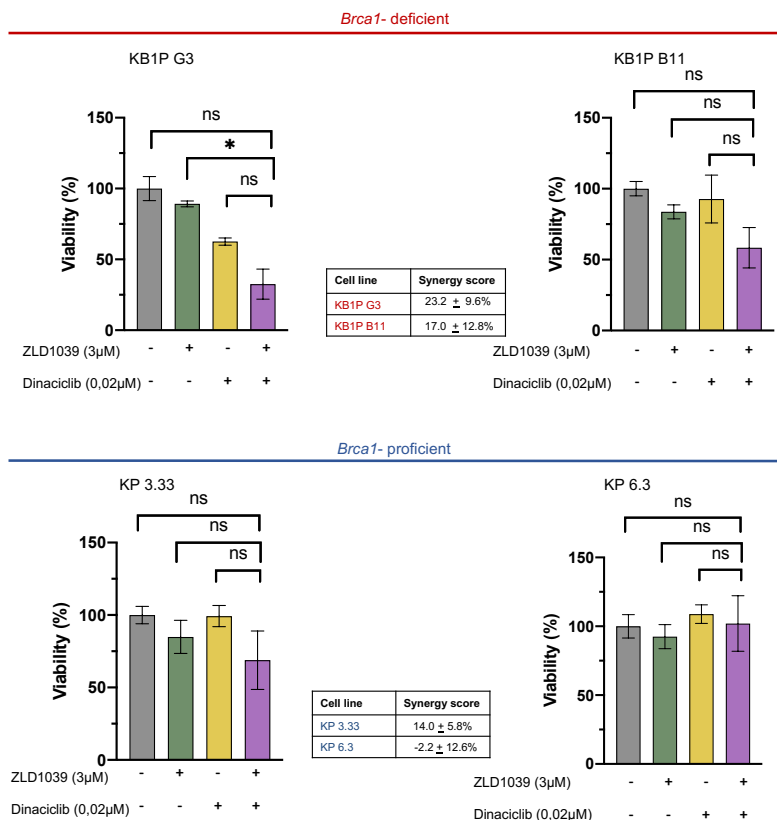


**Figure 9. Compound exchange of EZH2i in combination with dinaciclib does not significantly inhibit growth of *Brca1*-deficient cell lines.**

Pharmacological exchange of compounds was analyzed with CTG experiments for 72 h for (KB1P G3, KB1P B1, KP 3.33 and KP 6.3) cell lines. DMSO served as a vehicle control. Viability (in %) of cells is normalized to DMSO values. Cells were treated with ZLD1039 in combination with dinaciclib.  These experiments were conducted and analyzed by L. Bartke. This figure is

## 4.4 Knockdown of *Ezh2* in combination with ATM inhibition by AZD1390 is synergistic in *Brca1*-deficient breast tumor cells.

For a genomic validation of synergy, we made use of a Doxycycline (Dox) -dependent shRNA *Ezh2* knockdown. After 7 days of Dox treatment, a knockdown of *Ezh2* was achieved in both KB1P G3 and KP 33 cell lines (fig. 10.A) [70]. Trimethylation levels of H3K27 were down-regulated upon *Ezh2* knockdown. In order to genetically confirm the synergistic effect of EZH2i and ATMi, we performed a colony formation assay with *Ezh2* knockdown cells in combination with the ATMi AZD1390 (fig. 10.B, C, D, E) [70]. These experiements contain data from Ratz et al. [70] and show a synergistic (synergy score of 27.6%; SD +/- 14.6%) growth inhibition of about 70% upon combined *Ezh2* knockdown and AZD1390 treatment (fig. 10.B).

**Knockdown of *Ezh2* in combination with PI3K inhibition by BKM120 is not synergistic in *Brca1*-deficient breast tumor cells.**

Next, we tested the effect of *Ezh2* knockdown and PI3K inhibition. Figure 10.B displays a growth inhibition of approximately 50% upon *Ezh2* knockdown in combination with BKM120 in *Brca1*-deficient cell lines. No effect on growth inhibition was observed for the *Brca1*-proficient cells lines (fig. 10.D). However, the synergy score of 26.6 % for KB1P G3 sh*Ezh2* cells treated with Dox and BKM120 cannot faithfully prove synergy as the standard deviation of +/- 25% indicates discrepancy within the experiment (fig. 10.B). These experiments are based on Ratz et al. [70].
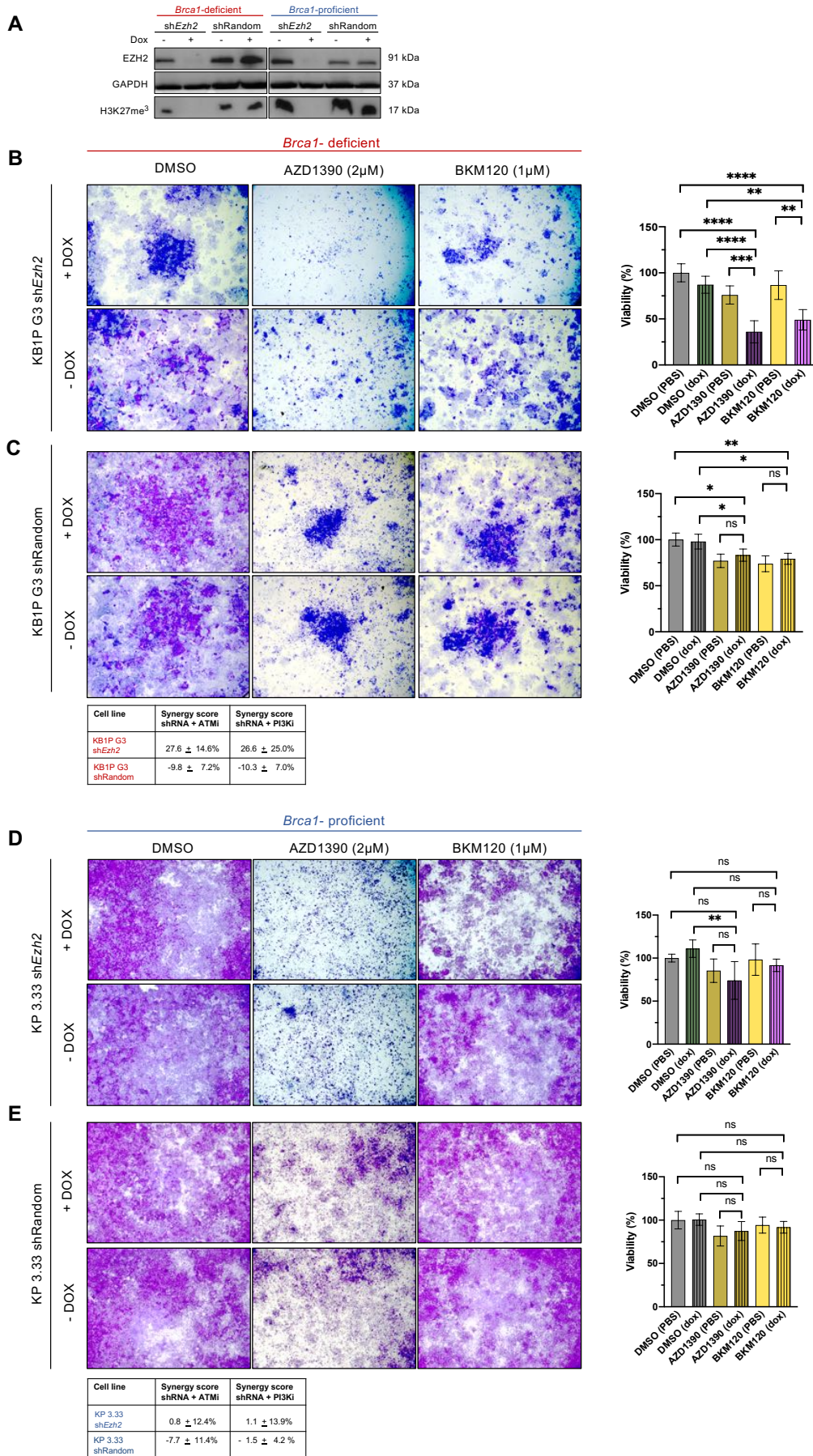
Figure 10. Knockdown of *Ezh2* in combination with ATMi is synergistic in *Brca1*-deficient tumor cells.

(A) KB1P G3 sh*Ezh2*, KB1P G3 shRandom, KP 3.33 sh*Ezh2* and KP 3.33 shRandom cell lines were treated with DOX or PBS for 7 days. Protein lysates were then stained with EZH2 and H3K27me[3] antibodies, GAPDH antibody serves as a control. One representative image out of three independent experiments is shown. KB1P G3 sh*Ezh2* (B), KB1P G3 shRandom (C), KP 3.33 sh*Ezh2* (D) and KP 3.33 shRandom (E) cell lines were treated with DOX or PBS for 7 days and then incubated with DMSO, AZD1390 or BKM120 for 7 days. Representative images (2.0 magnification) from one experiment out of at least three independent experiments are shown. Combination of *Ezh2* knockdown and AZD1390 or BKM120 are outlined in purple. Colony forming units were counted with the *clono counter* and normalized to DMSO (PBS treated) controls. These experiments were conducted and analyzed by L. Ratz and L. Bartke. This figure contains data from Ratz et al. [70]. If not otherwise specified, shown experiments exhibit values from at least three independent experiments. Synergy scores (in %) were calculated according to the Bliss Independence Model. Significances were calculated with Tukey's multiple comparison testing (ns= not significant; *, $p < 0.0332$; **, $p < 0.0021$; ***, $p < 0.0002$; ****, $p < 0.0001$) with GraphPad Prism (Version 8.0, Graphpad Software, Inc.).

## 4.5 Combination of EZH2i and ATMi induces high levels of DNA damage in *Brca1*-deficient cell lines.

ATM is a key mediator of DDR by phosphorylating H2AX to yH2AX, which is highly involved in DNA damage signaling of DSBs [27]. In order to understand the mechanistic behind the synergistic growth inhibition of GSK126 and AZD1390 upon *Brca1*-deficiency, we further investigated its effect on DNA damage signaling. Therefore, we made use of immunofluorescence to stain yH2AX foci per cell, according to the same set up previously described by Jachimowicz et al. [70,117]. Cisplatin is known to induce double strand breaks and therefore served as a positive control for the induction of high levels of yH2AX foci/cell [117].

These experiments contain data from Ratz et al. [70]. Cisplatin increased yH2AX foci/cell significantly in all four displayed cell lines (fig. 11). We observed significantly higher levels of yH2AX foci per cell upon combinatory GSK126 and AZD1390 treatment in comparison to vehicle control in both *Brca1*-deficient cell lines (fig. 11). Furthermore, combination therapy elevated yH2AX foci levels per cell more significantly than the respective monotherapies did (fig. 11). *Brca1*-proficient cell lines did not show any increase of yH2AX foci when treated with combinatory EZH2 / ATM inhibition.
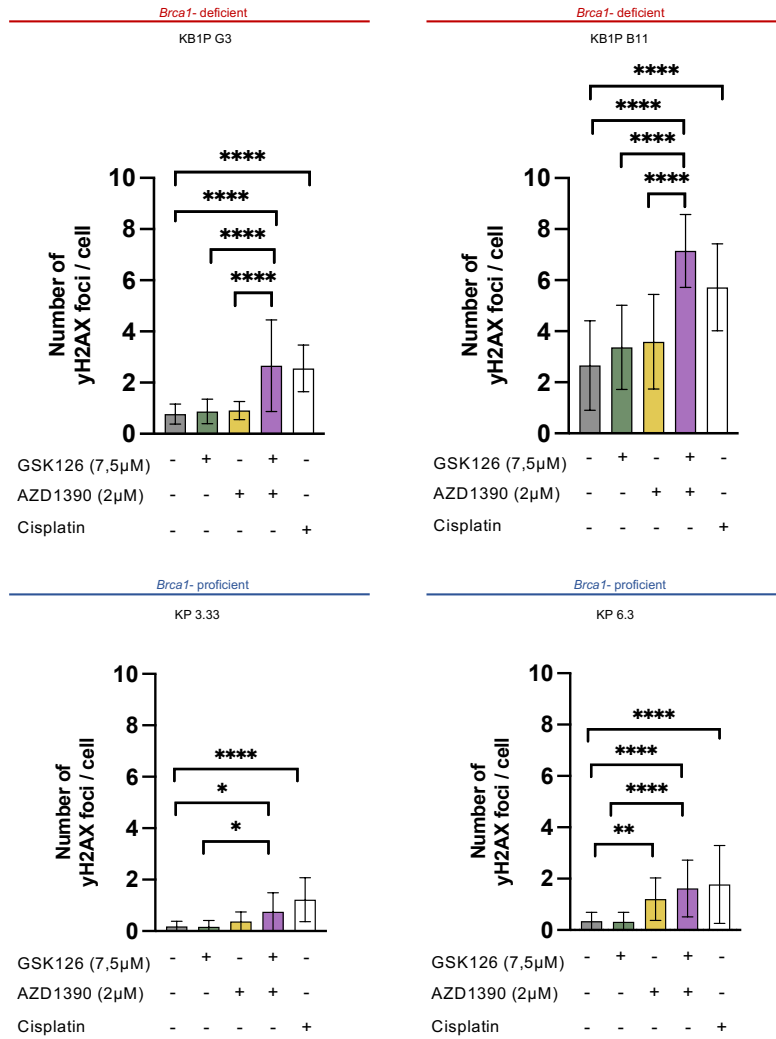
**Figure 11. Combination of EZH2i and ATMi induces high levels of DNA damage in *Brca1*-deficient cell lines.**

KB1P G3, KB1P B11, KP 3.33 and KP 6.3 cell lines were incubated for 48 h according to the displayed compounds. DMSO (7.5µM) served as control. Cells were stained with yH2AX primary antibody and an immunofluorescent secondary antibody, visualized with DAPI by high-throughput microscopy. The number of yH2AX foci per cell is shown. Analyzed data is derived from at least three independent experiments. This experiment was conducted by L. Ratz and L. Bartke and analyzed with the help of J. Isensee. This figure contains data from Ratz et al. [70]. This figure is adapted from Ratz et al. with kind permission [70]. Statistical analysis was calculated with Tukey's multiple comparison testing (ns= not significant; *, p<0,0332; **, p<0,0021; ***, p<0,0002; ****, p<0,0001) with GraphPad Prism (Version 8.0, Graphpad Software, Inc.)..

# 5    DISCUSSION

## 5.1    *Brca1*-deficient breast cancer cells overexpress EZH2 and are sensitive to EZH2 inhibition

The rational for targeting *BRCA1*-deficient breast cancers with EZH2i was based on previous observations of our group that EZH2 is overexpressed in *BRCA1*-associated breast carcinomas [65,100]. In this study, we could confirm that EZH2 RNA-levels were overexpressed in *Brca1*-deficient mammary murine tumors (fig. 3.A) [70]. In line with our findings, Yomtoubian et al. found that high levels of EZH2 in TNBC lead to characteristics of *BRCA1*-deficient tumors, such as increased metastasis formation and an undifferentiated basal-like cancer phenotype [102]. Therefore, EZH2 emerges as a potential target for *BRCA1*-mutant breast cancers. Our group has already previously established, that *Brca1*-deficient murine breast cancer cells are more sensitive to the EZH2 inhibitor GSK126 [65]. Our *in vivo* experiments show a significant impact of GSK126 monotherapy in contrast to vehicle control in *Brca1*-deficient murine breast tumors (fig. S1) [70].

Several studies provide potential explanations for a reciprocal regulation of *EZH2* overexpression and loss of *BRCA1*. Wang et al. postulate that direct binding of BRCA1 to EZH2 can inhibit the EZH2 activity. Additionally, an inhibition of cell differentiation and an enhancement of metastasis have been associated with EZH2 expression in cells with lower levels of BRCA1 [93]. Another study revealed that low levels of nuclear p-BRCA1 were detected upon high EZH2 levels and upregulated p-AKT [99]. Kumari et al. could identify several EZH2 target genes by ChIP (Chromatin Immunoprecipitation) analyses of invasive breast tumor tissues, with some serving as oncogenes and others as tumor suppressor genes, which further portrays the inconclusive understanding of the role of EZH2 in cancer [118]. Others identified more specific targets of EZH2 as high levels of H3K27me$^3$ were found at the promotor site of transcription factor GATA3, which results in a basal-like TNBC phenotype similar to the *Brca1*-deficient breast cancer phenotype [102]. To further properly study the impact of EZH2 inhibition in the context of *Brca1*-deficiency, ChIP sequencing of gene sites with high H3K27me$^3$ levels in KB1P cell lines compared to KP cell lines would be interesting.

In general, EZH2-mediated histone methylation in breast cancer can be assumed to promote genomic instability and is associated with an aggressive cancer phenotype [87-89,102]. In line with our hypothesis that EZH2 inhibition could sensitize *Brca1*-deficient tumor cells to synthetic lethal partners, our large-scale synergy screen identified synergistic interactions of AZD1390 (ATMi), BKM120 (PI3Ki) or dinaciclib (panCDKi) in combination with EZH2i upon *Brca1*-deficiency [70]. The tumor suppressor gene ATM is relevant for DDR upon DSBs [28], PI3K is

involved in cell cycle progression and oncogenic signaling [4] and CDKs are essential for cell cycle regulation [17]. In the context of GI, as caused by defects of HR upon *BRCA1*-deficiency, these pathways therefore play a crucial role in either maintaining genomic integrity (ATM) or promoting uncontrolled proliferation (PI3K and CDKs).

Consequently, our study confirms the previous finding that *BRCA1*-deficiency can be proclaimed as a prognostic marker for high EZH2 levels [65,70]. As Puppe et al. has previously established, EZH2 could thus function as a biomarker for identifying tumors with a *BRCA*ness phenotype [65]. Moreover, high EZH2 levels may constitute a novel target for specific treatment of *BRCA1*-deficient breast cancers. However, further investigation of the involvement of H3K27me$^3$ levels in the tumorigenesis of *BRCA1*-deficient breast cancer with e.g. ChIP analyses is required. In order to exploit the defects of HR upon *BRCA1*-deficiency, simultaneous inhibition of EZH2, with its context dependent oncogenic role and involvement in DDR [15], in combination with inhibition of ATM, PI3K or CDKs are incentives to efficiently induce growth inhibition of *BRCA1*-deficient breast cancer cells [70].

## 5.2 Combined treatment of EZH2i and ATMi is synergistic *in vitro* and leads to significant prolonged overall survival *in vivo* upon *Brca1*-deficiency.

Our functional *in vitro* experiments verified that combined EZH2 inhibition and ATM inhibition in murine and human *BRCA1*-deficient mammary tumor cell lines leads to synergistic growth inhibition [70]. Furthermore, our group validated this treatment *in vivo* (fig. S1) as combined GSK126 and AZD1390 treatment results in significantly prolonged progression-free survival of mice [70].

Chiara Brambillasca and others from The Netherlands Cancer Institute in Amsterdam performed an *in vivo* drug intervention study with our *Brca1*-deficient tumor model (fig. S1) [70]. The optimal dose was determined in previous MTD (maximum tolerated dose) studies (data not shown) [70]. Monotherapies with GSK126 (p = 0.002) and AZD1390 (p = 0.038) led to an increased survival, compared to vehicle exposure (fig. S1) [70]. However, a combination therapy consisting of GSK126 and AZD1390 increased the progression-free survival (PFS) compared to vehicle control (p = 0.0006) and the single agents (AZD1390 vs. GSK126+AZD1390: p = 0.048; GSK126 vs. GSK126+AZD1390: p = 0.21) [70]. Combination treatment showed an excellent toxicity profile with no significant weight loss (data not shown) [70].

To ensure target inhibition *in vivo*, tumor tissue from samples of sacrificed mice, which responded to the treatment, was stained by immunohistochemistry. As expected, GSK126 and AZD1390 led to a reduction of H3K27me$^3$ and pATM after 7 days of treatment (data not shown)

[70]. This is in accordance with previous studies, where others achieved good tolerance for the concentration of 20mg/kg bodyweight *in vivo* and 88% of p-ATM inhibition over a period of 24 hours [119]. We can therefore assume that the *in vivo* AZD1390 concentrations used in this study were ATM specific [70].

We validated target specificity of AZD1390 *in vitro* on a protein (fig. 3.E) and pharmacological (fig. 7.B) level [70]. However, we did not study target specificity of AZD1390 on a genomic level. Therefore, we were not able to fully rule out possible off-target effects of AZD1390. Moreover, others observed inhibition of other targets than ATM at very high concentrations of 1mM AZD1390 [120]. To fully prove target specificity of the compound, validation on the genomic level should be shown by using siRNA (small interfering RNA) to cause an ATM knockdown. Growth inhibition analyses of GSK126 in combination with siATM knockdown cells should then prove synergy.

AZD1390 is currently in a phase I clinical trial for the treatment of brain tumors in combination with radiotherapy (ClinicalTrials.gov identifier NCT03423628), as radiation induces high levels of DSBs, which then triggers ATM activity [121]. Durant et al. state that especially *TP53*-deficient brain tumors are sensitive for such treatment. With its role as the "guardian of the genome", mutant *TP53* already destabilizes DDR and thus results in a more efficient radio-sensitization in combination with ATM inhibition, also leading to higher levels of genomic instability [120]. These observations are therefore in line with our rational to use ATM inhibition for exploiting defects in genome integrity caused by loss of *Brca1* and *Tp53* in our murine breast cancer cell lines. In this study, we were able to describe sensitivity of *Brca1*- and *Tp53*-mutated breast cancer cell lines to ATM inhibition [70].

We showed that EZH2 inhibition in combination with ATM inhibition leads to significantly higher levels of the "DSB-marker" yH2AX upon *Brca1*-deficiency [70]. We hypothesized that combination treatment of EZH2i/ATMi results in dysfunctional and dysregulated DDR, which consequently abrogates DSB repair. High yH2AX levels upon combination treatment therefore strongly indicate that the combination of EZH2i/ATMi leads to higher levels of unrepaired DSBs [70]. Mak et al. describe a synthetic lethal interaction of ATMi/PARPi as both inhibitors individually cause transient DNA damage, but when combined result in high levels of yH2AX and G2-M arrest, followed by apoptosis [122]. Based on the previously assessed role of EZH2 in breast cancer, it would also be interesting to evaluate the level of HR by staining GSK126 treated *BRCA1*-deficient cells for RAD51 foci [70]. Adapting the results of Chang et al. to our setting, we would expect an increase in RAD51 foci upon EZH2 inhibition, indicating a shift in

DDR towards HR. Consequently, this might be synthetic lethal when HR is abrogated due to *BRCA1*-deficiency and additional ATM inhibition [48].

Beyond the potential impact of the combination treatment on DDR, synergistic growth inhibition may also be the result of an interaction between the EZH2 protein levels and ATM expression. Naskou et al. observed a negative influence of EZH2 on ATM as loss of EZH2 led to an overactivation of ATM in ovarian cancer cell lines [123]. Responding to DNA damage upon loss of EZH2, cell cycle checkpoints can thus be initiated more efficiently, leading to a stall of proliferation that makes the cancer cells less accessible for chemotherapies that specifically target the cell's proliferation machinery [123]. Consequently, high levels of ATM and low levels of EZH2 in ovarian cancer patients are assumed to contribute to chemotherapy resistance and decreased progression-free survival [123]. Therefore, a synthetic lethal interaction between ATMi and EZH2i can be assumed [70]. Li et al. discovered phosphorylation of EZH2 by ATM and reciprocally an upregulation of EZH2 upon *ATM*-deficiency in Ataxia-telangiectasia (A-T) [124]. An increase of H3K27me$^3$ was then associated with cell cycle reentry and checkpoint abrogation. *Ezh2* knockdown in *Atm*-deficient mice consequently improved A-T symptoms and resulted in cell cycle arrest, further supporting the idea of simultaneous EZH2 and ATM inhibition as synthetic lethal partners [124]. As these approaches are based on the DNA damage machinery, the effect could consequently be enhanced upon *BRCA1*-deficiency, where an additional defect in HR might be lethal in combination with ATM inhibition. To formally prove an interaction between EZH2 and ATM as synthetic lethal partners in the setting of this study, an assessment of protein interaction between ATM and EZH2 in *BRCA1*-deficient breast cancer cell lines would be interesting [70].

As an outlook, patient-derived xenograft (PDX) murine models of *BRCA1*-deficient human breast carcinomas could be a next step to further validate this synergistic combination treatment by mimicking human conditions. As a perspective for a clinical use of this treatment, it might also be interesting to assess an impact on metastasis formation, as EZH2 is supposedly highly involved in EMT-pathways. Wang et al. describe that an increase in breast cancer metastasis upon *BRCA1*-deficiency is dependent on EZH2 [93]. Yomtoubian et al. suggest implementing EZH2 inhibition for the treatment of metastatic TNBC [102]. Another clinical application for this combination treatment could be upon PARP inhibitor resistance. Jaspers et al. found PARP inhibitor resistance in the setting of *BRCA1*-deficiency to be caused by restored HR [125]. As ATM is a key mediator of promoting HR, dual inhibition of EZH2 and ATM upon *BRCA1*-deficiency could rationalize overcoming PARP inhibitor resistance by reintroducing an abrogation of HR.

## 5.3 Combined inhibition of EZH2 and PI3K is additive *in vitro* upon *Brca1*-deficiency.

We furthermore describe a significant growth inhibition of *Brca1*-deficient breast cancer cells upon combination of EZH2 inhibition with PI3K inhibition.

BKM120 leads to a down-regulation of phosphorylated AKT protein levels (fig. 3.F). Exchanging BKM120 with alpelisib, a PI3K catalytic subunit p110 alpha (PIK3CA) inhibitor, proved PI3K target specific growth inhibition of combination treatment (fig. 8.B). For BKM120, high *in vitro* concentrations have been observed to result in off-target effects [126]. Besides that, a PI3K independent effect for *in vivo* murine models was observed above a concentration of 40mg/kg [126]. As we used lower concentrations of BKM120 in this study, the observed effects could be considered as PI3K specific. However, we did not study target specificity on a genomic level.

BKM120 is a pan class 1 PI3K inhibitor that showed efficient anti-tumor activity for hormone receptor positive metastatic breast cancers in combination with endocrine therapy during the phase III clinical trial BELLE 2 (ClinicalTrials.gov identifier NCT01610284) [127]. Due to its high toxicity profile and strong psychiatric side effects, current studies are focusing on the new generation of specific PI3K alpha isoform inhibitors, such as alpelisib [54]. Alpelisib led to good anti-tumor activity during the SOLAR1 clinical trial and is now approved for the treatment of metastatic hormone receptor positive breast cancers with *PIK3CA* mutations in combination with fulvestrant (selective estrogene receptor degrader) [128]. The PI3K pathway is known to be upregulated in various breast cancers, along with basal-like breast cancers [129]. BKM120 has been proposed to synergistically induce tumor cell death in combination with olaparib for *Brca1*-deficient cancers in various studies [130,131], as well as *Brca1*-proficient TNBC [132]. Juvekar et al. explain the synergy with an increase in yH2AX levels and simultaneous decrease of RAD51 levels as a result of BKM120 treatment [130]. In accordance with this, Oeck et al. propose AKT1 to promote NHEJ in the face of genomic stress [133]. Besides supporting DSB repair, AKT1 functions as a mediator between cell cycle arrest, apoptosis and cell survival [133]. These findings thus suggest an involvement of PI3Ki in targeting genome integrity of breast cancer cells and deliver a rational to use PI3Ki in the setting of *BRCA1*-deficiency.

Numerous studies describe a relation between high EZH2 levels and upregulated AKT activity [99,134,135]. AKT is thought to upregulate phosphorylated EZH2 levels leading to oncogenic STAT3 signaling in glioblastoma stem-like cells [134] and *KRAS* mutated NSCLC [135]. Riquelme et al. highlight a possible beneficial effect of dual EZH2 and PI3K inhibition as *AKT* depletion leads to decreased phosphorylated EZH2 levels [135]. Rizk et al. conducted *in vitro* functional analysis of dual AKT1 and EZH2 inhibition for the treatment of multiple myeloma [136]. In that

matter, they found a compensatory EZH1 upregulation resulting in high H3K27me$^3$ levels, which was driven by binding of FOXO3 to the EZH1 promoter as a consequence of abrogated AKT1 activity. The study thus points out a more effective anti-tumor activity by using AKT pathway inhibition in combination with a dual EZH2- and EZH1-inhibitor instead of GSK126 [136]. Based on this, further studies should test such dual EZH2/1 inhibitors in combination with PI3Ki to possibly gain synergistic growth inhibition due to more efficient H3K27me$^3$ depletion. Besides that *in vivo* analysis of the combination treatment with alpelisib for our *Brca1*-deficient murine model should be conducted.

## 5.4 Combination of EZH2i and panCDKi is additive upon *Brca1*-deficiency *in vitro*.

We describe an additive effect of combinatory therapy with panCDK inhibition and EZH2 inhibition for our *Brca1*-deficient breast cancer cell lines [70]. Dinaciclib is a small molecule panCDK inhibitor with most specificity towards CDK1, CDK2, CDK5 and CDK 9 inhibition [137]. We could observe a trend of down-regulated pRB levels upon dinaciclib treatment (fig. 3.G). Others describe a strong down-regulation of pRB levels after treatment with similar doses of dinaciclib *in vitro* [137]. Dinaciclib has been reported to induce apoptosis in osteosarcoma [138] and melanoma cells *in vitro* and to inhibit tumor growth of xenograft melanoma murine models *in vivo* [139]. Others state that *in vitro* apoptosis induction was dependent on TP53 expression in melanoma cells [140]. This is, however, in conflict with our murine cell lines as both *Brca1*-deficient and -proficient cell lines exhibit a *Tp53* knockdown, which thus could be a reason for insufficient growth inhibition after dinaciclib treatment.

Overexpressed CDK activity, caused by mutations of CDK regulators or hyperactive cyclines, is an emerging target for cancer therapies [141]. While CDK4/6 inhibitors are already established for the treatment of metastatic hormone receptor positive breast cancers (ClinicalTrials.gov identifier NCT01942135) [53], CDK1 inhibition is emerging as a target for TNBCs [142]. Dinaciclib is being investigated for metastatic breast cancer as monotherapy [143]. A randomized phase II clinical trial for metastatic breast cancer found insufficient anti-tumor activity in comparison to standard chemotherapy with capecitabine while the drug was tolerated well [144]. However, since dinaciclib monotherapy does not seem to reach sufficient anti-tumor activity in clinical trials, there is a tendency to use it in combination therapies [143]. A phase I study found the combination of dinaciclib and epirubicin for the treatment of metastatic TNBC to be toxic (ClinicalTrials.gov identifier NCT01624441) [145]. Nevertheless, dinaciclib is currently subject to investigation in a phase I study for the treatment of metastatic TNBCs in combination with pembrolizumab (PD-1 inhibitor) (ClinicalTrials.gov identifier NCT01676753) [146]. The, so far, rather negative trial

results concerning dinaciclib for the treatment of TNBCs don't suggest an incentive for further *in vivo* analysis of this combination treatment.

Recently, an evolving number of molecules have been identified as synthetic lethal partners of CDKs, such as MYC, K-RAS, PI3K and PARP [141]. This is particularly interesting as CDKs appear to have an impact on maintaining genome integrity by contributing to DNA repair. CDK2 has been found to contribute to the repair of radiation-induced DSBs [147] and CDK1 activity has been pinpointed to start-off HR by enabling ssDNA resection [148]. In the face of the described correlation between CDK activity and DDR in literature and our findings of the synergy screen [70], we hypothesized that a possible new synthetic lethal partner of CDKs could be BRCA1. This is supported by findings of Deans et al., who describe a sensitivity of *BRCA1*-deficient cancer cells to CDK2 inhibition due to down-regulation of CHK1, TP53 and RAD51 signaling in the face of DNA damage [149]. In accordance with this, others found that CDK1 inhibition compromises HR by deregulating BRCA1 and RAD51 signaling, leaving *BRCA1*-proficient cancer cells more sensitive to PARP inhibition and enabling *BRCA1*-deficient cancers to overcome PARP inhibitor resistance [142,150]. Besides the correlation of CDKs and DDR, growing evidence also links the cell cycle regulatory kinases to epigenetic gene suppression. Both CDK1 and CDK2 evidently phosphorylate EZH2 at its activating site and thus enhance global H3K27me$^3$ levels [151]. Therefore, CDKs can be assumed to promote EZH2 mediated oncogenic signaling, thus providing for an incentive of dual EZH2 and CDK inhibition in our study.

However, we could not prove the combination treatment of GSK126 and dinaciclib to be of synergistic character. We can therefore only assume that the significant growth inhibition of combined EZH2i/panCDKi upon *Brca1*-deficiency is due to an additive effect. Furthermore, we cannot support scientific evidence of previous studies that claim a synthetic lethal interaction of CDKs and BRCA1. Treatment with single agent dinaciclib did not sufficiently inhibit growth of *Brca1*-deficient cancer cells *in vitro*. Our data, however, indicate that combined EZH2i/panCDKi is more effective upon *Brca1*-deficiency than *Brca1*-proficiency. As an outlook, we therefore suggest that further analyses will be necessary to determine specific CDKs responsible for a potential synthetic lethal interaction with EZH2 in *BRCA1*-deficienct breast cancer cells. Once these are identified, a more specific targeted and less toxic compound should be used.

## 5.5 Conclusion

Conclusively, we hereby found a novel synergistic combination of EZH2i/ATMi for the treatment of *BRCA1*-mutant breast cancers as it results in significant synergistic growth inhibition *in vitro* and prolongs progression-free survival *in vivo* [70]. Indicated by a significant increase of yH2AX foci for the combination of EZH2 inhibition and ATM inhibition, a potential explanation for the observed synergy could be higher levels of unrepaired DSB occurring in the face of impaired HR due to *BRCA1*-deficiency [70]. To further establish this synergy, dual EZH2- and ATM-inhibition should be administered in PDX murine models in order to mimic the human setting.

The rational of combining EZH2i/PI3Ki for the treatment of *BRCA1*-deficient breast cancer also seems to be promising. However, our *in vitro* data suggest an additive effect of combined GSK126 (EZH2i) and BKM120 (PI3Ki) treatment. The PI3Ki alpelisib, which inhibits the alpha unit of PI3K specifically, showed comparable *in vitro* anti-tumor activity to BKM120 in our study. In this context, further *in vivo* validation studies with alpelisib should be conducted, as alpelisib was recently approved for breast cancer therapy.

Combined EZH2i/panCDKi proved to not be synergistic for our *Brca1*-deficient cell lines. This indicates that specific CDKs, which are mechanistically involved with EZH2, should be analyzed to target *BRCA1*-deficiency more efficiently.

# 6  LITERATURE

1.    The global challenge of cancer. *Nat Cancer* 2020; 1(1): 1-2.
2.    Weinberg RA. The biology of cancer. Second edition. ed. New York: Garland Science, Taylor & Francis Group; 2014.
3.    Hanahan D, Weinberg RA. The hallmarks of cancer. *Cell* 2000; 100(1): 57-70.
4.    Hanahan D, Weinberg RA. Hallmarks of Cancer: The Next Generation. *Cell* 2011; 144(5): 646-74.
5.    Kalimutho M, Nones K, Srihari S, Duijf PHG, Waddell N, Khanna KK. Patterns of Genomic Instability in Breast Cancer. *Trends Pharmacol Sci* 2019; 40(3): 198-211.
6.    Negrini S, Gorgoulis VG, Halazonetis TD. Genomic instability--an evolving hallmark of cancer. *Nat Rev Mol Cell Biol* 2010; 11(3): 220-8.
7.    Balmain A. Cancer genetics: from Boveri and Mendel to microarrays. *Nat Rev Cancer* 2001; 1(1): 77-82.
8.    Weinstein IB, Joe A. Oncogene addiction. *Cancer Research* 2008; 68(9): 3077-80.
9.    Weinberg RA. The Retinoblastoma Protein and Cell-Cycle Control. *Cell* 1995; 81(3): 323-30.
10.   Knudson AG. Mutation and Cancer - Statistical Study of Retinoblastoma. *P Natl Acad Sci USA* 1971; 68(4): 820-&.
11.   Petrucelli N, Daly MB, Feldman GL. Hereditary breast and ovarian cancer due to mutations in BRCA1 and BRCA2. *Genet Med* 2010; 12(5): 245-59.
12.   Lane DP. Cancer - P53, Guardian of the Genome. *Nature* 1992; 358(6381): 15-6.
13.   Esteller M, Corn PG, Baylin SB, Herman JG. A gene hypermethylation profile of human cancer. *Cancer Research* 2001; 61(8): 3225-9.
14.   Sparmann A, van Lohuizen M. Polycomb silencers control cell fate, development and cancer. *Nat Rev Cancer* 2006; 6(11): 846-56.
15.   Comet I, Riising EM, Leblanc B, Helin K. Maintaining cell identity: PRC2-mediated regulation of transcription and cancer. *Nat Rev Cancer* 2016; 16(12): 803-10.
16.   Riising EM, Comet I, Leblanc B, Wu XD, Johansen JV, Helin K. Gene Silencing Triggers Polycomb Repressive Complex 2 Recruitment to CpG Islands Genome Wide. *Molecular Cell* 2014; 55(3): 347-60.
17.   Massague J. G1 cell-cycle control and cancer. *Nature* 2004; 432(7015): 298-306.
18.   Yu QY, Geng Y, Sicinski P. Specific protection against breast cancers by cyclin D1 ablation. *Nature* 2001; 411(6841): 1017-21.
19.   Reinhardt HC, Yaffe MB. Phospho-Ser/Thr-binding domains: navigating the cell cycle and DNA damage response. *Nat Rev Mol Cell Biol* 2013; 14(9): 563-80.
20.   Hannon GJ, Beach D. P15(Ink4b) Is a Potential Effector of Tgf-Beta-Induced Cell-Cycle Arrest. *Nature* 1994; 371(6494): 257-61.
21.   Reinhardt HC, Yaffe MB. Kinases that control the cell cycle in response to DNA damage: Chk1, Chk2, and MK2. *Current Opinion in Cell Biology* 2009; 21(2): 245-55.
22.   Keyomarsi K, Tucker SL, Buchholz TA, et al. Cyclin E and survival in patients with breast cancer. *New Engl J Med* 2002; 347(20): 1566-75.
23.   Luo J, Manning BD, Cantley LC. Targeting the PI3K-Akt pathway in human cancer: rationale and promise. *Cancer Cell* 2003; 4(4): 257-62.
24.   Liang J, Zubovitz J, Petrocelli T, et al. PKB/Akt phosphorylates p27, impairs nuclear import of p27 and opposes p27-mediated G1 arrest. *Nature Medicine* 2002; 8(10): 1153-60.
25.   Olivier M, Hollstein M, Hainaut P. TP53 Mutations in Human Cancers: Origins, Consequences, and Clinical Use. *Csh Perspect Biol* 2010; 2(1).
26.   Lord CJ, Ashworth A. The DNA damage response and cancer therapy. *Nature* 2012; 481(7381): 287-94.
27.   Kinner A, Wu W, Staudt C, Iliakis G. Gamma-H2AX in recognition and signaling of DNA double-strand breaks in the context of chromatin. *Nucleic Acids Res* 2008; 36(17): 5678-94.

28. Shiloh Y. ATM and related protein kinases: Safeguarding genome integrity. *Nat Rev Cancer* 2003; 3(3): 155-68.

29. Sun YR, McCorvie TJ, Yates LA, Zhang XD. Structural basis of homologous recombination. *Cell Mol Life Sci* 2020; 77(1): 3-18.

30. Isono M, Niimi A, Oike T, et al. BRCA1 Directs the Repair Pathway to Homologous Recombination by Promoting 53BP1 Dephosphorylation. *Cell Reports* 2017; 18(2): 520-32.

31. Helleday T. Homologous recombination in cancer development, treatment and development of drug resistance. *Carcinogenesis* 2010; 31(6): 955-60.

32. Fischbach MA. Combination therapies for combating antimicrobial resistance. *Curr Opin Microbiol* 2011; 14(5): 519-23.

33. Erber J, Steiner JD, Isensee J, et al. Dual Inhibition of GLUT1 and the ATR/CHK1 Kinase Axis Displays Synergistic Cytotoxicity in KRAS-Mutant Cancer Cells. *Cancer Research* 2019; 79(19): 4855-68.

34. Frei E, 3rd, Karon M, Levin RH, et al. The effectiveness of combinations of antileukemic agents in inducing and maintaining remission in children with acute leukemia. *Blood* 1965; 26(5): 642-56.

35. Kummar S, Chen HX, Wright J, et al. Utilizing targeted cancer therapeutic agents in combination: novel approaches and urgent requirements. *Nat Rev Drug Discov* 2010; 9(11): 843-56.

36. World-Health-Organization. WHO position paper on mammography screening. World Heath Organization; 2014.

37. Koch-Institut R, e.V. GdeKiD. Krebs in Deutschland 2015/2016. 2019.

38. Eisemann N, Waldmann A, Katalinic A. Epidemiology of Breast Cancer - Current Figures and Trends. *Geburtshilfe Frauenheilkd* 2013; 73(2): 130-5.

39. AGO-Breast-Committee. Diagnosis and Treatment of Patients with Primary and Metastatic Breast Cancer. Recommendations 2020. 2020. https://www.ago-online.de/fileadmin/ago-online/downloads/_leitlinien/kommission_mamma/2021/Alle_aktuellen_Empfehlungen_2021.pdf (Last consulted: March, 20th, 2021) (accessed 25.03.2020.

40. Leitlinienprogramm-Onkologie. S3-Leitlinie Früherkennung, Diagnose, Therapie und Nachsorge des Mammakarzinoms. 2020. https://www.leitlinienprogramm-onkologie.de/leitlinien/mammakarzinom/ (Last consulted: March, 10th, 2020) (accessed AWMF Registernummer: 032-045OL.

41. Mavaddat N, Rebbeck TR, Lakhani SR, Easton DF, Antoniou AC. Incorporating tumour pathology information into breast cancer risk prediction algorithms. *Breast Cancer Research* 2010; 12(3).

42. Tan PH, Ellis I, Allison K, et al. The 2019 World Health Organization classification of tumours of the breast. *Histopathology* 2020; 77(2): 181-5.

43. Skibinski A, Kuperwasser C. The origin of breast tumor heterogeneity. *Oncogene* 2015; 34(42): 5309-16.

44. Holm K, Hegardt C, Staaf J, et al. Molecular subtypes of breast cancer are associated with characteristic DNA methylation patterns. *Breast Cancer Res* 2010; 12(3): R36.

45. Coates AS, Winer EP, Goldhirsch A, et al. Tailoring therapies-improving the management of early breast cancer: St Gallen International Expert Consensus on the Primary Therapy of Early Breast Cancer 2015. *Annals of Oncology* 2015; 26(8): 1533-46.

46. Foulkes WD, Smith IE, Reis-Filho JS. Triple-negative breast cancer. *N Engl J Med* 2010; 363(20): 1938-48.

47. Lakhani SR, Reis-Filho JS, Fulford L, et al. Prediction of BRCA1 status in patients with breast cancer using estrogen receptor and basal phenotype. *Clin Cancer Res* 2005; 11(14): 5175-80.

48. Chang CJ, Yang JY, Xia WY, et al. EZH2 Promotes Expansion of Breast Tumor Initiating Cells through Activation of RAF1-beta-Catenin Signaling. *Cancer Cell* 2011; 19(1): 86-100.

49. Sarrio D, Rodriguez-Pinilla SM, Hardisson D, Cano A, Moreno-Bueno G, Palacios J. Epithelial-mesenchymal transition in breast cancer relates to the basal-like phenotype. *Cancer Res* 2008; 68(4): 989-97.

50. von Minckwitz G, Schneeweiss A, Loibl S, et al. Neoadjuvant carboplatin in patients with triple-negative and HER2-positive early breast cancer (GeparSixto; GBG 66): a randomised phase 2 trial. *Lancet Oncol* 2014; 15(7): 747-56.

51. Gluz O, Nitz U, Liedtke C, et al. Comparison of Neoadjuvant Nab-Paclitaxel+Carboplatin vs Nab-Paclitaxel+Gemcitabine in Triple-Negative Breast Cancer: Randomized WSG-ADAPT-TN Trial Results. *J Natl Cancer Inst* 2018; 110(6): 628-37.

52. Cortazar P, Zhang L, Untch M, et al. Pathological complete response and long-term clinical benefit in breast cancer: the CTNeoBC pooled analysis. *Lancet* 2014; 384(9938): 164-72.

53. Loibl S, Turner NC, Ro J, et al. Palbociclib (PAL) in combination with fulvestrant (F) in pre-/peri-menopausal (PreM) women with metastatic breast cancer (MBC) and prior progression on endocrine therapy - results from Paloma-3. *J Clin Oncol* 2016; 34(15).

54. Andre F, Ciruelos EM, Juric D, et al. Alpelisib plus fulvestrant for PIK3CA-mutated, hormone receptor-positive, human epidermal growth factor receptor-2-negative advanced breast cancer: final overall survival results from SOLAR-1. *Ann Oncol* 2021; 32(2): 208-17.

55. Robert NJ, Dieras V, Glaspy J, et al. RIBBON-1: randomized, double-blind, placebo-controlled, phase III trial of chemotherapy with or without bevacizumab for first-line treatment of human epidermal growth factor receptor 2-negative, locally recurrent or metastatic breast cancer. *J Clin Oncol* 2011; 29(10): 1252-60.

56. Schmid P, Adams S, Rugo HS, et al. Atezolizumab and Nab-Paclitaxel in Advanced Triple-Negative Breast Cancer. *N Engl J Med* 2018; 379(22): 2108-21.

57. Nielsen FC, Hansen TV, Sorensen CS. Hereditary breast and ovarian cancer: new genes in confined pathways. *Nat Rev Cancer* 2016; 16(9): 599-612.

58. Engel C, Rhiem K, Hahnen E, et al. Prevalence of pathogenic BRCA1/2 germline mutations among 802 women with unilateral triple-negative breast cancer without family cancer history. *Bmc Cancer* 2018; 18.

59. Paluch-Shimon S, Cardoso F, Sessa C, et al. Prevention and screening in BRCA mutation carriers and other breast/ovarian hereditary cancer syndromes: ESMO Clinical Practice Guidelines for cancer prevention and screening. *Ann Oncol* 2016; 27(suppl 5): v103-v10.

60. Stevens KN, Vachon CM, Couch FJ. Genetic Susceptibility to Triple-Negative Breast Cancer. *Cancer Res* 2013; 73(7): 2025-30.

61. Foulkes WD, Stefansson IM, Chappuis PO, et al. Germline BRCA1 mutations and a basal epithelial phenotype in breast cancer. *J Natl Cancer Inst* 2003; 95(19): 1482-5.

62. Turner NC, Reis JS, Russell AM, et al. BRCA1 dysfunction in sporadic basal-like breast cancer. *Oncogene* 2007; 26(14): 2126-32.

63. Turner N, Tutt A, Ashworth A. Hallmarks of 'BRCAness' in sporadic cancers. *Nat Rev Cancer* 2004; 4(10): 814-9.

64. Schouten PC, Grigoriadis A, Kuilman T, et al. Robust BRCA1-like classification of copy number profiles of samples repeated across different datasets and platforms. *Molecular Oncology* 2015; 9(7): 1274-86.

65. Puppe J, Opdam M, Schouten PC, et al. EZH2 Is Overexpressed in BRCA1-like Breast Tumors and Predictive for Sensitivity to High-Dose Platinum-Based Chemotherapy. *Clin Cancer Res* 2019; 25(14): 4351-62.

66. Schouten PC, Marme F, Aulmann S, et al. Breast Cancers with a BRCA1-like DNA Copy Number Profile Recur Less Often Than Expected after High-Dose Alkylating Chemotherapy. *Clinical Cancer Research* 2015; 21(4): 763-70.

67. Na B, Yu X, Wither T, et al. Therapeutic targeting of BRCA1 and TP53 mutant breast cancer through mutant p53 reactivation. *Cancer Research* 2019; 79(4).

68. Brachova P, Mueting SR, Carlson MJ, et al. TP53 oncomorphic mutations predict resistance to platinum- and taxane-based standard chemotherapy in patients diagnosed with advanced serous ovarian carcinoma. *Int J Oncol* 2015; 46(2): 607-18.

69. Liu X, Holstege H, van der Gulden H, et al. Somatic loss of BRCA1 and p53 in mice induces mammary tumors with features of human BRCA1-mutated basal-like breast cancer. *Proc Natl Acad Sci U S A* 2007; 104(29): 12111-6.

70. Ratz L, Brambillasca C, Bartke L, et al. Combined inhibition of EZH2 and ATM is synthetic lethal in BRCA1-deficient breast cancer. *Breast Cancer Research* 2022; 24(1).

71. Hill DP, Harper A, Malcolm J, et al. Cisplatin-resistant triple-negative breast cancer subtypes: multiple mechanisms of resistance. *Bmc Cancer* 2019; 19(1): 1039.

72. Byrski T, Huzarski T, Dent R, et al. Pathologic complete response to neoadjuvant cisplatin in BRCA1-positive breast cancer patients. *Breast Cancer Res Treat* 2014; 147(2): 401-5.

73. Tutt A, Tovey H, Cheang MCU, et al. Carboplatin in BRCA1/2-mutated and triple-negative breast cancer BRCAness subgroups: the TNT Trial. *Nat Med* 2018; 24(5): 628-37.

74. Hahnen E, Lederer B, Hauke J, et al. Germline Mutation Status, Pathological Complete Response, and Disease-Free Survival in Triple-Negative Breast Cancer: Secondary Analysis of the GeparSixto Randomized Clinical Trial. *JAMA Oncol* 2017; 3(10): 1378-85.

75. Lord CJ, Ashworth A. The DNA damage response and cancer therapy. *Nature* 2012; 481(7381): 287-94.

76. Farmer H, McCabe N, Lord CJ, et al. Targeting the DNA repair defect in BRCA mutant cells as a therapeutic strategy. *Nature* 2005; 434(7035): 917-21.

77. Lord CJ, Ashworth A. Targeted therapy for cancer using PARP inhibitors. *Curr Opin Pharmacol* 2008; 8(4): 363-9.

78. Fong PC, Boss DS, Yap TA, et al. Inhibition of Poly(ADP-Ribose) Polymerase in Tumors from BRCA Mutation Carriers. *New Engl J Med* 2009; 361(2): 123-34.

79. Leitlinienprogramm Onkologie (Deutsche Krebsgesellschaft DK, AWMF). S3-Leitlinie Diagnostik, Therapie und Nachsorge maligner Ovarialtumoren. 2022. https://www.leitlinienprogramm-onkologie.de/fileadmin/user_upload/LL_Ovarialkarzinom_Langversion_5.1.pdf (accessed 19.01.2023 2022).

80. Litton JK, Rugo HS, Ettl J, et al. Talazoparib in Patients with Advanced Breast Cancer and a Germline BRCA Mutation. *N Engl J Med* 2018; 379(8): 753-63.

81. Tutt ANJ, Garber JE, Kaufman B, et al. Adjuvant Olaparib for Patients with BRCA1- or BRCA2-Mutated Breast Cancer. *N Engl J Med* 2021; 384(25): 2394-405.

82. Li BH, Chng WJ. EZH2 abnormalities in lymphoid malignancies: underlying mechanisms and therapeutic implications. *J Hematol Oncol* 2019; 12(1).

83. Cao R, Wang L, Wang H, et al. Role of histone H3 lysine 27 methylation in Polycomb-group silencing. *Science* 2002; 298(5595): 1039-43.

84. Margueron R, Reinberg D. The Polycomb complex PRC2 and its mark in life. *Nature* 2011; 469(7330): 343-9.

85. Whitcomb SJ, Basu A, Allis CD, Bernstein E. Polycomb Group proteins: an evolutionary perspective. *Trends Genet* 2007; 23(10): 494-502.

86. Italiano A. Role of the EZH2 histone methyltransferase as a therapeutic target in cancer. *Pharmacol Therapeut* 2016; 165: 26-31.

87. Varambally S, Dhanasekaran SM, Zhou M, et al. The polycomb group protein EZH2 is involved in progression of prostate cancer. *Nature* 2002; 419(6907): 624-9.

88. Kleer CG, Cao Q, Varambally S, et al. EZH2 is a marker of aggressive breast cancer and promotes neoplastic transformation of breast epithelial cells. *P Natl Acad Sci USA* 2003; 100(20): 11606-11.

89. Bachmann IM, Halvorsen OJ, Collett K, et al. EZH2 expression is associated with high proliferation rate and aggressive tumor subgroups in cutaneous melanoma and cancers

of the endometrium, prostate, and breast. *Journal of Clinical Oncology* 2006; 24(2): 268-73.

90. Cao Q, Yu J, Dhanasekaran SM, et al. Repression of E-cadherin by the polycomb group protein EZH2 in cancer. *Oncogene* 2008; 27(58): 7274-84.

91. Tiwari N, Tiwari VK, Waldmeier L, et al. Sox4 Is a Master Regulator of Epithelial-Mesenchymal Transition by Controlling Ezh2 Expression and Epigenetic Reprogramming. *Cancer Cell* 2013; 23(6): 768-83.

92. Ito T, Teo YV, Evans SA, Neretti N, Sedivy JM. Regulation of Cellular Senescence by Polycomb Chromatin Modifiers through Distinct DNA Damage-and Histone Methylation-Dependent Pathways. *Cell Reports* 2018; 22(13): 3480-92.

93. Wang L, Zeng XZ, Chen S, et al. BRCA1 is a negative modulator of the PRC2 complex. *Embo J* 2013; 32(11): 1584-97.

94. Campbell S, Ismail IH, Young LC, Poirier GG, Hendzel MJ. Polycomb repressive complex 2 contributes to DNA double-strand break repair. *Cell Cycle* 2013; 12(16): 2675-83.

95. Song XJ, Gao TT, Wang NY, et al. Selective inhibition of EZH2 by ZLD1039 blocks H3K27methylation and leads to potent anti-tumor activity in breast cancer. *Sci Rep-Uk* 2016; 6.

96. Wang L, Huang HJ. EZH2 takes the stage when BRCA1 loses. *Cell Cycle* 2013; 12(23): 3575-6.

97. Pietersen AM, Horlings HM, Hauptmann M, et al. EZH2 and BMI1 inversely correlate with prognosis and TP53 mutation in breast cancer. *Breast Cancer Research* 2008; 10(6).

98. Lee ST, Li Z, Wu Z, et al. Context-specific regulation of NF-kappaB target gene expression by EZH2 in breast cancers. *Mol Cell* 2011; 43(5): 798-810.

99. Gonzalez ME, DuPrie ML, Krueger H, et al. Histone methyltransferase EZH2 induces Akt-dependent genomic instability and BRCA1 inhibition in breast cancer. *Cancer Res* 2011; 71(6): 2360-70.

100. Puppe J, Drost R, Liu X, et al. BRCA1-deficient mammary tumor cells are dependent on EZH2 expression and sensitive to Polycomb Repressive Complex 2-inhibitor 3-deazaneplanocin A. *Breast Cancer Res* 2009; 11(4): R63.

101. Hirukawa A, Smith HW, Zuo D, et al. Targeting EZH2 reactivates a breast cancer subtype-specific anti-metastatic transcriptional program. *Nat Commun* 2018; 9(1): 2547.

102. Yomtoubian S, Lee SB, Verma A, et al. Inhibition of EZH2 Catalytic Activity Selectively Targets a Metastatic Subpopulation in Triple-Negative Breast Cancer. *Cell Rep* 2020; 30(3): 755-70 e6.

103. McCabe MT, Ott HM, Ganji G, et al. EZH2 inhibition as a therapeutic strategy for lymphoma with EZH2-activating mutations. *Nature* 2012; 492(7427): 108-12.

104. Italiano A, Soria JC, Toulmonde M, et al. Tazemetostat, an EZH2 inhibitor, in relapsed or refractory B-cell non-Hodgkin lymphoma and advanced solid tumours: a first-in-human, open-label, phase 1 study. *Lancet Oncol* 2018; 19(5): 649-59.

105. Pawlyn C, Bright MD, Buros AF, et al. Overexpression of EZH2 in multiple myeloma is associated with poor prognosis and dysregulation of cell cycle control. *Blood Cancer J* 2017; 7.

106. Gounder M, Schoffski P, Jones RL, et al. Tazemetostat in advanced epithelioid sarcoma with loss of INI1/SMARCB1: an international, open-label, phase 2 basket study. *Lancet Oncol* 2020; 21(11): 1423-32.

107. Silver DP, Dimitrov SD, Feunteun J, et al. Further evidence for BRCA1 communication with the inactive X chromosome. *Cell* 2007; 128(5): 991-1002.

108. Niyazi M, Niyazi I, Belka C. Counting colonies of clonogenic assays by using densitometric software. *Radiat Oncol* 2007; 2: 4.

109. Herold MJ, van den Brandt J, Seibler J, Reichardt HM. Inducible and reversible gene silencing by stable integration of an shRNA-encoding lentivirus in transgenic rats. *P Natl Acad Sci USA* 2008; 105(47): 18507-12.

110. Dobin A, Davis CA, Schlesinger F, et al. STAR: ultrafast universal RNA-seq aligner. *Bioinformatics* 2013; 29(1): 15-21.
111. Liao Y, Smyth GK, Shi W. featureCounts: an efficient general purpose program for assigning sequence reads to genomic features. *Bioinformatics* 2014; 30(7): 923-30.
112. Anders S, Huber W. Differential expression analysis for sequence count data. *Genome Biol* 2010; 11(10): R106.
113. Ianevski A, Giri AK, Aittokallio T. SynergyFinder 2.0: visual analytics of multi-drug combination synergies. *Nucleic Acids Res* 2020; 48(W1): W488-W93.
114. Yamaguchi H, Du Y, Nakai K, et al. EZH2 contributes to the response to PARP inhibitors through its PARP-mediated poly-ADP ribosylation in breast cancer. *Oncogene* 2018; 37(2): 208-17.
115. Puppe J, ter Brugge P, Seressi M, et al. Combination therapy of the EZH2 inhibitor GSK126 and the PARP inhibitor Olaparib shows in vivo synergy in a patient-derived xenograft model of BRCA1-deficient breast cancer. *Geburtshilfe Frauenheilkd* 2014; 74(S 01): FV_02_.
116. Golding SE, Rosenberg E, Valerie N, et al. Improved ATM kinase inhibitor KU-60019 radiosensitizes glioma cells, compromises insulin, AKT and ERK prosurvival signaling, and inhibits migration and invasion. *Molecular Cancer Therapeutics* 2009; 8(10): 2894-902.
117. Jachimowicz RD, Beleggia F, Isensee J, et al. UBQLN4 Represses Homologous Recombination and Is Overexpressed in Aggressive Tumors. *Cell* 2019; 176(3): 505-19 e22.
118. Kumari K, Das B, Adhya AK, Rath AK, Mishra SK. Genome-wide expression analysis reveals six contravened targets of EZH2 associated with breast cancer patient survival. *Sci Rep* 2019; 9(1): 1974.
119. Reddy VP, Sykes A, Colclough N, et al. A preclinical PK/PD model based on a mouse glioblastoma survival model for AZD1390, a novel, brain-penetrant ATM kinase inhibitor, to predict the inhibition of DNA damage response induced by radiation and the human efficacious dose. *Cancer Res* 2019; 79(13).
120. Durant ST, Zheng L, Wang Y, et al. The brain-penetrant clinical ATM inhibitor AZD1390 radiosensitizes and improves survival of preclinical brain tumor models. *Sci Adv* 2018; 4(6): eaat1719.
121. Ngoi NYL, Pham MM, Tan DSP, Yap TA. Targeting the replication stress response through synthetic lethal strategies in cancer medicine. *Trends Cancer* 2021; 7(10): 930-57.
122. Mak JPY, Ma HT, Poon RYC. Synergism between ATM and PARP1 inhibition involves DNA damage and abrogating the G2 DNA damage checkpoint. *Mol Cancer Ther* 2019.
123. Naskou J, Beiter Y, van Rensburg R, et al. EZH2 Loss Drives Resistance to Carboplatin and Paclitaxel in Serous Ovarian Cancers Expressing ATM. *Mol Cancer Res* 2020; 18(2): 278-86.
124. Li J, Hart RP, Mallimo EM, Swerdel MR, Kusnecov AW, Herrup K. EZH2-mediated H3K27 trimethylation mediates neurodegeneration in ataxia-telangiectasia. *Nat Neurosci* 2013; 16(12): 1745-53.
125. Jaspers JE, Kersbergen A, Boon U, et al. Loss of 53BP1 causes PARP inhibitor resistance in Brca1-mutated mouse mammary tumors. *Cancer Discov* 2013; 3(1): 68-81.
126. Brachmann SM, Kleylein-Sohn J, Gaulis S, et al. Characterization of the mechanism of action of the pan class I PI3K inhibitor NVP-BKM120 across a broad range of concentrations. *Mol Cancer Ther* 2012; 11(8): 1747-57.
127. Baselga J, Im SA, Iwata H, et al. Buparlisib plus fulvestrant versus placebo plus fulvestrant in postmenopausal, hormone receptor-positive, HER2-negative, advanced breast cancer (BELLE-2): a randomised, double-blind, placebo-controlled, phase 3 trial. *Lancet Oncol* 2017; 18(7): 904-16.
128. Andre F, Ciruelos E, Rubovszky G, et al. Alpelisib for PIK3CA-Mutated, Hormone Receptor-Positive Advanced Breast Cancer. *N Engl J Med* 2019; 380(20): 1929-40.

129. Marty B, Maire V, Gravier E, et al. Frequent PTEN genomic alterations and activated phosphatidylinositol 3-kinase pathway in basal-like breast cancer cells. *Breast Cancer Res* 2008; 10(6): R101.

130. Juvekar A, Burga LN, Hu H, et al. Combining a PI3K inhibitor with a PARP inhibitor provides an effective therapy for BRCA1-related breast cancer. *Cancer Discov* 2012; 2(11): 1048-63.

131. Kimbung S, Biskup E, Johansson I, et al. Co-targeting of the PI3K pathway improves the response of BRCA1 deficient breast cancer cells to PARP1 inhibition. *Cancer Lett* 2012; 319(2): 232-41.

132. Ibrahim YH, Garcia-Garcia C, Serra V, et al. PI3K inhibition impairs BRCA1/2 expression and sensitizes BRCA-proficient triple-negative breast cancer to PARP inhibition. *Cancer Discov* 2012; 2(11): 1036-47.

133. Oeck S, Al-Refae K, Riffkin H, et al. Activating Akt1 mutations alter DNA double strand break repair and radiosensitivity. *Sci Rep-Uk* 2017; 7.

134. Kim E, Kim M, Woo DH, et al. Phosphorylation of EZH2 activates STAT3 signaling via STAT3 methylation and promotes tumorigenicity of glioblastoma stem-like cells. *Cancer Cell* 2013; 23(6): 839-52.

135. Riquelme E, Behrens C, Lin HY, et al. Modulation of EZH2 Expression by MEK-ERK or PI3K-AKT Signaling in Lung Cancer Is Dictated by Different KRAS Oncogene Mutations. *Cancer Research* 2016; 76(3): 675-85.

136. Rizk M, Rizq O, Oshima M, et al. Akt inhibition synergizes with polycomb repressive complex 2 inhibition in the treatment of multiple myeloma. *Cancer Sci* 2019; 110(12): 3695-707.

137. Parry D, Guzi T, Shanahan F, et al. Dinaciclib (SCH 727965), a novel and potent cyclin-dependent kinase inhibitor. *Mol Cancer Ther* 2010; 9(8): 2344-53.

138. Fu W, Ma L, Chu B, et al. The cyclin-dependent kinase inhibitor SCH 727965 (dinacliclib) induces the apoptosis of osteosarcoma cells. *Mol Cancer Ther* 2011; 10(6): 1018-27.

139. Abdullah C, Wang X, Becker D. Expression analysis and molecular targeting of cyclin-dependent kinases in advanced melanoma. *Cell Cycle* 2011; 10(6): 977-88.

140. Desai BM, Villanueva J, Nguyen TT, et al. The anti-melanoma activity of dinaciclib, a cyclin-dependent kinase inhibitor, is dependent on p53 signaling. *PLoS One* 2013; 8(3): e59588.

141. Vymetalova L, Krystof V. Potential Clinical Uses of CDK Inhibitors: Lessons from Synthetic Lethality Screens. *Med Res Rev* 2015; 35(6): 1156-74.

142. Johnson N, Li YC, Walton ZE, et al. Compromised CDK1 activity sensitizes BRCA-proficient cancers to PARP inhibition. *Nat Med* 2011; 17(7): 875-82.

143. Cicenas J, Kalyan K, Sorokinas A, et al. Highlights of the Latest Advances in Research on CDK Inhibitors. *Cancers (Basel)* 2014; 6(4): 2224-42.

144. Mita MM, Joy AA, Mita A, et al. Randomized phase II trial of the cyclin-dependent kinase inhibitor dinaciclib (MK-7965) versus capecitabine in patients with advanced breast cancer. *Clin Breast Cancer* 2014; 14(3): 169-76.

145. Mitri Z, Karakas C, Wei CM, et al. A phase 1 study with dose expansion of the CDK inhibitor dinaciclib (SCH 727965) in combination with epirubicin in patients with metastatic triple negative breast cancer. *Invest New Drug* 2015; 33(4): 890-4.

146. Chien AJ, Gliwa AS, Rahmaputri S, et al. A phase Ib trial of the cyclin-dependent kinase inhibitor dinaciclib (dina) in combination with pembrolizumab (P) in patients with advanced triple-negative breast cancer (TNBC) and response correlation with MYC-overexpression. *Journal of Clinical Oncology* 2020; 38(15).

147. Muller-Tidow C, Ji P, Diederichs S, et al. The cyclin A1-CDK2 complex regulates DNA double-strand break repair. *Mol Cell Biol* 2004; 24(20): 8917-28.

148. Aylon Y, Kupiec M. Cell cycle-dependent regulation of double-strand break repair: a role for the CDK. *Cell Cycle* 2005; 4(2): 259-61.

149. Deans AJ, Khanna KK, McNees CJ, Mercurio C, Heierhorst J, McArthur GA. Cyclin-dependent kinase 2 functions in normal DNA repair and is a therapeutic target in BRCA1-deficient cancers. *Cancer Res* 2006; 66(16): 8219-26.

150.   Johnson SF, Cruz C, Greifenberg AK, et al. CDK12 Inhibition Reverses De Novo and Acquired PARP Inhibitor Resistance in BRCA Wild-Type and Mutated Models of Triple-Negative Breast Cancer. *Cell Reports* 2016; 17(9): 2367-81.

151.   Chen S, Bohrer LR, Rai AN, et al. Cyclin-dependent kinases regulate epigenetic gene silencing through phosphorylation of EZH2. *Nat Cell Biol* 2010; 12(11): 1108-14.

# 7  APPENDIX

## 7.1  Supplementary figure
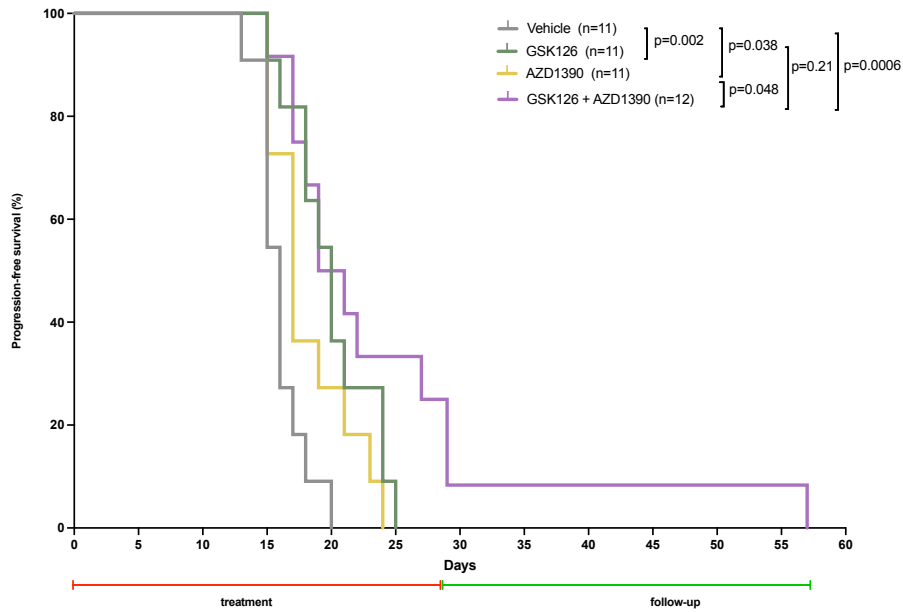


**Figure S1. Combination treatment of murine breast tumors with GSK126 and AZD1390 prolongs progression-free survival of *Brca1*-deficient mice.**

Kaplan-Meier-Curve for mice treated (murine model *K14Cre;Brca1$^{fl/fl}$;Tp53$^{fl/fl}$*) with DMSO control (Vehicle), GSK126 (150 mg/kg), AZD1390 (2 x 20mg/kg) or combined GSK216 and AZD1390. Mice were treated up to the timepoint of 28 days and then observed as a follow-up until 60 days after the first treatment. The statistical survival-analysis was calculated with Log-rank (Mantel-Cox) test with GraphPad Prism (Version 8.0, Graphpad Software, Inc.). This figure is adapted from Ratz et al. with kind permission [70]. Experiments were carried out by Chiara Brambillasca and others as stated in the publication.

## 7.2   Table of Figures

## 8 VORABVERÖFFENTLICHUNG VON ERGEBNISSEN

Diese Doktorarbeit enthält unpublizierte Daten der Kombinationstherapie aus EZH2 Inhibierung und PI3K Inhibierung, sowie der Kombinationstherapie aus EZH2 Inhibierung und panCDK Inhibierung. Eine Bestätigung über die Benutzungserlaubnis dieser Daten liegt dem Promotionsbüro vor.